Photonics · Plasmonics
Magneto-Optics
PPM 2011

PPM Posters (38)

Coupling effects in arrays of Infrared Gold Nanoantennas

Pablo Albella[1] , Javier Aizpurua[1], D. Enders[2], T. Nagao[2], D. Weber[3], F. Neubrech[3] and A. Pucci[3]

[1] Material Physics Center CSIC-UPV/EHU and Donostia International Physics Center, Paseo Manuel de Lardizabal 5, Donostia-San Sebastian, Spain.
[2] World Premier International (WPI) Research Center for Materials Nanoarchitectonics National Institute for Materials Science (NIMS), 1-1 Namiki, Tsukuba, Ibaraki, 305-0044, Japan.
[3] Kirchhoff Institute for Physics, University of Heidelberg, INF 227, D-69120 Heidelberg, Germany.
pablo_albella@ehu.es

Since the resonant excitation of metallic nanostructures by light can yield considerable electromagnetic near field enhancement, the optical properties of metal nanoparticles have been subject of many studies [1]. In particular, interaction between particles in multimers and arrays of nanoantennas modifies and influences the optical properties of the system. The interaction properties depend on the separation distances to adjacent neighbors as well as on the distribution of the particles within the array. These effects have been broadly analyzed experimentally and theoretically in the visible spectral range for many different arrangements of particles [2,3] while only few studies have analyzed the IR range [4], where retardation is especially important.

Here, we report on the effect of coupling in the electromagnetic properties of 2D gold nanorod arrays in the IR range (1–12 µ m). We numerically and experimentally investigate the influence of interaction between neighboring antennas along the longitudinal and transversal direction in an ordered rectangular array of wire nanoantennas prepared on a silicon substrate. As an example, we show in Fig.1, the experimental and calculated resonance wavelength, λres vs the rod length L for nanoantenna arrays of three different longitudinal separation distances between the antennas, d_x. A red shift of the resonance wavelength is clearly observed for small values of d_x (40 nm) while for larger longitudinal separation distances (1µm) the results are almost identical to the non-interacting antennas (d_x = 5µm). This spectral red shift for small d_x can be understood in terms of coupled dipoles that include retardation. Regarding the transversal interaction (not shown here), significant blue shift of the extinction cross-sections and extraordinary broadening can be experimentally and theoretically observed for transversal separation distances, d_y smaller than $\lambda_{res} / n_{substrate}$.
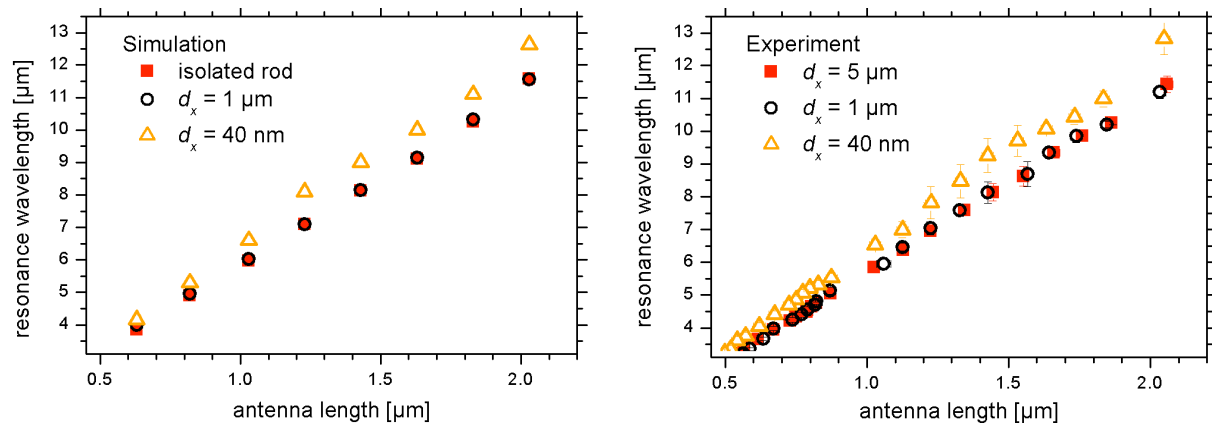
Fig.1: (Top) Calculated and (bottom) experimental resonance wavelength vs. rod length for different longitudinal separation distances between rods d_x .

The modification of optical properties by antenna arrays due to interaction effects can be exploited for sensing applications like surface enhanced infrared spectroscopy (SEIRS) [5].

The sensitivity in SEIRS strongly depends on where the resonant excitation is spectrally located compared to the molecular vibration that is to be enhanced. Therefore, the relation between spectral resonance positions and geometrical properties of the nanostructures, as presented here, is essential for the optimization of sensing devices.

References

[1] S.A. Maier and H.A. Atwater, J. Appl. Phys. 98, 011101 (2005).
[2] E.M. Hicks, S. Zou, G.C. Schatz, K.G. Spears, R.P. Van Duyne, L. Gunnarsson, T. Rindzevicius, B. Kasemo, and Mikael Käll, Nano Lett. 5, 6, 1065-1070 (2005).
[3] B. Lamprecht, G. Schider, R.T. Lechner, H. Ditlbacher, J.R. Krenn, A. Leitner, and F.R. Aussenegg, Phys. Rev. Lett. 84, 20 (2000).
[4] R. Adato, A.A. Yanik, C.-H. Wu, G. Shvets, and H. Altug, Optics Express 18, 5, 4526 (2010).
[5] F. Neubrech, A. Pucci, T. Cornelius, S. Karim, A. Garcia-Etxarri, and J. Aizpurua, Phys. Rev. Lett. 101, 157403 (2008).

Synthesis of nanogaps between smooth and porous nanowires

I. Alber[1], S. Müller[1], O. Picht[1], M. Rauber[1,2], R. Neumann[1], M. E. Toimil Molares[1]

[1] GSI Helmholtz Centre for Heavy Ion Research GmbH, Planckstr.1, Darmstadt, Germany
[2] Darmstadt University of Technology, Karolinenplatz 5, Darmstadt, Germany
i.alber@gsi.de

By interaction of metallic nanowires (NW) with electromagnetic radiation of appropriate wavelength, resonant surface charge density oscillations, called surface plasmons, can be excited. These oscillations are responsible for a large electromagnetic field enhancement in the NW near-field, which makes these wires suitable as functional elements in devices for e.g. highly sensitive detection of molecules using surface enhanced infrared spectroscopy[1] and Raman spectroscopy[2,3], and selectively killing of cancer cells by photothermal therapy [4,5].

The even stronger field enhancements achieved by plasmon coupling at nanogaps between narrowly spaced nanostructures [6,7,8] have recently been, experimentally and theoretically, a subject of increasing scientific interest. However, controllable fabrication of nanogaps between well-defined nanostructures continues being an experimental challenge.

Here, we report the synthesis of closely spaced smooth and porous nanowires by electrochemical deposition in etched ion-track membranes. Polycarbonate foils were irradiated at the GSI linear accelerator UNILAC with heavy ions accelerated to an energy of 11.1 MeV/u. The irradiated foils were track-etched with a 6 mol/l sodium hydroxide solution at 50° C to produce cylindrical pores randomly distributed in the foils. Au/Ag/Au nanowires were grown by pulsed-deposition using a single-electrolyte containing both silver and gold cyanide ions.

Figure 1 shows a scanning electron microscopy (SEM) image of two multisegment nanowires. Segments with higher concentration of gold appear brighter than the ones with higher silver content.

To selectively etch out the silver of the segmented nanowires, the nanostructures were treated with nitric acid. This results in the formation of nanogaps with sizes down to about 8 nm as shown in Figure 2. In addition, composition and concentration of the electrolyte, and pulse parameters determined the Au and Ag content of the segments, and thus the morphology of the wires after dissolution of the Ag. Using different concentrations of $KAg(CN)_2$ in the electrolyte, smooth segments enclosing the gap (Figure 2) as well as very porous segments (Figure 3) were obtained.

In conclusion, segmented silver gold nanowires and small nanogaps down to 8 nm were created. Furthermore, the morphology of the segments enclosing the gap can be varied by adjusting the deposition parameters. Plasmon resonance measurements on these structures are under way.

References
[1] F. Neubrech et al., Phys. Rev. Lett. **101** (2008) 157403.
[2] S. Nie et al., Science **275** (1997) 1102.
[3] K. Kneipp et al., Phys. Rev. Lett. **78** (1997) 1667.
[4] J.N. Anker et al., Nature Mater. **7** (2008) 4.
[5] I. H. El-Sayed et al., Nano Lett. **5** (2005) 829.
[6] S. Li et al., Nano Lett. **10** (2010) 1722.
[7] L. Qin et al., PNAS **103** (2006) 13300.
[8] W. Wei et al., Nano Lett. **8** (2008) 344.

Figures
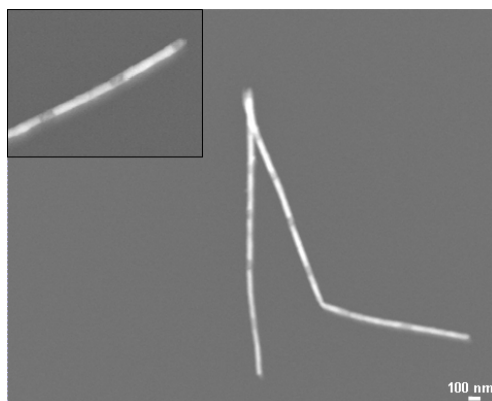
Figure 1: SEM image of two nanowires displaying the gold and silver segments. The inset shows a zoom in at higher magnification.
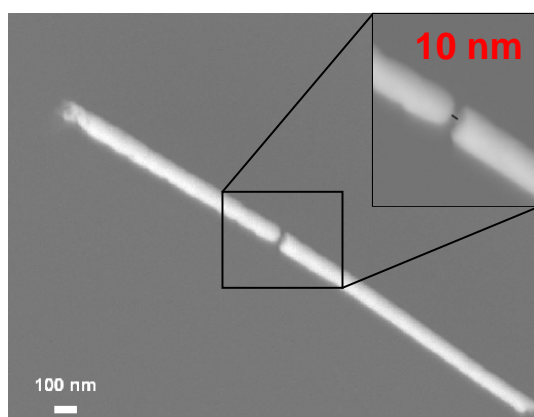
Figure 2: 10 nm gap between two smooth Au nanowires. The inset shows the gap at higher magnification.
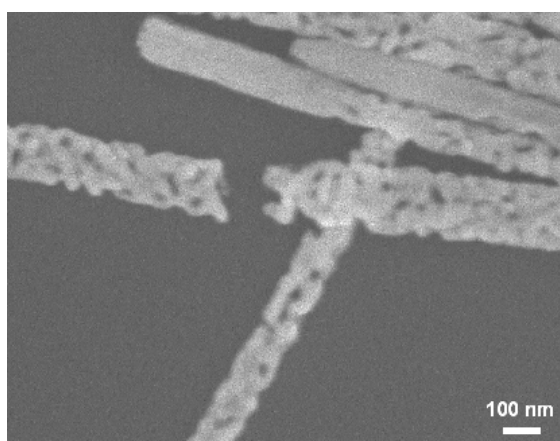
Figure 3: Porous nanowires enclosing a nanogap

4

Optical and magneto-optical response of magnetic nano-scale disks: size effects

R. Alcaraz de la Osa[1,2], J. M. Saiz[1], F. González[1], F. Moreno[1], P. Vavassori[2,3] and A. Berger[2]

[1] Grupo de Óptica, Dpto. de Física Aplicada. Universidad de Cantabria,
Avda. de Los Castros s/n, Santander, Spain
[2] CIC nanoGUNE Consolider, Tolosa Hiribidea 76, E-20018 Donostia-San Sebastián, Spain
[3] IKERBASQUE, Basque Foundation for Science, E-48011 Bilbao, Spain
alcarazr@unican.es

The recent rise of interest in magnetoplasmonics –materials that combine magnetic and plasmonic functionalities– has accelerated fundamental studies of the interplay of light-matter coupling and magnetism in nano-sized structures. The combination of optical and magnetic properties of nanostructurized materials has been employed to address active tuning in nanoplasmonic devices, thermal magnetization switching, and enhancement of magneto-optical Kerr effect (MOKE) [1].

The experimental exploration of the mutual relations between magnetism, magneto-optical activity and light-matter coupling in spatially confined geometries poses questions and brings a new impulse to the modeling efforts. As a first approximation, the infinite film approach has been often applied to model light interaction with finite size magnetic particles by researchers in magneto-optics. This approach worked extremely well for magnetic structures whose geometric dimensions are larger than the wavelength of the incident light (>1µm). However, the recent move to the nanometer range is expected to require a revision of the current numerical models and approximations.

In order to address the fundamental question of the limits of applicability of the infinite film approach, we have compared its predictions of the optical and magneto-optical response of ferromagnetic nano-scale disks with those by a more specific model. The latter approach considered relies on the recently developed E-DDA code, based on an extension of the discrete dipole approximation [2], which has been specifically devised to deal with nano-scale optical objects. In order to make this comparison meaningful, we worked out an equivalent discretization formulation of the infinite film approach. In doing so, we introduced the same structural discretization used for the E-DDA approach, so that the numerical specifics related to the discretization process show up in exactly the same way in the two cases. More specifically, we considered an electric dipole interacting with an infinite number of surrounding dipoles in order to get an effective polarizability expression for that reference dipole. The nano-scale particle is then built up by inserting this reference dipole in each cell of the discretization mesh (no further interaction is considered). While in this modified infinite film approach the shape of the particle only affects the scattered field through the phase of each electric dipole, in E-DDA near field interactions produce additional shape effects.

We applied these two approaches to predict the optical and magneto-optical response of Cobalt disks of several sizes illuminated with a wavelength of λ=632.8nm under normal incidence, in a typical transverse MOKE configuration (Fig. 1). The comparison of the predictions of the two methods is summarized in Fig. 2, which shows the optical and magneto-optical dipole moment distributions calculated with E-DDA and normalized to that obtained using the discretization formulation of the infinite film. Figure 3 shows the corresponding far-field intensity patterns calculated in the x-y plane.

The main conclusion we can draw from the comparison is that, for large enough disks (diameter comparable to the wavelength), both approaches provide similar results (see Fig. 3, D equal to 1000 and 600 nm), meaning that in these cases the infinite film approximation produces almost exact results. However, as the size of the disks is decreased below the wavelength, both optical and magneto-optical components show size-induced enhancement effects (see Fig. 3, D equal to 100 and 200 nm). It is worth noting that, since optical and magneto-optical contributions to the far field intensity scale nearly in

the same way, the normalized magneto-optical response, which is the quantity measured in experiments, is only weakly affected even in the case of disks of sub-wavelength size.

References

[1] V. V. Temnov, et al., Nat Photon **4**, 107 (2010); B. C. Stipe, et al., Nat Photon **4**, 484 (2010); V. I. Belotelov, et al., Phys. Rev. Lett. **98**, 077401 (2007).
[2] R. Alcaraz de la Osa, P. Albella, J. M. Saiz, F. González, and F. Moreno, Optics Express, Vol. 18, **23**, 23865 (2010).

Acknowledgements
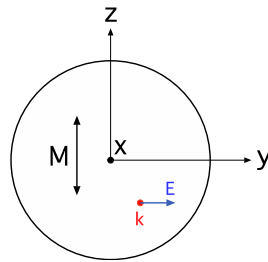
Figures

Figure 1: Transverse MOKE configuration, where the incoming light wave-vector is in the x-direction, the electric field linearly polarized along the y-direction, and the magnetization M being perpendicular to the scattering plane (considering X-Y plane).
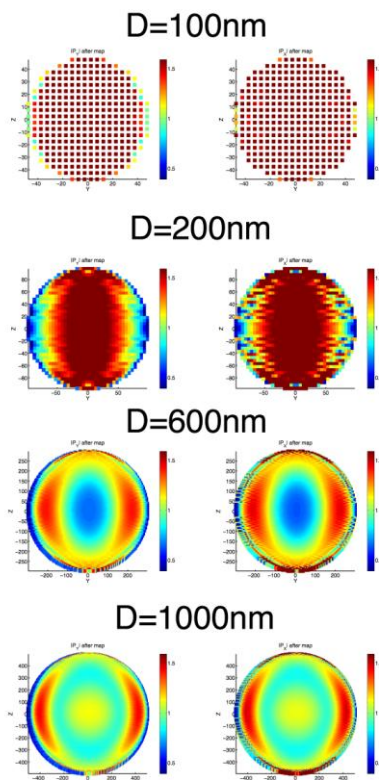
Figure 2: Absolute value of the y (left column) and x (right column) components of the induced dipole moment for several sizes normalized to the infinite film calculation. Notice that the x-component of the dipole moment is the "magneto-optically induced" component, while the y-component is the "optically induced" component.
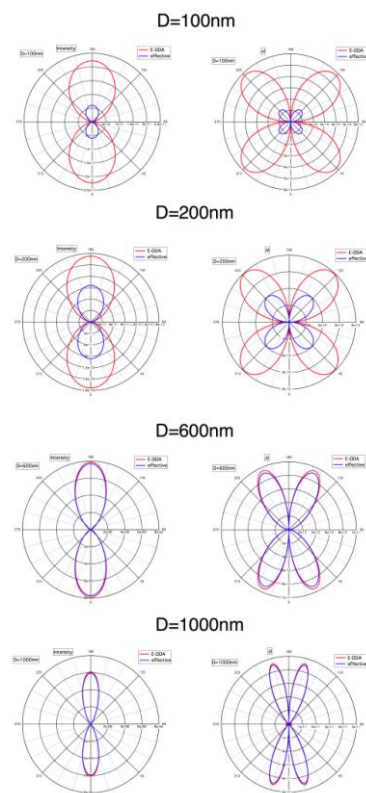
Figure 3: Far-field scattered intensity patterns and ΔI patterns for several sizes for both the E-DDA calculation and the film approach (effective). The ΔI patterns are obtained by computing the difference in scattered intensity under magnetization reversal.

Infrared phononic nanoantennas: Localized surface phonon polaritons in SiC disks.

AMEEN Mohamed[1], GARCIA-ETXARRI Aitzol[1], SCHNELL Martin[2], HILLENBRAND Rainer[2], AIZPURUA Javier[1].

1. Donostia International Physics Center, DIPC & Centro de Fisica de Materiales, CSIC-UPV/EHU, San Sebastian 20018, Spain.
2. Nanooptics Group, CIC Nanogune Consolider, San Sebastian 20018, Spain.

aizpurua@ehu.es

Electromagnetic interaction of light with the interfaces of polar materials shows a sharp and well defined electromagnetic response in the infrared (IR) region that consists mainly of excitation of optical phonons. Similar to surface plasmons in the visible region, surface phonons can couple efficiently to infrared light in micron-sized particles made of polar materials. This interaction forming localized surface phonon polaritons cause antenna effects, like enhanced absorption and scattering of electromagnetic radiation in some particular frequencies and enhancement & localization of electromagnetic field, allowing micron sized-structures of polar materials to act as micro/nano antennas in the infrared.

We apply the boundary element method to calculate the infrared electromagnetic response of single SiC disks acting as effective infrared antennas as a function of different parameters such as disk size (800 – 1200 nm) and thickness (50 – 100 nm). We also analyzed the effect of locating a near-field probing metallic tip near the SiC disk to scatter light, thereby obtaining new spectral peaks connected with localized modes between the tip and the SiC disk. We then further investigated their application in IR scanning probe microscopy. A near-field map of the phononic resonances improves the understanding of the nature of the IR extinction peaks. Finally, the effect of placing the nanoantenna on different substrates is studied.

References

[1] Ameen Mohamed, Garcia-Etxarri Aitzol, Schnell Martin, Hillenbrand Rainer & Aizpurua Javier., Chinese Science Bulletin, 2010, vol 55, 2625-2628.
[2] P. Mühlschlegel et al., Science 308, (2005), 1607-1609.
[3] R. Hillenbrand, T. Taubner F. Keilmann., Nature Vol 418, 2002, 159-162

Figures
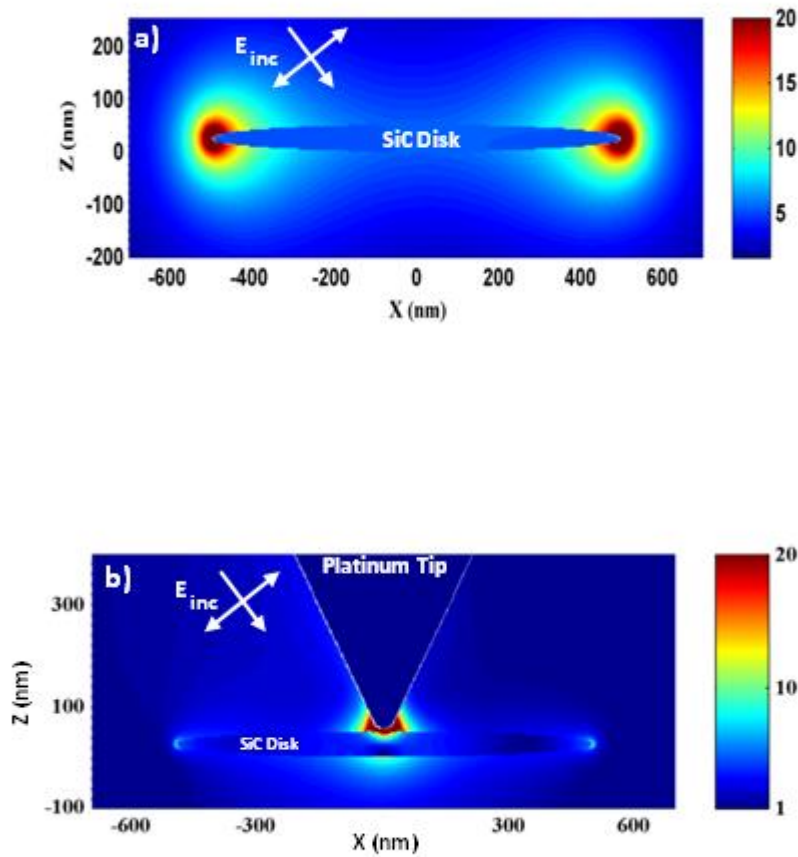
Figure caption

a) Near-field amplitude distribution around a SiC disk nanoantenna with size 1000 nm and thickness 50 nm at an incident wavelength of 12.1 micrometer. Incident field E_{inc} is displayed in the figure.

b) Same situation as in Figure a, but in the presence of a metallic probing tip. Localized electromagnetic mode emerges from the interaction of the metallic probing tip with the nanoantenna. The incident wavelength is 11.6 micrometer.

Characterization of slow light regime in 2D photonic crystal waveguides

Imanol Andonegui Artegui[1], Andrea Blanco Redondo[1], Angel J. Garcia-Adeva[2]

[1]Tecnalia-Telecom ,Zamudio (Biscay), Spain
iandonegui@gmail.com
andrea.blanco@tecnalia.com

[2]University of the Basque Country,
Department of applied physics I
Bilbao (Biscay), Spain
angel.garcia-adeva@ehu.es

We present a comprehensive study of the slow light behavior in photonic crystal waveguides as key elements in optical buffer devices.

Photonic band gap materials are now recognized as excellent candidates for novel applications in the area of all-optical telecommunication networks. Systems based on these novel materials could outperform current generation optoelectronic devices in applications related to optical buffering [1,4,5,8,9], low-threshold lasing [10], or interferometry [7], just to cite a few examples.

In photonic crystal structures, where the dielectric permittivity varies periodically, a complete photonic band gap (CPBG) can appear. This gives rise to a frequency range where no light can propagate into the crystal structure independently of its propagation direction. If the periodicity is broken in certain ways (such as introducing point or line defects), localized light modes are formed around the defect region [3]. In this way, a photonic crystal waveguide can be tailored in such a way that light is guided from one point in the photonic crystal to another, no matter the geometrical complexity of the defect pathway. Moreover, in certain cases, light propagating through this waveguide can exhibit extremely low group velocity, which yields to considerable delays over the light pulse [11].

This work presents an exhaustive study of CPBG maps for two-dimensional photonic crystals based on the square and triangular lattices. These maps have been obtained by gradually sweeping rods/holes radii and dielectric contrasts. To perform the corresponding simulations, the finite element method (FEM) [2] and the plane wave expansion method [6] were used. FEM has also been applied to the study of PCWs, where harmonic propagation and eigenvalue analysis simulations have been done, showing that localized modes tend to present an extremely low group velocity. Finally, defect mode group velocity, group velocity dispersion (GVD), resulting bandwidth, and power loss are reported for different defect line widths in standard PCWGs. Taking into account these criteria, an optimum PCW is proposed, implementing the best combination of hole/rod radii, index contrast, waveguide width, and operational frequency bandwidth. The so obtained structures possess a great potential for the development of low-power consuming on-chip photonic buffers, whose impact on future telecommunication networks and optical computing will be of decisive importance.

References

[1] Andrey A. Sukhorukov, Yuri S. Kivshar, Physycal Review Letters, **Vol.97** (2006)，pp. 97-101

[2] Comsol multiphysics and Electromagnetics module, http://www.comsol.com.

[3] J. D. Joannopoulos, R. D. Meade, J. N. Winn, Princeton, NJ: Princeton Univ. Press, **Photonic Crystals Molding the Flow of Light** (2008)**.**

[4] M.D. Settle, R.J.P. Engelen, M. Salib, A. Michaeli, L. Kuipers, T.F. Krauss, Optics express, **Vol. 15** (2007) pp. 219-226.

[5] Pei-Cheng Ku, Connie J. Chang-Hasnain, Jungho Kim, Shun-Lien Chuang, Electronic Letters**, Vol. 38, n.24** (2002), pp.1581-1583.

[6] S. G. Johnson The MIT photonic-bands (MPB) package, MIT http://ab-initio.mit.edu/mpb/.

[7] T. Kampfrath, D. M. Beggs, T. P. White, A. Melloni, T. F. Krauss, L. Kuipers, Physical review A**., Vol. 81** (2010), pp.1-6.

[8] Toshihiko Baba, Nature Photonics**, Vol. 2** (2008), pp.465-473.

[9] Yurii A. Vlasov, Martin O. Boyle, Hendrik F. Hamann, Sharee J. McNab, Nature**, Vol. 438** (2005), pp. 65-69.

[10] Marko Loncar,, Tomoyuki Yoshie, Axel Scherer, Pawan Gogna and Yueming Qiu, Applied Physics Letters, **Vol. 81 n. 15** (2002), pp. 2680-2682.

[11] Daisuke Mori and Toshihiko Baba, Applied Physics Letters, **Vol. 85, n. 7 (2004)**, pp. 1101-1103.

Theoretical analysis of the effective optical properties of gold-nanoparticle-loaded polymer films and their transition from surface to bulk values with varying thickness

O. Merchiers, J. Vieaud, V. Ponsinet, A. Aradian

Centre de Recherche Paul Pascal UPR 8641, 115 Avenue Schweitzer, 33600 Pessac, France
merchiers@crpp-bordeaux.cnrs.fr

Systems of resonant gold nanoparticles embedded in a dielectric matrix have been studied for a long time from a fundamental point of view [1], and present interesting optical properties. The optical response of such systems in the visible region of the spectrum is dominated by the Localized Surface Plasmon Resonance (LSPR) of the particles. As a consequence, by varying the actual amount of nanoparticles, effective properties like permittivity or optical index of the composite film can be tuned, and at high enough loading fractions, they can exhibit large values or negative regions in the neighborhood of the LSPR. We study this system as a first step towards more complex systems with highly-engineered resonant particles which could give birth to metamaterial-type responses (e.g., double negativity).

Interestingly, even a simple system like this one still presents significant challenges in the understanding of the effective optical response. On the particle scale, the exact position of the LSPR directly depends on the dielectric function of the metal and matrix but also on the particles' shape [2]. For very small ones (around 10nm in diameter), confinement effects become important and there still exists uncertainty about the correct dielectric function that should be used. On the global scale, the volume fraction (density) and the spatial distribution of the particles in the matrix (dispersed in volume or located on a substrate) also strongly alter the LSPR spectrum and hence the optical response of the whole system. All these aspects should be integrated correctly into a suitable model. For dilute bulk geometries (3D), where particles are far from the substrate supporting the film, effective medium approaches such as the Maxwell-Garnett mixing rule, have shown to be quite satisfactory [3]. On the other hand, 2D-like systems with nanoparticles directly deposited on substrates require more sophisticated modeling tools. These have been developed during the 1970's and 1980's [4] and were later applied to determine for instance surface densities from spectroscopic ellipsometry measurements [5].

In this work we analyze the optical response of polymer films doped with gold nanoparticles (AuNP). Different spectra are obtained by means of UV\vis transmission spectroscopy an ellipsometric spectroscopy for different polymer film configurations: monolayer or volume dispersion of AuNP, supported either by a transparent (glass) or a reflective substrate (Si\SiO$_2$). Comparison of the results for the doped polymer film with those obtained for AuNP suspended in water shows strong differences in the width of the plasmon peak. The inclusion of AuNP's in the polymer matrix tends to broaden this peak. This effect can be related to the modified dielectric environment of the nanoparticles and possibly to some amount of aggregation occurring during the process of polymerization [6].

A model is proposed which takes into account the effect of the electron confinement, size polydispersity due to chemical synthesis and the substrate on the effective optical properties. In the case of thin polymer films (particle monolayers), interaction with the substrate has to be introduced by means of the image method. A modified polarizability is obtained by keeping only the dipole term in the expansion. With these physical ingredients, we propose a simple generalization of the Maxwell-Garnett mixing rule where we include both "volume" particles, and "surface" particles with modified polarizabilities (see figure 1).

This extended Maxwell-Garnett model brings several noteworthy features: first, it allows us to study mixed 2D-3D films, by describing continuously the evolution of the effective electromagnetic properties when the thickness of the composite film is varied from a fully 2D-situation (monolayer of nanoparticle on a substrate) to a fully 3D-situation (thick films), passing through all intermediate cases. This is interesting as, to the best of our knowledge, only purely 2D or purely 3D models were available to date. Second, our model also allows to separately change the amount of particles in the bulk of the material and the amount sitting at the surface of the substrate. We are therefore able to study the influence of repulsive, attracting or neutral substrates over the global electromagnetic response of the composite material.

References

[1] Maxwell-Garnett, J.C., *Philos.Trans.R.Soc.London*, **A203**, (1904), 385-420

[2] Maier, S.A., Plasmonics, fundamentals and applications. Springer, New York (2007)

[3] Doyle, W.T., *Phys.Rev.B*, **39**(14), (1989) 9852-9858.

[4] Bedeaux & Vlieger, Optical properties of surfaces, Imperial College Press (2004)

[5] Kooij, E.S. et al., *Langmuir* **18**(11), (2002) 4401-4413

[6] Mackay, M.E. et al., *Science* **311**(5768), (2006) 1740 --1743.

Figures
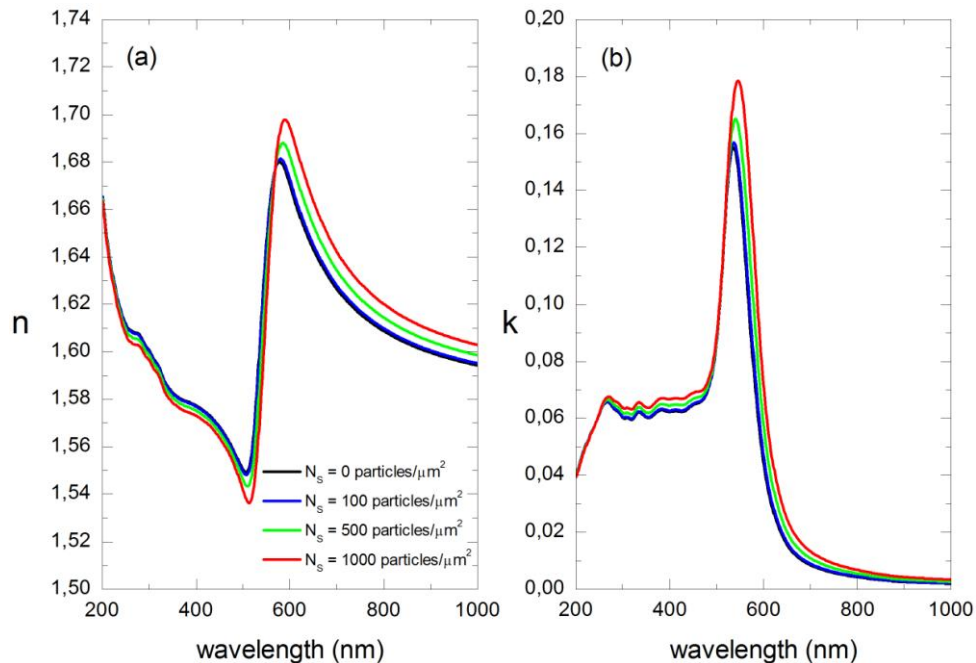
Figure caption

Figure 1 : (a) real part and (b) imaginary part of the refractive index. The curves were produced by applying the Maxwell-Garnett formula considering gold spherical inclusions in a polymer matrix. The volume fraction of the AuNP is 3%. For N_s=0, no substrate effect is taken into account.

12

Generalized Scattering-Matrix Approach for the Description of Wave Propagation in Nanostructured Magneto-Plasmonic Systems

B. Caballero[1,2], A. García-Martín[1], J.C. Cuevas[2]

[1]Instituto de Microelectrónica de Madrid (CNM-CSIC), Isaac Newton 8, PTM, 28760 Tres Cantos, Madrid, Spain; [2]Departamento de Física Teórica de la Materia Condensada, Universidad Autónoma de Madrid, E-28049 Madrid, Spain.

blanca.caballero@uam.es

In recent years a lot of attention has been paid to the study of the optical properties of nanostructured materials with both plasmonic and magneto-optic activity [1]. Here the key idea is to use hybrid nanostructures contaning both noble metals, which exhibit plasmon resonances, and ferromagnetic materials, which provide the magneto-optical activity, to profit from the best of the worlds of plasmonics and magneto-optics. In these hybrid structures one can make use of the excitation of the plasmons supported by the noble metals to enhance the magneto-optical signals (Kerr effect, Faraday effect, etc.), which can be of great importance, in particular, for sensing applications [2].

The nanostructuring in these magneto-plasmonic structures plays a fundamental role for several reasons. First of all, it provides a convenient way to couple the light of an external source to the plasmons supported by these hybrid systems, avoiding so the typical wave vector mismatch in unstructured systems. On the other hand, by nanostructuring these hybrid systems one can manipulate light at the nanometer scale in several ways. In particular, one can concentrate light in reduced volumes with the subsequent enhancement of the electric field. This fact leads in turn to the enhancement of the different magneto-optical properties of these hybrid systems.

In view of the relevance of these novel hybrid structures, and in order to guide their design, it is crucial to have theoretical methods that are able to describe the wave propagation in nanostructured magneto-plasmonic systems. A powerful approach, which is widely used to describe nanostructed systems without magneto-optical activity, is the so-called *scattering matrix formalism* [3]. In recent years, this method has been extended to describe also different magneto-optical effects in magneto-plasmonic systems [4]. However, there are still basic situations and problems that lie out of the scope of the existent implementations of the scattering formalism. As an example, the Kerr and the Farady effect in nanostructured multilayer systems in the transverse configuration cannot be addressed with the existent theoretical methods. In this context, we present in this work a generalization of the scattering-matrix approach to describe the magneto-optics of hybrid nanostructured systems which is able to handle any combination of materials and to describe the magneto-optical effects in any configuration. We illustrate the power of the method by addressing a recent experiment where the Transverse Magneto-Optical Kerr Effect (TMOKE) was measured in a periodically perforated Fe film [5]. We show that, in excellent agreement with the experimental results, the excitation of plasmon-like modes in these structures enhances the TMOKE signal (see Fig. 1). More importantly, our theoretical method paves the way for studying the interplay between emblematic plasmon-driven effects, like the extraordinary optical transmission [6], and the magneto-optics in a wide variety of hybrid nanostructures.

References

[1] G. Armelles, A. Cebollada, A. García-Martín, J.M. García-Martín, M.U. González, J.B. González-Díaz, E. Ferreiro-Vila, and J.F. Torrado, J. Opt. A: Pure Appl. Opt., **11** (2009) 114023.
[2] A.G. Brolo, R. Gordon, B. Leathem, and K.L.. Kavanagh *et al.*, Langmuir, **20** (2004) 4813.
[3] D.M. Whittaker and I.S. Culshaw, Phys. Rev. B, **60** (1999) 2610.
[4] A. García-Martín, G. Armelles and S. Pereira, Phys. Rev. B, **71** (2005) 205116.
[5] J.F. Torrado, E. Th. Papaioannou, G. Ctistis, P. Patoka, M. Giersig, G. Armelles, and A. García-Martín, Phys. Status Solidi (RRL), **4** (2010) 271.
[6] F.J. García-Vidal, L. Martín-Moreno, T.W. Ebbesen, and L. Kuipers, Rev. Mod. Phys., **82** (2010), 729.

Figures
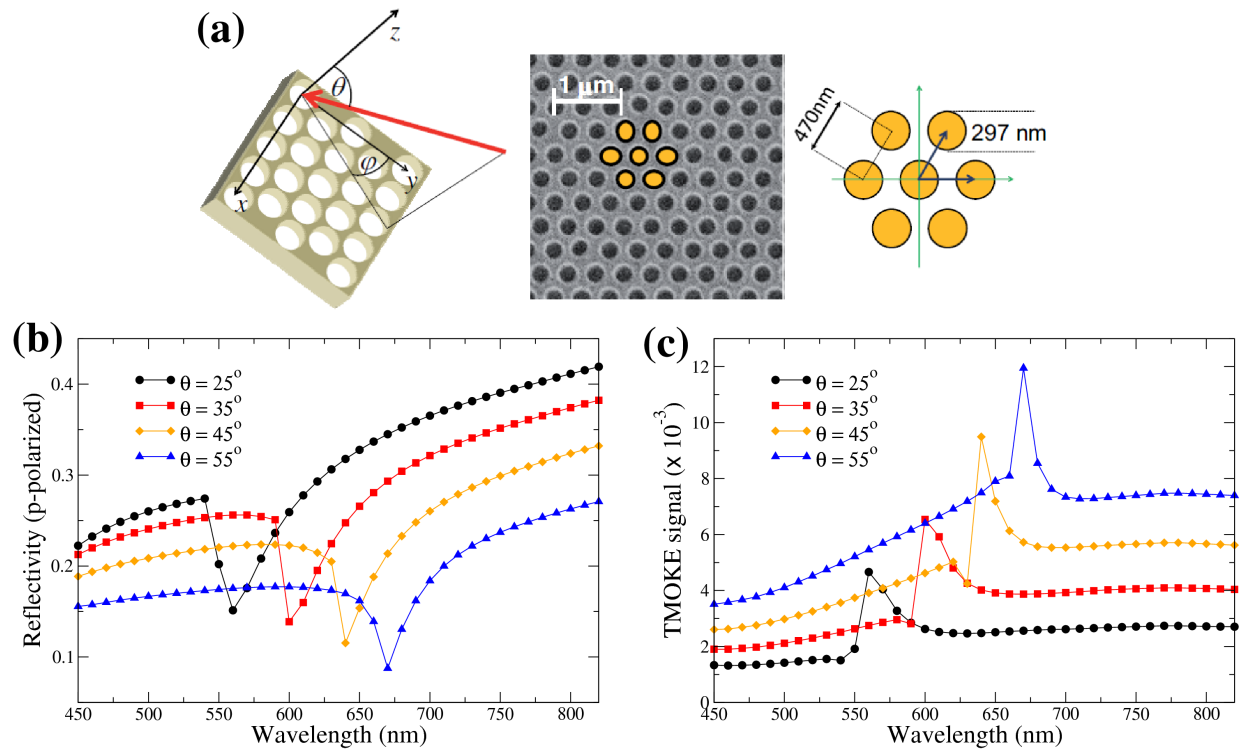
Fig. 1: **(a)** The left figure shows a schematic view of the periodically perforated Fe film studied experimentally in Ref. [5] and considered here in our theoretical work. Here, one can also see the angles defining the direction of the incident light. The central figure shows a SEM micrograph of the structure [5], and on the right hand side one can see the relevant dimensions of the system (lattice constant and radius of the holes). **(b)** Calculated reflectivity for p-polarized light for different incidence angles along the line φ = 30°. **(c)** Calculated TMOKE signal as a function of the wavelength and incidence angle θ for the crystal orientation φ = 30°.

Magneto-plasmonic colloidal hybrid nanostructures:
A double-faced magneto optical behaviour

L. I. Cabrera[1], F. Pineider[1,2], C. de Julián Fernández[1], G. Campo[1], E. Fantechi[1], C. Innocenti[1], C. Sangregorio[1,3], A. Caneschi[1], D. Gatteschi[1]

[1]INSTM- Università di Firenze, via della Lastruccia 3, 50019 Sesto Fiorentino, Italy; [2]CNR- ISTM, Via Marzolo 1, 35131 Padova, Italy; [3] CNR-ISTM, Via C. Golgi 19, 20133 Milano, Italy
lourisa. cabrera@yahoo.com

The conjugation of magnetic and plasmonic moieties at the nanoscale offers a wide variety of opportunities, both from the point of view of theoretical understanding and for exciting applications. In particular, magnetic-plasmonic hybrids have been proposed as bi-functional systems for a variety of applications in theranostics, in which the gold shell acts as a protecting agent for the magnetic core, [1] as a highly functonalisable surface, [2] as an optical heater [3] or as an active optical beacon. [4]

The most interesting aspect of this type of systems however, is probably that of conjugating the two functions to obtain novel effects: active magneto-plasmonics (the modulation of plasmon resonance with an external magnetic field) has been recently demonstrated, [5] and several reports of plasmon-mediated enhancement of the magneto-optical response of hybrids have been described. [6-9]

Our study uses magnetic circular dichroism (MCD) in the visible range as an information-rich tool to enucleate the relations between magneto-optical (MO) terms in hybrid magnetic-plasmonic systems.

Using colloidal chemistry methods we have been able to obtain systems containing gold and ferrites in different geometries, that exhibit different levels of conjugation, thus a variable extent of interaction of magnetic and plasmonic functions, ranging from no interaction (separate gold and ferrite particles), to weak (particle heterodimers) and strong interaction (gold core@ferrite and ferrite core@gold shell particles).
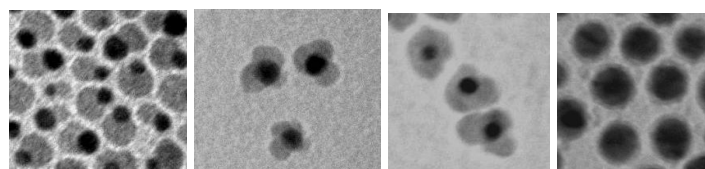
Our very recent results indicate that the MCD response of the hybrid magnetoplasmonic particles can clearly be divided into distinct components from the two moieties, and that these do not necessarily sum in linear way. This interesting observation represents a key factor to promote the investigation from the mere effect of plasmon-mediated MO amplification a more mature and fascinating level, which consists in the use MCD to investigate complex wavelength-dependent behaviour of magnetoplasmonic nanostructures.

References

[1] L. Wang et al., J. Mater. Chem. **15** (2005) 1821.

[2] X. Zhao et al., Anal. Chem. **80** (2008) 9091.

[3] L. Wang et al., Angew. Chem. Int. Ed. **47** (2008) 2439.

[4] Q. Wei et al., J. Am. Chem. Soc. **131** (2009) 9728.

[5] V. Temnov et al., Nature Photon. **4** (2010) 107.

[6] P. Jain et al., Nano Lett. **9** (2009) 1644.

[7] Y. Li et al., Nano Lett. **5** (2005) 1689.

[8] J. B. González-Díaz et al. Adv. Mater. **19** (2007) 2643.

[9] J. B. González-Díaz et al. Small **4** (2008) 202.

Magneto-optical study of the dipolar coupling between magnetism and plasmonic nanoparticles

G. Campo[1], C. de Julián Fernández[1], F. Pineider[2,1], E. Fantechi[1], G. Poneti[1], C. Innocenti[1], C. Sangregorio[3,1] and A. Caneschi[1]

[1]INSTM- Università di Firenze, via della Lastruccia 3, 50019 Sesto Fiorentino, Italy; [2] CNR- ISTM, Via Marzolo 1, 35131 Padova, Italy; [3] CNR-ISTM, Via C. Golgi 19, 20133 Milano, Italy
giulio.campo@unifi.it

The magneto-optical (MO) properties of nanomaterials that combines localize surface plasmon resonances (SPR) with magnetic properties is the centre of this study. In the last years an intense activity is being devoted to interconnect two different nanowords: the optic and the magnetic ones. Nanomaterials that exhibit SPR or photoluminescence in simple combination with magnetic properties or, more interesting, in which the magnetic and optical properties are in synergy so one part can be controlled by the counterpart are being looking for. The development of novel photo-detectable, photoswitchable and in general multifunctional nanomaterials are quite interesting for biomedicine, spintronics and data recording. The expected effect of the SPR on the magnetic properties is the change of its MO features. The few studies in hybrid core-shell nanoparticles [1] hetero-dimers nanostructures [2] or simply plasmonic dots on magnetic surfaces [3] have shown effects like enhancement of the MO signal and/or changes in the MO spectra in correspondence to the SPR. The origin of these phenomena is under discussion, they can be due to the effect of the strong electromagnetic fields (EMFs) linked to the localized plasmons but also can be related to the electronic and structural changes at the interface of the two parts. It is well known that the EMFs generated by the SPR gives rise to changes in the optical properties of the structures/compounds near the particles like the huge enhancement of Raman activity or the enhanced photoluminescence. Instead the influence of the plasmonic resonance on MO activity has not been investigated.

In this work we present one combination of magnetic and magneto-optical characterizations of composite films containing magnetic and plasmonic nanoparticles well dispersed in a transparent matrix. Cobalt ferrite ($Co_{0.5}Fe_{2.5}O_4$) and Au nanoparticles were synthesized by colloidal methods. TEM characterizations reveal that the two type of nanoparticles exhibit narrow particle size distributions being the average particle sizes: 8.6 nm for Cobalt ferrite and 7.0 nm for Au nanoparticles. Both nanoparticles are capped by 2.0 nm size shell of oleylamine and oleic acid. The reference nanocomposite has 3%wt of the Co-ferrite nanoparticles in polystyrene matrix. Three spin-coated films including also the gold nanoparticles were prepared with 1/4, 3/8, and 1/2 weight of Au with respect to the cobalt ferrite content, that corresponds to packing factors of 0.035%, 0.05%, and 0.07% respectively.

The optical extinction spectra of the three Au-cobalt ferrite films exhibit similar structure characterized by one broad SPR peak centred around 570 nm with a large tail that extends to the nIR. Magnetic circular dichroism (MCD) spectra and MCD hysteresis loops were recorded in the 400 -1000 nm spectral range and applying a maximum field of 1.3 T. In opposite to the optical properties, the MO properties are strongly depending on the Au content (Figure 1). We observe a decreasing of the MO strength when include Au nanoparticles that depends on the Au content. Moreover, in the spectral region in coincidence with the SPR, the line-shapes change including the sign. We record also MCD hysteresis loops at different wavelengths. This allows to observe the presence of different MO contributions in the different spectral regions. Considering the different transitions involved in the MO spectrum of the cobalt ferrite [4] we conclude that the EM field generated by the plasmons coincide with Charge-transfer transitions of the Co-ferrite giving rise to their strong dumping and to a new type of MO

transitions are activated. Also crystal-field transitions are dumped even if plasmon resonance are very weak. Such changes depend in one non-linear way of the Au concentration. The differences in the MO spectral with the Au-contain precludes the use of MO techniques due to the sensibility and selectivity to different magnetic and optical environments.

References

[1] P. Jain *et al.* Nano Letters, **9** (2009) 1644

[2] Y. Li *et al.* Nano Lett., **5** (2005) 1689

[3] S. Tomita *et al.* Phys. Rev. Lett., **96,** (2006) 167402

[4] E. Tirosh, G. Shemer, G. Markovich Chem. Mater., **18** (2006) 465

Figures
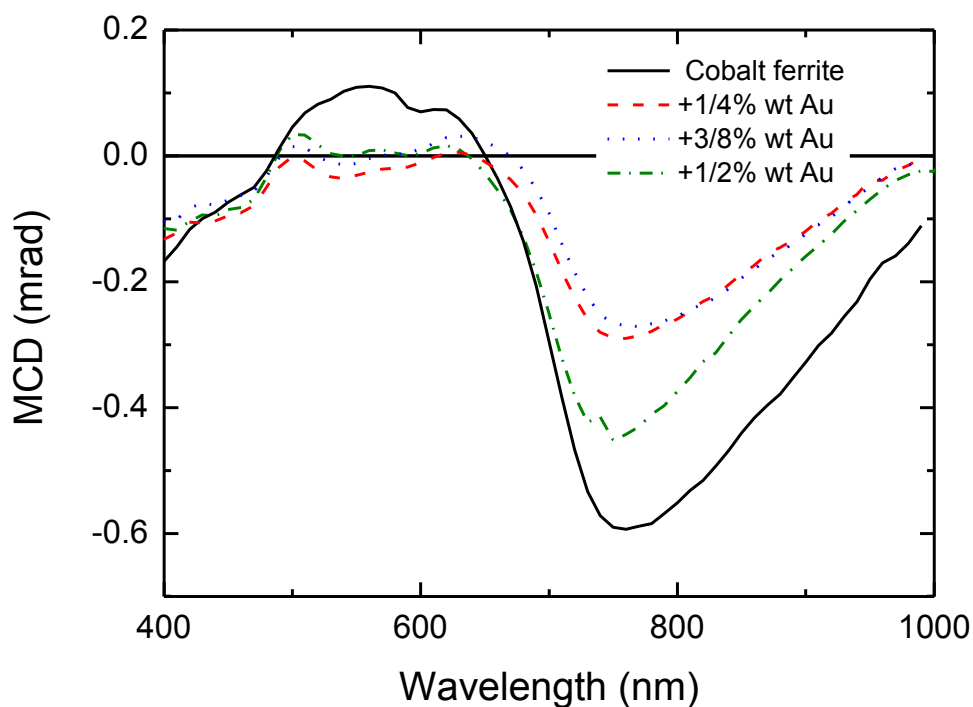
Figure 1. Magnetic circular dichroism spectra of the films containing only Cobalt ferrite nanoparticles and of the films including ¼%wt. , 3/8% wt. and ½% wt. of Au nanoparticles.

Localized Extraordinary Optical Transmission of THz radiation through subwavelength apertures

S. Carretero-Palacios[1], Sergio G. Rodrigo[2], L. Martín-Moreno[1], F.J. García-Vidal[3]

[1]Instituto de Ciencia de Materiales de Aragón and Departamento de Física de la Materia Condensada, CSIC-Universidad de Zaragoza, E-50009 Zaragoza, Spain

[2]Institute of Optics, University of Rochester, Rochester, New York 14627, USA

[3]Departamento de Física Teórica de la Materia Condensada, Universidad Autónoma de Madrid, Madrid 28049, Spain
sol@unizar.es

Sub-wavelength apertures periodically arranged may transmit electromagnetic waves beyond the cut-off wavelength with a much higher intensity than if they were isolated. It has been established that resonant excitation of surface plasmons creates huge electric fields at the surface that force light through the holes, giving very high transmission coefficients. This is the so-called Extraordinary Optical Transmission [1].

We analyze theoretically resonances appearing at wavelengths beyond the cut-off of the holes [2], [3]. We name this phenomenon Localized Extraordinary Optical Transmission (LEOT). Interestingly, no surface modes are involved; therefore, the physical mechanism is valid for both single holes (SH) and hole arrays (2DHA).

In particular, we will give analytical expressions for the LEOT peak position as a function of the film thickness (h), and the dielectric constants of the environment (the cover, the substrate, and inside the holes, ε_1, ε_3, ε_2, respectively) for both symmetric ($\varepsilon_1 = \varepsilon_3$) and asymmetric ($\varepsilon_1 \neq \varepsilon_3$) configurations, for any hole shape of high aspect ratio (See Fig.1). Furthermore, the peak position is not the only spectral property affected by the dielectric environment, but also LEOT peak intensities are drastically modified.

These results explain the unexpected fact reported by some experiments in the THz regime about enhanced transmission [4] through isolated holes at wavelengths red-shifted from the cutoff wavelength.

References

[1] T. W. Ebbesen et al. Nature (London) 391, 667 (1998)

[2] A. Degiron et al., Opt. Commun 239 (2004)

[3] K. J. Klein Koerkamp et al., Physs. Rev. Lett. 92, 1839901 (2004)

[4] M. A. Seo et al., Opt. Express, 16, 20484, (2008)
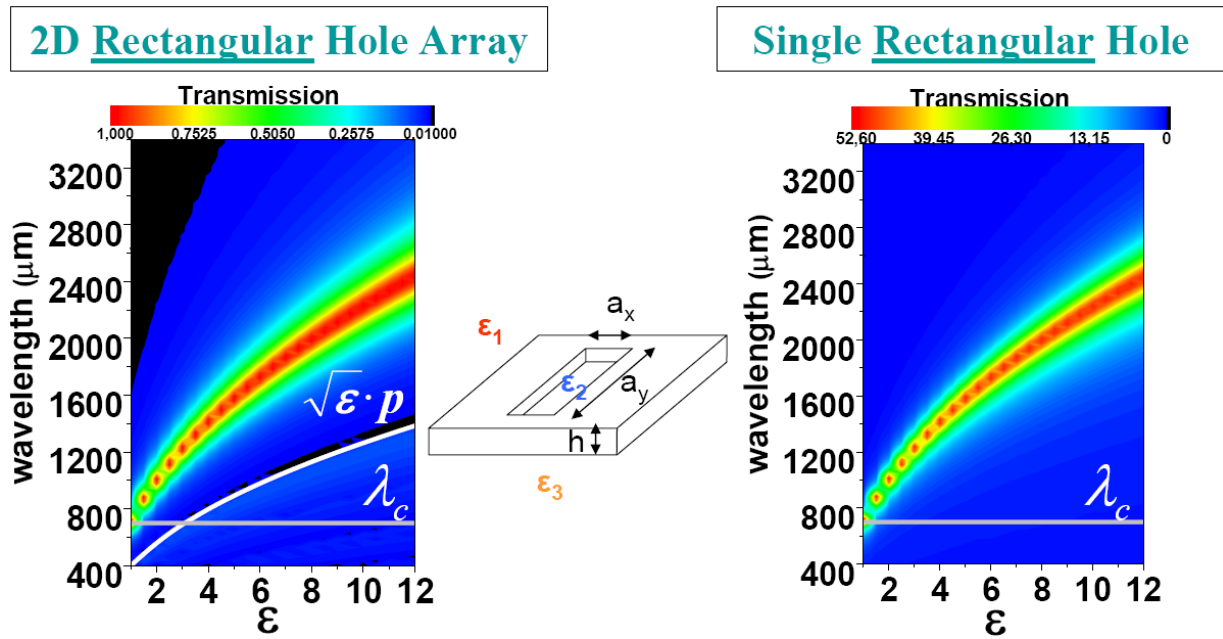
Fig.1. *Transmission of light as a function of the wavelength and the dielectric constant ε, through a 2DHA with rectangular holes on it (left panel, P=400μm) and through an isolated rectangular hole (right panel) placed in a symmetric environment (ε=ε₁=ε₃). The film thickness is chosen to be h = 1μm, for the rectangular holes aₓ = 10μm, aᵧ = 350μm, and ε₂ = 1.0. The horizontal grey line in both graphs depicts the cut-off wavelength of the holes, and the white line in the array corresponds to the Rayleigh condition.*

Flexible Terahertz Metamaterial Narrow Bandpass Filter

Choon-Gi Choi[1,3], Muhan Choi[1], Jaehyung Han[1,3], Byungsoo Kang[1,2], and Bumki Min[2]

[1]Convergence Components & Materials Research Lab (CCMRL), Electronics and Telecommunications Research Institute (ETRI), Daejeon, 305-700, Republic of Korea

cgchoi@etri.re.kr

[2]Department of Mechanical Engineering, Korea Advanced Institute of Science and Technology (KAIST), Daejeon 305-751, Republic of Korea

[3]School of Engineering for Advanced Device Technology, Korea University of Science and Technology (UST), Daejeon 305-333, Republic of Korea

Electromagnetic metamaterials have been fabricated to obtain material properties that are not available in naturally existing conventional materials. These are composed of micro- and nano-structures exhibiting the required values of permittivity and permeability in a desired frequency regime. Metamaterials in terahertz (THz) frequency regime have attracted much attention due to its potential application in lenses, switches, filters, modulators and detectors [1-5]. One of the important devices in the THz range is bandpass filters. These could be widely used in the field of imaging, spectroscopy, molecular sensing, security, drug identification.

In this paper, a multi-layered flexible THz metamaterial narrow bandpass filter is proposed, fabricated, and demonstrated. The key idea of the metamaterial filter is that it consists of a combination of three metallic layers filled with the polyimide substrate. The top and bottom layers have a fishnet metallic structure working as a high-pass FSS (frequency selective surface) with 40μm unit cell and line width 5μm and the mid-layer as a low-pass FSS has complementary metallic structure of the outer fishnet layers as shown in Fig. 1. The simulated transmission spectra of the single fishnet layer, the single square layer (complementary structure of fishnet), and the composite three layer as shown in Fig. 2.(a) reveal the function of each layer. The sharp transmission peak is obtained near at 1 THz frequency. It is also shown in Fig. 2.(b) that the transmission and the operating bandwidth can be tuned by adjusting the interlayer spacing parameter (s).

The transmission properties are calculated by the finite-difference time-domain (FDTD) method, adopting the Drude model to take into account the dispersion of metal in THz regime. The single layer of metamaterial filter is fabricated by Au/Cr metal patterning with 100 nm thickness using photolithography, e-beam metal deposition, and lift-off process on the polyimide substrate. The multilayered structure is completed by repeating the above single-layer processes. Experimentally, the transmission spectra of the metamaterial filter were measured by using the THz Time-domain spectroscopy (TDS) with the frequency window from 0.2 to 2.5 THz.

In conclusion, we introduced the flexible narrow bandpass filter designed through intuitive and robust method using the fishnet metamaterial layer and its complementary layer. It will be expected to be used in various THz optical applications.

References

[1] H. T. Chen, W. J. Padilla1, J. M. O. Zide, A. C. Gossard, A. J. Taylor, and R. D. Averitt, *Nature* **444** (2006) 597.

[2] H. T. Chen, J. F. O'Hara, A. J. Taylor, R. D. Averitt, C. Highstrete, M. Lee, and W. J. Padilla1, *Opt. Express* **15** (2007) 1084.

[3] D.J. Shelton, J.W. Cleary, J.C. Ginn, S.L. Wadsworth, R.E. Peale, D.K. Kotter, and G.D. Boreman, *Electronics Letters*, **44** (2008) 1288.

[4] J. Bonache, I. Gil, J. García-García, and F. Martín, *IEEE Trans. Microw. Theory Tech.,* **54** (2006) 265.

[5] A. J. Gallant, M. A. Kaliteevski, S. Brand, D. Wood, M. Petty, R. A. Abram, and J. M. Chamberlain, *J. Appl. Phys.* **102** (2007) 023102.

Figures
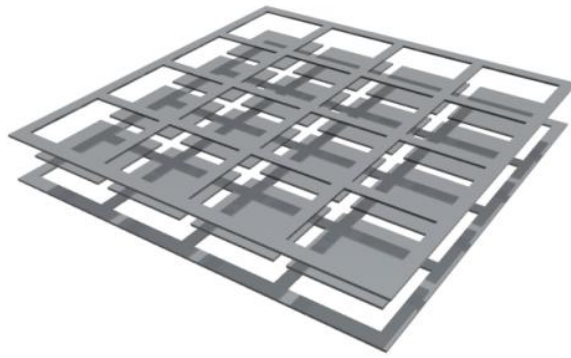
Fig. 1: The schematic of the metamaterial narrow bandpass filter with triple layers. Top and bottom layers are fishnet metal layer with 40μm unit cell and line width 5μm, and mid-layer is the complementary structure of the fishnet layer.

(a)   (b)
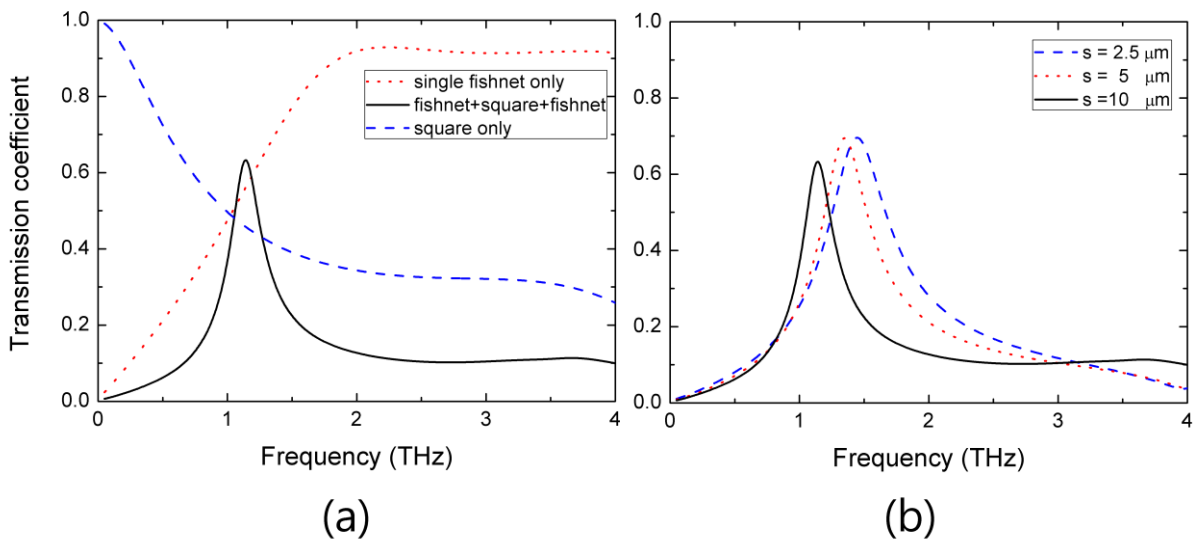
Fig. 2: (a) Simulated transmission spectra of the metamaterial filter (black solid line), the square layer only (blue dash line), and the single fishnet only (red dot line). (b) Simulated transmission spectra of the metamaterial filter with varying interlayer spacing (s) as 10 μm (black solid line), 5 μm (blue dash line), and 2.5 μm (red dot line), respectively.

Frequency analysis of magneto-optical SPR signals

Sorin David[1], Cristina Polonschii[1], Mihnea Rosu-Hamzescu[2], Dumitru Bratu[1], Eugen Gheorghiu[1]

1. International Centre of Biodynamics, Intrarea Portocalelor, Nr. 1B, 060101, Bucharest, Romania

2. University "Politehnica" of Bucharest, Faculty of Automatic Control and Computers, Splaiul Independentei, Nr. 313, 060042, Bucharest, Romania

sdavid@biodyn.ro

Materials with combined magneto-plasmonic elements allow for a highly improved sensitivity of the SPR measurements when applying an oscillating magnetic field across the sensor's magneto-optical surface.

The aim of this work is to investigate the sensitivity of a magneto optical surface plasmon resonance (MOSPR) sensor chip, to refractive index variations of the medium above its surface in a microfluidic set-up.

The system comprises an SPR measuring unit, custom made MOSPR chip, flow chamber and magnetic field generator.

The SPR measuring unit provides via an array of photodetectors the reflectivity of the incident light for a series of incident angles in total internal reflection conditions providing an SPR curve (reflectivity vs. incidence angle).

The custom made MOSPR sensor chip has alternating gold and cobalt layers and is prepared by thermal evaporation in a PVD system. The metallic structure Ti/Au/Co/Au [1], with no intermediate adhesion layer between Co and Au proved stable under flow conditions. Titanium and Gold were evaporated from tungsten boats while Cobalt was evaporated from an Al_2O_3 crucible.

A 100 µm deep flow chamber ensures the flow of the liquids above the surface of the sensor chip and is connected to a flow injection system with automatic valves.

The oscillating magnetic field is applied via a custom made electromagnet, perpendicular to the plane of the propagation of the incident light within the SPR measuring unit.

In contrast to the "classical" approach where the refractive index of the media above the surface of the sensor is related to the angle corresponding to the minimum value of the SPR curve, for MOSPR determinations, the angle pertaining for the largest reflectivity variation within the SPR curve is selected via the corresponding photodetector in the detection array.

The data from this photodetector is collected at a high rate and analyzed using the Fast Fourier Transform. Since the frequency of the oscillating magnetic field is known, from the amplitude of the oscillation of the light intensity for the chosen angle of incidence one can straightforwardly derive the reflectivity for each direction of magnetization $R_{pp}(M)$ and $R_{pp}(-M)$, respectively.

The data is processed using the formula $\dfrac{\Delta R_{pp}}{R_{pp}} = \dfrac{\left| R_{pp}(M) - R_{pp}(-M) \right|}{R_{pp}(0)}$ [2], where $R_{pp}(0)$ represents the

reflectivity without magnetization.

For comparing the sensitivity of both "classical" SPR and MOSPR methods as function of the refractive indices of the media presented at the surface of the sensor, the values are normalized using the formula:

$V\% = \dfrac{\left| V_i - V_1 \right|}{V_1} \times 100$, where V_i is the current value and V_1 is the value corresponding to the

measurement of the solution with the lowest refractive index. The results are presented in figure 1 and demonstrate a steeper slope and, correspondingly, ~4 times higher sensitivity of the MOSPR data in comparison to the classical SPR sensor chip and data processing. Adding a functionalization layer of self assembled thiols has no effect on the increased sensitivity of the MOSPR chip paving the way for biosensing applications.

Acknowledgements:
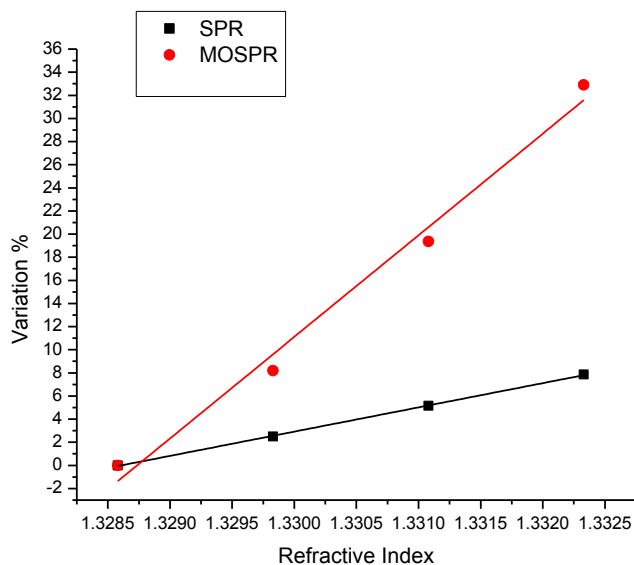
Fig. 1 Calibration curves for SPR (Black) and MOSPR (Red) showing improved sensitivity of the latter

References

[1] B. Sepúlveda, A. Calle, L. M. Lechuga, and G. Armelles, OPTICS LETTERS, **Vol. 31**, No. 8 (2006) 1085-1087

[2] D. Regatos, D. Fariña, A. Calle, A. Cebollada, B. Sepúlveda, G. Armelles, and L. M. Lechuga, J. Appl. Phys. **108**, 054502 (2010); doi:10.1063/1.3475711

24

Optical properties of disordered metallic clusters

R. Esteban[1], *Richard W. Taylor*[2]*, Tung-Chun Lee*[3]*, Sumeet Mahajan*[2]*, Jeremy J. Baumberg*[2]*, Oren A. Scherman*[3] *and* J. Aizpurua[1]

[1]*Centro de Fisica de Materiales, Centro Mixto CSIC-UPV/EHU and Donostia International Physics Center (DIPC), 20018 Donostia-San Sebastián, Spain*
[2]*NanoPhotonics Centre, Cavendish Laboratory, University of Cambridge, CB3 0HE, U.K.*
[3]*Melville Laboratory for Polymer Synthesis, Department of Chemistry, University of Cambridge,Cambridge, CB2 1EW, U.K.*
ruben_esteban@ehu.es

Metallic particles of sub-wavelength dimensions separated by distances smaller than their size support strong optical resonances. Intense fields at the separating gaps characterize these resonances, which are thus of interest for SERS spectroscopy. Cucurbiturils[1] are molecular linkers that result in a very good control of the inter-particle distance providing reproducible optical properties. We study both theoretically and experimentally the optical response of clusters of gold particles separated by Cucurbiturils. The position of each particle depends on random processes, therefore we consider the effect of disorder on the optical properties[2].

We are able to experimentally monitor the behavior of gold spherical clusters as they grow in size[3]. Notably, the lower energy extinction peak considerably redshifts up to a saturation value, and the Raman Signal can strongly increase as dimers or longer chains are formed. We perform simulations using both BEM[4] and Open-Max [5] to better understand the experimental results.

We first consider the response of the clusters to be dominated by linear chains of an average length that increases with the size of the cluster. Straight linear chains of increasing length present a low energy peak that redshifts up to a saturation value[6]. This behavior helps to understand the redshift observed in the experiments. Since the chains are not perfectly straight, we consider next chains with different degree of disorder (Figure 1). Even substantial disorder affects weakly the position of the low energy peak, and only moderately its strength. The spectra of the disordered chains already reproduce much of the observed spectral behavior of the experimental clusters.

To further approach the experimental system, we consider branching clusters composed by several tens of spheres. Similarly to the measurements and chain simulations, a clear low-energy extinction peak appears at a wavelength considerably redshifted with respect to the resonance of the single sphere.

The extinction cross-section is a property of the whole cluster and it is not straightforward to extract much information about the local behavior at a particular position. To obtain this local information, we are presently looking at the near-field spectrum obtained at the gap between the particles. This near fields also allow to estimate the expected SERS signal. Initial results indicate a good correspondence between simulated and measured results. Simulations of complex clusters with well defined gap distances are thus of interest for a complete understanding of optical networks.

References

[1] Lee, T-C. and Scherman, O. A., Chem. Comm. **46**, (2010) 2438
[2] C. Girard et al Phys. Rev. lett. **97**, (2006) 100801
[3] R. Taylor et al., submitted to ACS Nano (2010)
[4] F. J. García de Abajo and A. Howie, Physical Review B **65,** (2002) 115418
[5] T. Sannomiya, J. Vörös, and C. Hafner, J. Comput. Theor. Nanosci. **6**, (2009) 749
[6] Harris et al. J. Phys. Chem C **113**, (2009) 2784

Figure 1

(a)   (b)
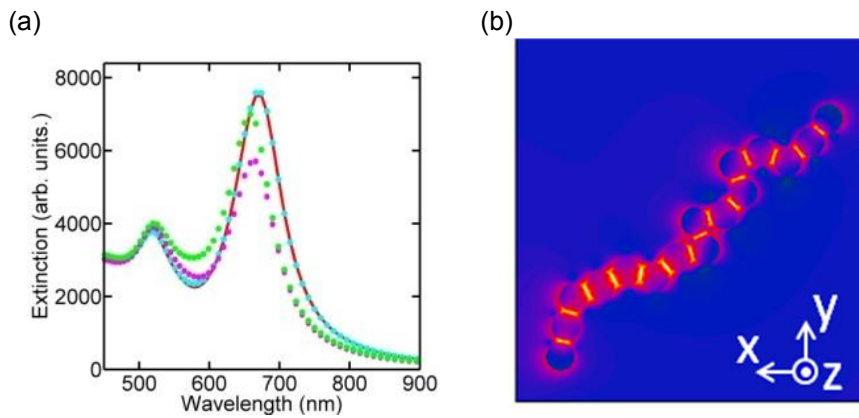
(a) Extinction spectra for chains composed by 16 gold spheres and different degrees of disorder. The values for a straight chain oriented along -1x+1y are plotted with a red line, while the green symbols correspond to the situation in (b). Other traces correspond to intermediate values of disorder. The sphere radius is 10nm and the separation is 0.9nm. Both the propagation vector and the E field are contained in the xz plane, making a 45 degree angle with the z axis.

Enhanced Magnetic field modulation of surface Plasmon wavevector in ultraflat Au/Fe/Au trilayers

E. Ferreiro-Vila[1], M. Iglesias[2], E. Paz[2], F. J. Palomares[2], J. M. González[3], J. M. García-Martín[1], A. Cebollada[1] and G. Armelles[1]

[1]IMM-Instituto de Microelectrónica de Madrid (CNM-CSIC)
Isaac Newton 8, PTM, E-28760 Tres Cantos, Madrid, Spain.

[2]Instituto de Ciencia de Materiales de Madrid (CSIC), Cantoblanco, 28049 Madrid, Spain.

[3]Unidad Asociada ICMM-CSIC/IMA-UCM, Sor Juana Inés de la Cruz 3, 28049 Madrid, Spain.
elias@imm.cnm.csic.es

A crucial aspect for the advance of plasmonics is the development of active elements, i.e., systems whose plasmonic properties can be modified by an external agent. Magnetoplasmonic structures combine materials with magneto-optical (MO) activity (usually ferromagnetic metals such as Fe or Co) and materials with plasmonic properties (typically Au [1] or Ag [2,3]). This kind of structures allows for a magnetic field control of the plasmonic characteristics of the system. On the other hand, obtaining ultrasmooth metallic structures is a crucial point for the implementation of active, high performance plasmonic devices[4,5]. Therefore, the elucidation of the influence on the magnetoplasmonic properties of the morphology of the structure to be used in those devices is of major interest.

Two series of 10 nm Au/X nm Fe/10 nm Au structures, with Fe thickness varying between 0nm and 6nm, have been grown on MgO substrates. Buffer layers, namely 1 nm Fe and 2 nm Cr, were used to fabricate the otherwise equivalent series of samples. The Fe buffer layers were grown by PLD whereas the Cr ones and Au layers were deposited by MBE.

Representative AFM images of the topmost surface of two equivalent samples (4.5 nm and 5 nm of Fe interlayer thickness, respectively) of the series grown on top of PLD and MBE buffers are shown in Fig. 1 (a). It is interesting to remark that both AFM images are displayed with the same scales for better comparison. As it can be observed, the PLD sample exhibits an ultraflat surface with global differences in height of around 0.5 nm over the scanned area. On the other hand, the equivalent MBE sample shows a rougher surface including granular structures around 7 nm in height, correlated to the different buffer growth technique. In Fig. 1 (b) we have plotted the Fe interlayer thickness dependence of the RMS roughness of the topmost layer for both series of samples, which is systematically at least a factor of two larger in the MBE samples than in the PLD ones for every Fe interlayer thickness. To extract quantitative information about the roughness of this Fe interlayer, x-ray reflectometry is a very suitable tool, since it allows quantifying, not only the roughness of the topmost layer in a multilayered system, but also the roughness of buried interfaces. The obtained results for the Fe interlayer – top Au layer interface from XRR measurements are also shown in figure 1 (b). A similar trend to that mentioned in the case of AFM results is observed.

The experimental SPP wavevector modulation ($\Delta k/k)_{SPP}$ was extracted from the Reflectivity and Transverse Kerr signals measured both under SPP excitation (Kretschmann configuration) by means of the formalism detailed in ref. [2]. In Fig 2 we present in symbols the experimentally obtained modulation as a function of the Fe interlayer thickness for both series of samples. As it can be seen, $\Delta k/k$ increases with Fe interlayer thickness for both series of samples, with systematically larger values for the PLD samples, specially for Fe thickness above 2.5 nm, whereas the observed modulation is similar for both series below this value. Besides, experimental values are in agreement with the simulated ($\Delta k/k)_{SPP}$ (lines) using the Transfer Matrix Method and the actual MO constants from 6 nm Fe layers of both PLD and MBE sets of samples. The most relevant result is the magnitude of the SPP wavevector modulation obtained in the PLD series, which doubles that measured in the MBE ones for the samples having a Fe thickness above 2.5 nm. This difference is ascribable to the reduced effective MO constants of the Fe interlayer for the MBE series. This reduction of the effective MO constant can be mainly explained in two ways. On the one hand, a system with a rough interface can be optically considered as an effective medium composed by Fe and Au, and therefore with effective MO constants lower than those of bulk Fe. On the other hand, a purely interfacial effect where the properties of the Fe and Au atoms at this interface are different from bulk; structures with rough interfaces, and as a consequence of it with a larger interfacial area than equivalent structures with sharper interfaces, would exhibit reduced MO constants as it has actually been reported. In our specific case, this would explain the reduced SPP

wavevector modulation in the MBE samples, with rougher interface, with respect to the PLD ones. The use of deposition techniques that allow fabricating ultraflat magneto-plasmonic structures will facilitate obtaining novel devices whose plasmonic properties will be largely modulated by the application of a magnetic field.

References

[1] J. B. González-Díaz *et al.*, Phys. Rev. B, **76** (2007) 153402.
[2] E. Ferreiro *et al.*, IEEE Trans. Magn. **44**, 3303 (2008).
[3] E. Ferreiro-Vila *et al.*, Phys. Rev. B, **80** (2009)125132.
[4] P.Nagpal et al., Science, **325** (2009) 594-597.
[5] X.Zhu *et al.*, Advanced Materials, **22** (2010) 4345-4349.

Figures
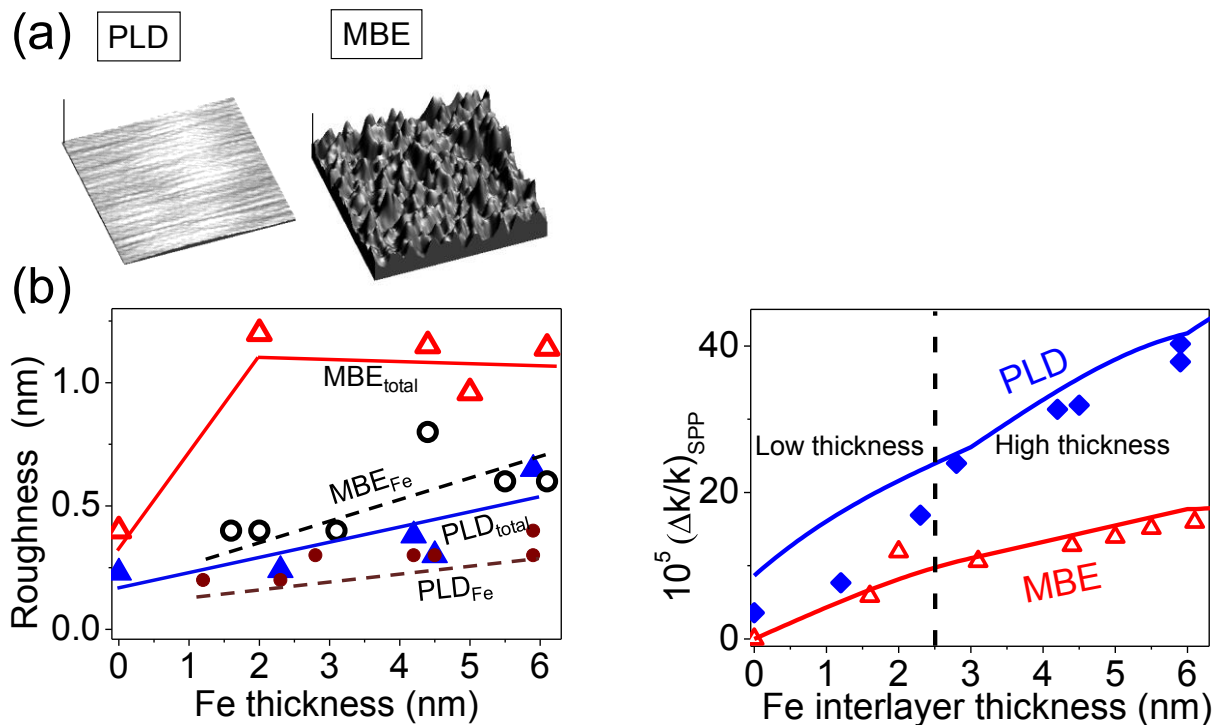
Figure 1: (a) AFM images for representative 4.5 nm and 5 nm Fe thickness of the PLD (left column) and MBE (right column) structures respectively. The AFM images have the same scale (7 nm vertical and 400 nm lateral). (b) Evolution of the surface (triangles) and Fe interlayer (circles) roughness, measured by AFM and XRR, respectively, with the Fe interlayer thickness for PLD (full symbols) and MBE (empty symbols) structures.

Figure 2: In the two remarked low (<2.5nmFe) and high (>2.5nmFe) thickness regions, Fe interlayer dependence of experimentally (symbols) and simulated (continuous lines) ($\Delta k/k)_{SPP}$ with actual MO constants from PLD (diamonds) and MBE (triangles) sets are shown.

Second Harmonic Generation in Hybrid Nanostructured Sol-Gel SiO$_2$:DR1 films

Alfredo Franco[1], Omar Torres-Mendieta[1], J. A. García-Macedo[1]

[1]Departamento de Estado Sólido, Instituto de Física, Universidad Nacional Autónoma de México,
México D.F. 04510
alfredofranco@fisica.unam.mx

To control the long-range order at nanometric level in hybrid films can improve their second-order non-linear optical properties[1]. Amorphous sol-gel SiO$_2$ films doped with dipolar chromophores have been subject of research for a long time due to their potential photonic applications[2], but the effects of nanostructures in the films have not been completely studied yet[3]. We synthesized SiO$_2$ films doped with the well known dipolar chromophore Disperse Red 1 (DR1). The films were synthesized by the sol-gel method, they were deposited on microscope slides by spin-coating technique and the chromophores were non-centrosymmetrically oriented by means of a Corona poling field. The films were bottom-up nanostructured through the use of ionic and neutral surfactants. The different kinds of nanostructures present in the films were determined by means of X-ray diffraction (XRD). The lattice parameter of all the nanostructures were in the range of 2.26 nm and 3.89 nm. The second-order non-linear optical properties of the films were mainly studied in resonance by transmission second harmonic generation, but the orientation of the chromophores inside the films was studied too by UV-vis spectroscopy. The second order parameter and the second harmonic generation intensity were studied for each sample as function of the poling time at three different temperatures: 80°C, 100°C and 120°C. The stability in the orientation of the chromophores was also studied at the same three different temperatures. The results were compared to those obtained in analogue films made with PolyMethylMetacrylate (PMMA) as the matrix of the films. It was found that some SiO$_2$:DR1 nanostructured films were able to generate a second harmonic signal even larger than that signal generated by SiO$_2$:DR1 amorphous films or by PMMA:DR1 amorphous films. Figure 1 shows the second harmonic generation signal of the films at 120°C as function of the incidence angle of the fundamental beam of light.

References

[1] Boyd R. W., Sipe J. E., J. Opt. Soc. Am. B, **11** (1994) 297.
[2] Chaumel F., Jiang H., Kakkar A., Chem. Mater., **13** (2001) 3389.
[3] García-Macedo J. A., Franco A., Valverde-Aguilar G., Aguilar-Gutiérrez C., J. Nanoresearch, **5** (2009) 135.

Figures
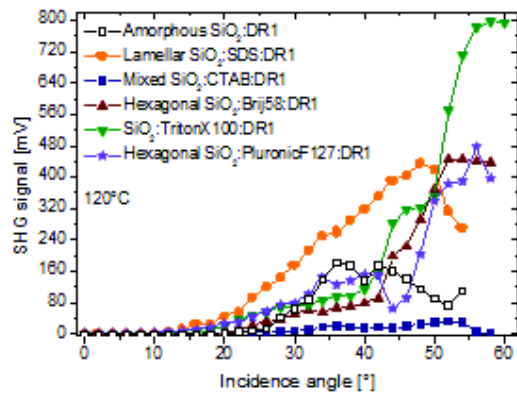
Second Harmonic Generation signal of the amorphous and nanostructured sol-gel SiO_2:DR1 hybrid films as function of the incidence angle of the fundamental beam of light.

Non-linear optical response of plate-like titanate-based nanoparticles in the region of fundamental absorption

Gorokhovsky A.V., Zimnyakov D.A., Ushakova O.V., Tretyachenko E.V., Pravdin A.B., Kudryashova A.

Saratov State Technical University, Saratov, Russia
algo54@mail.ru

The development of highly effective nonlinear optical (NLO) and optical limiting (OL) materials for application in protection from strong laser radiation is urgent [1]. Oxide semiconductors with high dielectric constants are good candidates for NLO and OL applications [2, 3]. Some homogeneously translucent titanate nanobelt suspensions demonstrated interesting physical and chemical properties due to strongly anisotropic structure different from those of the corresponding bulk material and those of isotropic nanoparticles. Such samples display remarkable NLO and OL effects at 532 nm, originating from nonlinear scattering [1].

This research is related to the NLO response of the potassium titanate nanoparticles characterized with plate-like shape as well as their aggregated forms. The NLO properties of the titanate suspensions were investigated in the region of fundamental absorption band using the Z-scan technique with open aperture at 337 nm and measurements of extinction spectra in UV and visible regions (300-600 nm). Various potassium titanate systems based on amorphous $K_2O \cdot 4.2TiO_2$ were examined. The parent potassium polytitanate was produced by molten-salt synthesis with the treatment of TiO_2 particles in the molten mixtures of KNO_3 and KOH at 500 ^{o}C [4]. Further, potassium polytitanate particles were ultrasonically dispersed in distilled water and treated with different cationic and non-ionic surfactants to obtain the suspensions characterized with different particles size distribution. The NLO response of the two suspensions was investigated: 1) consisted of single platy potassium titanate particles (effective diameter of 158 nm and thickness of 28 nm); 2) consisted of aggregated particles with the effective diameter of 1.93 μm.

The aqueous dispersions of pure TiO_2 (anatase) nanoparticles (25 nm) and colloidal Ag nanoparticles (40 nm) were also examined to compare non-linear optical response.

Z-scan measurements with open aperture were carried out with nitrogen laser radiation (λ=337 nm, average output power 40 mW, pulse duration 10 ns, repetition rate 1 kHz). The focal length of the used lens (fused silica) was equal to 30 mm, which gave the waist diameter and length in our Z-scan system equal to 6.5 μm and 390 μm, respectively. The peak value of power density of laser radiation was equal to $1.0 \cdot 10^{12}$ W/cm^2 approximately. The wavelength used corresponds to the spectral region of fundamental absorption of the wide variety of titanate-based systems.

It was shown that Ag and titanate-based systems exhibited different character of non-linearity. The extinction of Ag nanoparticles, for which a surface plasmon resonance near 400 nm is characteristical, falls down with a power density increasing. This phenomenon is obviously caused by positive non-linear absorption at the edge of surface-plasmon resonance [5-6].

At the same time, all the studied titanate samples exhibit the decreasing extinction with a power density increasing for the probe light (optical bleaching). For titanate-based nanoparticles the non-linear extinction can be approximated by the following relationship [7]:

$$\mu(I) = \mu_0 / \left[1 + (I/I_{sat})^{\beta_1} \right]^{\beta_2}, \qquad (1)$$

where μ_0 is the "base-line" for the extinction coefficient (evaluated, e.g., from spectral measurements at low intensities of the probe light; I_{sat} is the characteristic value of saturation intensity; β_1, β_2 are the dimensionless parameters, which are determined by predominating type of the optical bleaching mechanism. It was noted that, besides the non-linear absorption, the non-linear scattering also can contribute to optical bleaching near the fundamental absorption maximum.

The results of comparative analysis of phenomenological parameters I_{sat}, β_1, β_2 for the examined titanate-based systems are presented; the potential of their application for characterization of dispersed nanomaterials with specific optical properties (e.g., photocatalysts, dye-doped random media with optical gain, etc.) are discussed.

References

[1] M.Feng, H.Zhan, L.Miao, Nanotechnology, **21** (2010) 185707.

[2] D.Y.Guan, Z.H.Chen, Y.L.Zhou, K.J.Jin, G.Z.Yang, Appl. Phys. Lett., **88 (**2006) 111911.

[3] L.Irimpan, A.Deepthy, B.Krishnan, V.P.N.Nampoori, P.Radhakrishnan, Appl. Phys. B, **90** (2008) 547.

[4] T.Sanchez-Monjaras, A.V.Gorokhovsky, J.I.Escalante-Garcia., J.Am.Ceram.Soc., **91** (2008) 3058.

[5] L.Polavarapu, Q.H.Xu, M.S.Dhoni, W.Ji, Appl. Phys. Lett., **92** (2008) 263110.

[6] J.Wang, W.Blau, J. Opt. A: Pure Appl. Opt., **11** (2009) 024001.

[7] R.A.Ganeev, T.Usmanov, Quantum Electronics (Rus), **37** (2007) 605.

Figure
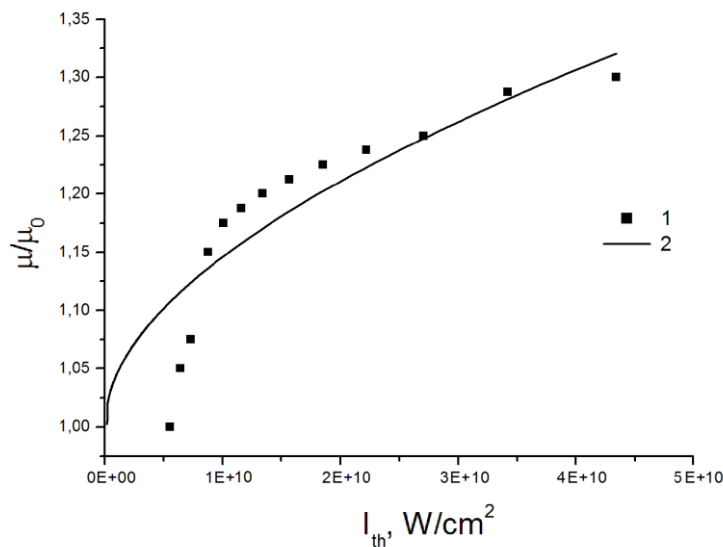
Experimental (1) and theoretical (2, Eq. 1) data on the normalized extinction coefficient μ/μ_0 versus the probe light intensity I_{th}. (for 2: $\beta_1 = 0.5, \beta_2 = 3.2$, $I_{sat} = 5.26\times10^{12}$ W/cm^2.

Nonreciprocal transmission through 2D magneto-photonic crystal

L. Halagacka[1,2], M. Vanwolleghem[1], K. Postava[2], J. Pistora[2], B. Dagens[1]

[1]Institut d'Electronique Fondamentale, UMR CNRS 8622, Universite Paris-Sud, Orsay, France

[2]Department of Physics and Regional Materials Science and Technology Centre,
Technical University of Ostrava, 708 33 Ostrava, Czech Republic

Lukas.halagacka@u-psud.fr, mathias.vanwolleghem@u-psud.fr,

kamil.postava@vsb.cz

A combination of unique magneto-optic (MO) non-reciprocity and photonic band gap in periodic structures is promising for efficient enhancement of optical isolation [1,2]. One very interesting concept that appears by combining magneto-optics and photonic crystal (PhC) effects is the possibility to obtain one-way band gaps [3]. We have recently theoretically proven the existence of such unidirectional regimes for TE modes in 2D integrated uniformly transversely magnetized magneto-optic photonic crystals [1].

In this paper we model and optimize rectangular magnetophotonic crystal structure shown on Fig. 1. This precise motif symmetry with its purely rectangular features is perfectly adapted for RCWA modelling. Its Brillouin zone along with its irreducible part is given in Fig. 1. The right pane shows the impact of the symmetry reduction on the resulting isofrequency contours in the Brillouin zone. These have been calculated using a standard plane wave expansion technique taking into account the anisotropic nonreciprocal character of the permittivity [4]. The model uses transparent magneto-optic material in transverse geometry (Bismuth iron garnet (ε_{xx} = 6.25 and ε_{yz} = 0.1 i) at wavelength λ = 1300 nm). We have plotted a single isofrequency contour (reduced frequency f^* = 0.4545) of the second photonic band at a frequency halfway those of the now non-degenerate K and K points. As expected from the symmetry arguments elaborated in the left panel of the Figure, a local interior gap without inversion symmetry in the reciprocal space opens up. This makes for an extremely compact one-way mirror that can be used as for instance a novel integrated isolator.

Transmission through the finite magneto-photonic crystal was modeled using Rigorous Coupled Wave Analysis (RCWA). Optical field in the anisotropic structures containing a periodic grating can be on the basis of Bloch theorem expressed using a Fourier expansion into plane waves [5-7]. In the following we consider the structure with the period of Λ = 590.85 nm (f^* = Λ/λ = 0.4545), the angle of incidence φ = 17.94 (N_y = $n \sin \varphi$ = 0.693), and the filling factor of the air holes f = 0.4. In backward direction the transmission rapidly decreases (reach value 10^{-5} for 22 double periods of air holes), which corresponds to exponential decay of optical field and photonic bandgap behavior. However in forward transmission we obtain value of 30%, which can be more optimized. Figure 2 shows calculated field (the x-component of the magnetic field H_x) inside the structure. Left subplot shows the complete structure of 22 double-periods of air holes in forward and backward regime. Note that the color scale is logarithmic to visualize strong decrease of the field in backward direction. In the forward direction (structure is illuminated from the top) the optical field is amplified in the structure and the structure is partially transparent (orange color on the bottom). However, in backward direction (illumination from the bottom) the field is exponentially decreasing and the photonic structure block the transmission (blue color on the top). Right subplot shows a detail of the field distribution in the central area of the structure. It is clearly visible that the field is concentrated in between air holes.

References
[1] Vanwolleghem M, Checoury X, Smigaj W, Gralak B, Magdenko L, Postava K, Dagens B, Beauvillain P and
 Lourtioz J M 2009 Phys. Rev. B 80 121102(R)–1–4
[2] Inoue M, Fujikawa R, Baryshev A, Khanikaev A, Lim P B, Uchida H, Aktsipetrov O, Fedyanin A, Murzina
T and Granovsky A 2006 J. Phys. D 39 R151–R161
[3] Z. Yu, Z. Wang, and S. Fan, Appl. Phys. Lett. 90 (2007) 121133.
[4] Johnson S and Joannopoulos J 2001 Optics Express 8 173.
[5] Neviere M and Popov E Light Propagation in periodic media: Differential theory and design (Marcel Dekker) 2002.
[6] Li L 2003 J. Opt. A: Pure Appl. Opt. 5 345–355
[7] S Visnovsky 2006 Optics in magnetic multilayers and nanostructures (CRC Press, Taylor & Francis)

Figures
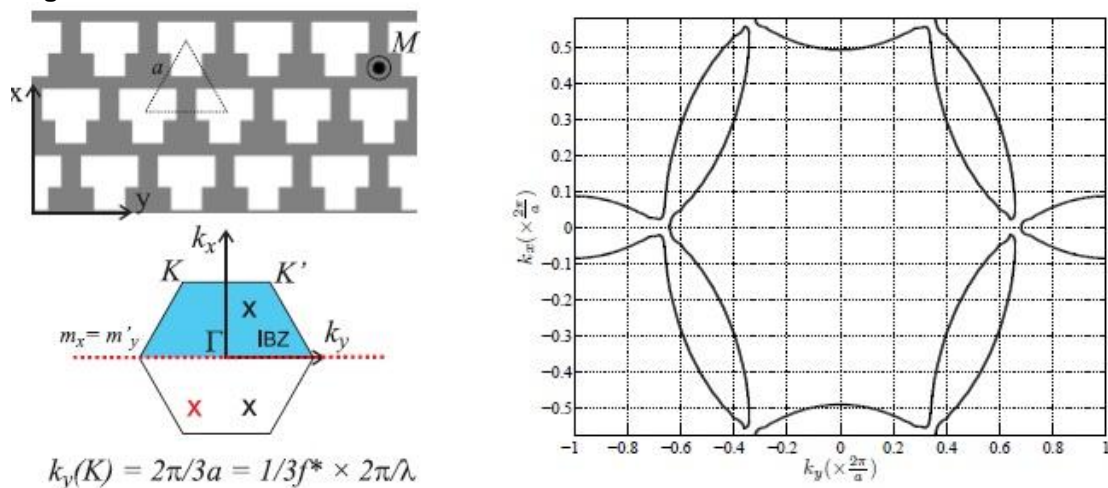
Figure 1. Scheme of photonics crystal structure in real and reciprocal space (left panel). The isofrequency contour at a reduced frequency of $f^* = \lambda = 0.4545$ of the uniformly magnetized MO PhC.
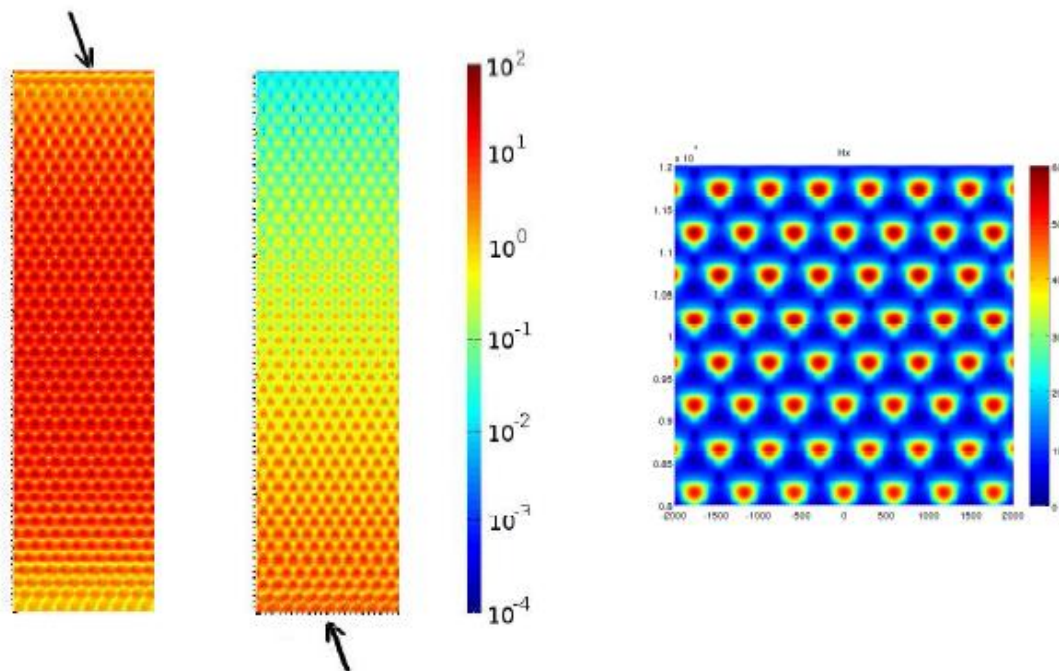

Figure 2. Field in the photonic-crystal structure

Optical properties of $Co_2FeAl_{0.4}Si_{0.6}$ and $Co_2FeGa_{0.5}Ge_{0.5}$ half-metallic Heusler compounds

Jaroslav Hamrle[1], Kamil Postava[1], David Hrabovský[1], Jaromír Pištora[1],
Enrique Vilanova[2], Gerhard Jakob[2]

[1]Department of Physics, VSB - Technical University of Ostrava, Czech Republic
[2]Institute of Physics, Mainz University, Germany
jaroslav.hamrle@vsb.cz

Commonly materials for plasmonic applications are gold and silver, as they provide low damping and negative value of real part of the permittivity. Nowadays, there is a need of new materials, which can provide both plasmonic excitations and magneto-optical activity. Co_2-based half metallic Heusler compounds are promising materials for this purpose, as there are several similarities in electronic band structure for exited states between gold, silver and the majority band of Co_2-based Heusler compounds. Namely in both cases the 3d-electrons are buried below the Fermi level and the electrons on the Fermi level are dominated by 4s electrons. Hence, for photon energies smaller than Heusler's minority band gap size (being typically 1eV), only majority electrons contribute to the photon absorption. Hence, for photon energies smaller than the minority electron gap size, the Heusler compounds are promising to provide similar optical properties as gold or silver. Furthermore, Co_2-based Heusler compounds have magneto-optical Kerr effect of similar strength as other 3d-ferromagnets (Fe, Co) as well as they provide high Curie temperature (up to 1000K) [1]. Hence, the half-metallic Heusler compounds are promising materials for magneto-plasmonic applications.

Within this contribution we present complex refractivity index, determined in range from mid-IR to near-UV, of half-metallic Heusler compounds $Co_2FeAl_{0.4}Si_{0.6}$ and $Co_2FeGa_{0.5}Ge_{0.5}$. Their composition optimizes half-metallic behavior [2], i.e. reducing contribution of minority band to the optical absorption for small (below 1eV) photon energies.

References

[1] S. Wurmehl, G.H. Fecher, H.C. Kandpal, V. Ksenofontov, C. Felser, Phys. Rev. B **72** (2005) 184434.
[2] I. Galanakis, Ph. Mavropoulos, J. Phys.: Condens. Matter **19** (2007) 315213

Optical reponse and Electron Energy Loss Spectroscopy of plasmonic systems by discrete dipoles approximation

Luc Henrard, Stéphane-Olivier Guillaume, Nicolas Geuquet

PMR, University of Namur (Belgium)
luc.henrard@fundp.ac.be

Plasmonic systems are mainly studied by optical spectroscopy and electron energy loss spectroscopy (EELS). We show here that the discrete dipoles approximation (DDA) is an efficient tool for numerical simulations and for the interpretation of experimental data obtained with both techniques [1], including for the effect interaction with a substrate and the coupling between nanoparticles.

Silver nanoparticles with triangular shape have been extensively study experimentally in the last year. The experimental size and aspect ratio dependance of their optical and EELS response is well described by DDA [2]. These modes have a symmetric charge distribution and result from the strong coupling of the upper and lower surface of the triangle. In other the explain the experimental results, we also explored the limit of very small and very large aspect ratio of particules and we analyzed the retardation effect on the mode excitation probability. We have also simulated the effects of the coupling between nanoparticles, with the substrate and with the environment.

Coupling between nanoparticles can result in induced transparency or Fano resonances. We report here on this effect with the example of noble metal nanorods as experimentally studied in [3] and of nanotriangle mentionned above (see Figure)

References

[1] N. Geuquet, L. Henrard. Ultramicroscopy, **110**, 1075 (2010)
[2] J. Nelayah et al., NanoLett **10,** 902 (2010)
[3] N. Verellen et al., NanoLett **10**, 2080 (2010)

Figure
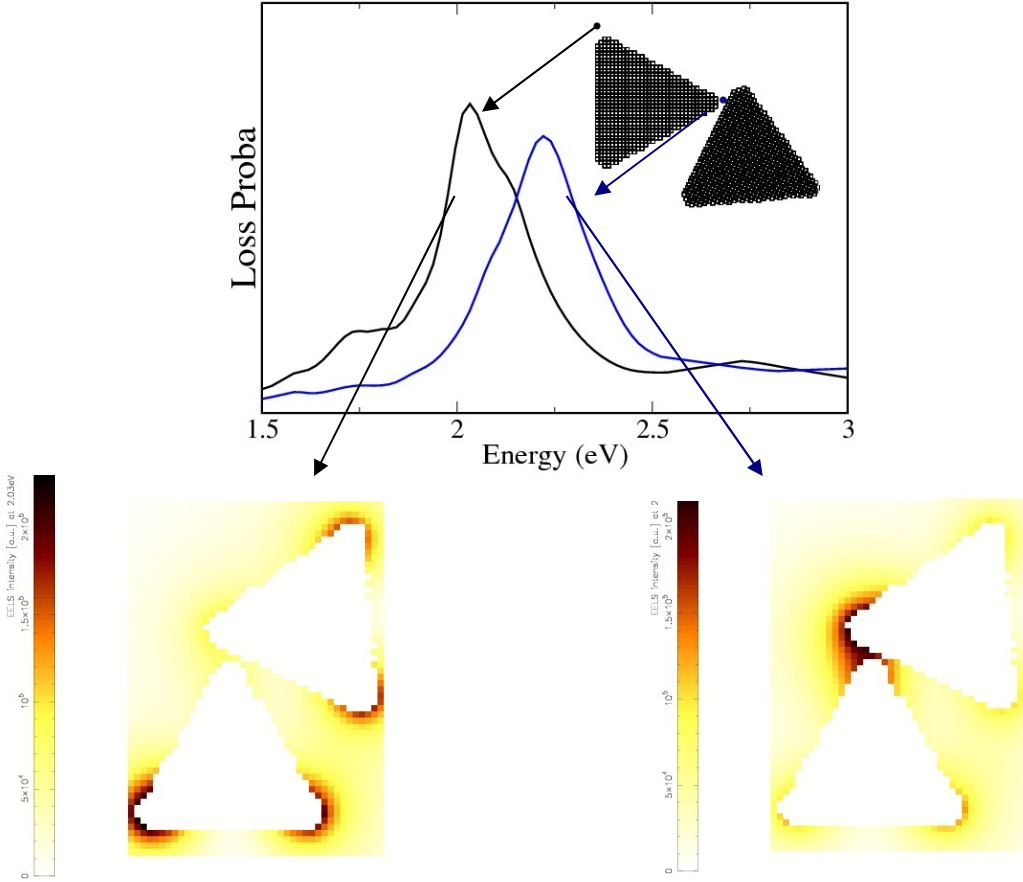
Caption :

2D-FDTD simulations of NSOM microscopy with magneto-optical capabilities

Aurelio Hierro-Rodriguez, Lucas Fernandez-Seivane, Jose Maria Alameda, Luis Manuel Alvarez-Prado

Departamento de Física, Universidad de Oviedo - CINN, Avd. Calvo Sotelo s/n 33007, Oviedo, Spain
hierroaurelio@uniovi.es

The study of magnetic nanostructures has a great interest from both, fundamental and technological point of view. At the nanoscale standard characterization tools can become uselessness and new kind of techniques are needed. Scanning probe microscopes (SPM) are very suitable in this length range for manipulation and characterization. The most popular SPM used to explore the magnetic properties is the MFM (Magnetic Force Microscopy) technique. The main problem of this microscopy system is the magnetic tip: it can strongly modify the magnetization configuration of the sample under study [1]. Another SMP technique called NSOM (Near field Scanning Optical Microscopy) has a great interest because it avoids this magnetization modification problem [2]. The NSOM with magneto-optical capabilities is a valuable technique to study the magnetic properties of the nanostructures as the conventional magneto-optical characterization does at larger scales [3].

Our group has been working with a M-O NSOM for the last years and the develop presented in this contribution is focused to understand certain aspects of our M-O NSOM experiments in order to get a deep understanding of the origin of the image formation. For this purpose we have developed a code based on the 2D-FDTD algorithm for the Maxwell equations [4]. As all possible materials need to be simulated with this algorithm we have had to extend the FDTD code to take into account metals with magneto-optical response. The main output of the code are the amplitude distributions over the simulation space of the Electric and Magnetic fields [Fig1]. With the 2D fields configuration we can simulate the Transversal Magneto Optical Kerr Effect (TMOKE) at the nanoscale [5].

First of all we have simulated the dependence of the magneto-optical response of a cobalt thin layer both uncoated and coated with a non magneto-optical media. The purpose of the last coating is to enhance the mageto-optical response from the Co layer at nanometric scale [6]. We have varied the magneto-optical response for different cobalt layer thickness and several values of the collector's angle. We have found a strong and non monotonic dependence of the magneto-optical response with the angle [Fig2].

In a second numerical experiment we have simulated a NSOM scanning over an inhomogeneous flat surface. The sample consists in a non magnetic matrix with cobalt stripes embedded inside. The objective of this experiment is to show the submicrometric resolution of the NSOM technique far above the Rayleigh's criterion.

References

[1] G Rodríguez-Rodríguez *et al J. Phys. D: Appl. Phys.* **40** (2007) 3051.
[2] LM Álvarez-Prado *et al Phys. Status Solidi A.* **203**, 6 (2006) 1425.
[3] C. Dehesa-Martínez *et al Phys. Rew. B.* **64** (2001) 024417.
[4] A. Taflove, S.C. Hagness, "Computational Electrodynamics, The Finite-Difference Time-Domain Method", Artech *House Antennas and Propagation Library* (2005).
[5] A.Hierro-Rodríguez *et al. ICM Poster reference Tu-B-7.6-04* (2009).
[6] Naser Qureshi *et al Nano Lett.***5**, 7 (2005) 1413.

**Figure1**

E_x　　　　E_y　　　　H_z
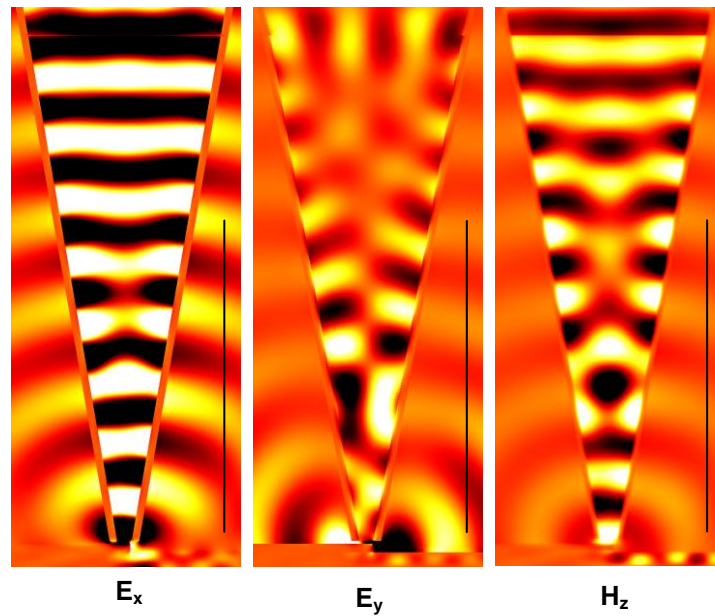
Fig.1 Amplitude distribution of the different Electric and Magnetic fields components over the simulation space. The black line at the right represents the collector's position.

Figure2
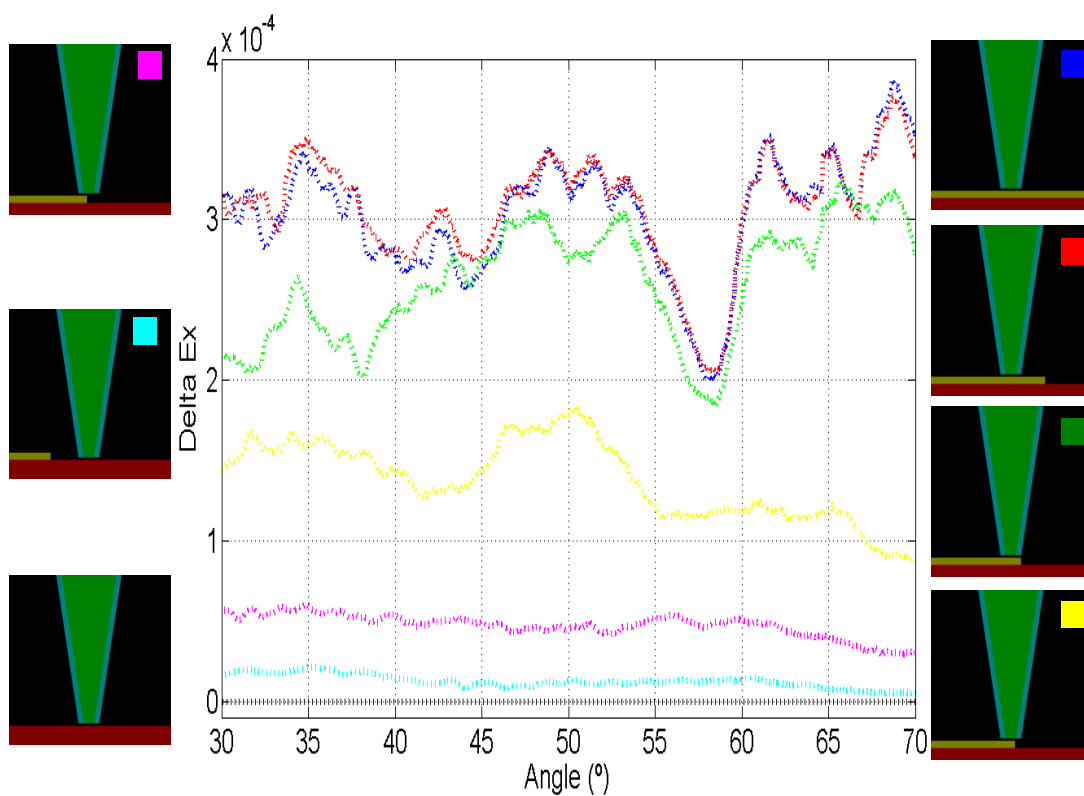
Fig.2 Dependence of the magneto-optical response measured as a function of the detector's angle for several position of the tip over the magneto-optical layer.

Fabrication of large-surface-area arrays of periodic nanostructures using azo-benzene containing polymer masks

Aleksandr Kravchenko[1], Andriy Shevchenko[1], Victor Ovchinnikov[2], Arri Priimagi[1], M. Kaivola[1]

[1] Department of Applied Physics, Aalto University, P.O. Box 13500, FI-00076 AALTO, Finland.
[2] Micronova Nanofabrication Centre, Aalto University, P.O. Box 13500, FI-00076 AALTO, Finland.

aleksandr.kravchenko@aalto.fi

During the last decades, arrays of periodic nanostructures have attracted an increasing interest of researchers and technologists. In particular, the fields of nanophotonics and optical metamaterials have undergone a significant progress. Traditional electron-beam and focused ion beam lithographies allow fabricating nanostructures with an unprecedented precision. However, their throughput is low and the fabrication of even a 1 cm^2-area pattern requires enormous time. On the other hand, modern optical lithography can as well be used for fabricating nanopatterns but on much larger surface areas in a much shorter time. For complicated patterns, high-precision photomasks still have to be fabricated by using the two above mentioned techniques, but for simple geometries, such as periodic nanostrip and nanopillar arrays, the exposure of a photoresist with interfering laser beams and a simple post-processing can yield rather high-quality periodic nanopatterns.

We report on the development of an optical interference lithography technique that is based on using azobenzene functionalized polymers (azo-polymers) instead of conventional photoresists. Starting with recording a surface relief grating in a thin polymeric film, spin-coated on a stack of intermediate layers on a silicon substrate, we finally perform reactive ion etching (RIE) of the substrate and obtain the desired structures. Large-area patterns (1cm^2 or so) with feature sizes on the order of 100 nm can be fabricated by using this fast and straightforward technique.

An advantage of this technique is the relative simplicity of obtaining surface relief gratings in azo-polymer films. The grating formation in the azo-polymers we use is governed not only by the irradiance, but also (and especially) by the polarization distribution within the illuminating interference pattern. Owing to this, grating inscriptions can be done under ordinary room illumination [1, 2]. Furthermore, no chemical development of the irradiated azo-polymer film is needed. We can use one or several subsequent illuminations of the azo-polymer film with different interference patterns to produce one- or two-dimensional patterns of the modulated film thickness. With more than two subsequent illuminations, rather complicated patterns can be obtained.

A thin layer of Al_2O_3 beneath the azo-polymer film is needed to obtain a hard mask from the inscribed surface relief grating in the polymer for etching silicon. An example of a hard mask obtained in this way is shown in Fig. 1. Figure 2 shows a mask prepared for fabricating a periodic nanopillar array; this mask is obtained by using two subsequent illuminations of the polymer film with two orthogonal interference fringe patterns. Further reactive ion etching yields either rounded (Fig. 3) or flat (Fig. 4) bottom profiles, depending on the processing parameters. Periodic nanopillar arrays with different sizes and bottom geometries are shown in Figs. 5 and 6. The silicon nanostrutures like these can be further processed, e.g., by covering them with metal for applications in plasmonics or nanoimprinting. They also can find applications in diffractive optics and surface enhanced Raman scattering spectroscopy, as well as in fabricating metamaterials and hydro- and oleophobic surfaces.

Figures
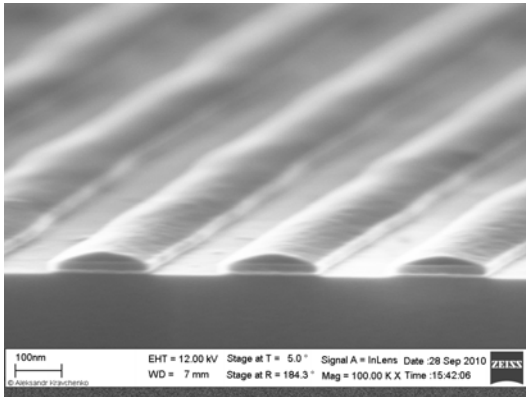
Figure 1. SEM image of a hard mask with remaining azo-polymer on the top of it after single exposure.
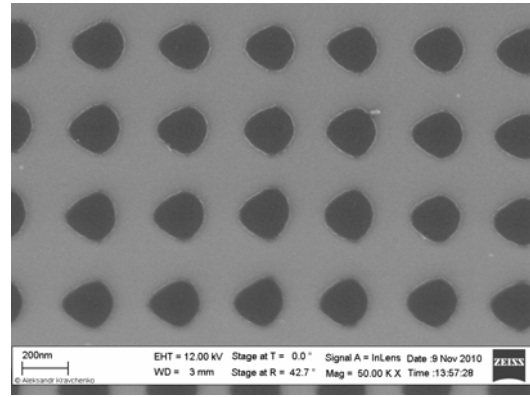
Figure 2. SEM image of a hard mask obtained by using two subsequent exposures of the azo-polymer.
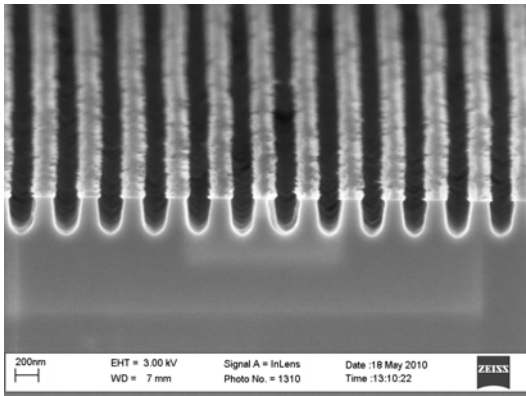
Figure 3. SEM image of a silicon substrate etched with a hard mask by inductively coupled plasma RIE (ICP-RIE).
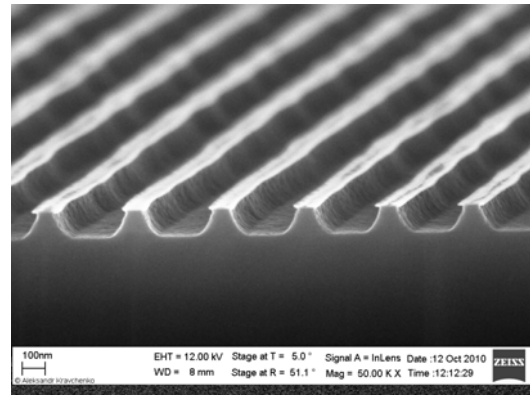
Figure 4. SEM image of a silicon substrate etched with a hard mask by conventional RIE.
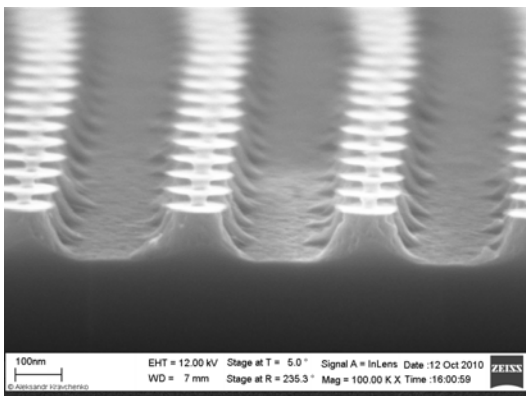
Figure 5. SEM image of a silicon nanopillar array etched with a hard mask by RIE.
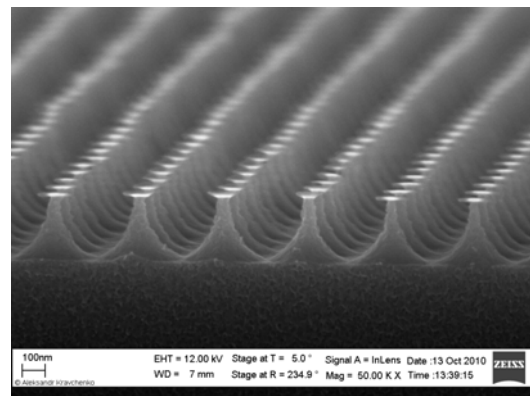
Figure 6. Silicon nanopillar array etched at different processing parameters compared to that in Fig. 5.

References

[1] N. K. Viswanathan, D.Y. Kim, S. Bian, J. Williams, W. Liu, et al., J. Mater. Chem., **9** (1999) 1941.
[2] C.J. Barrett, A.L. Natansohn, P.L. Rochon, J. Phys. Chem., **100** (1996) 8836.

Raman Pressure in Metallic Nano-Objects: a Picture of the Acousto-Plasmonic Interactions

Nicolas Large,[1,2,*] Lucien Saviot,[3] Adnen Mlayah,[2] and Javier Aizpurua[1]

[1] Centro Mixto de Física de Materiales CSIC-UPV/EHU and Donostia International Physics Center DIPC, Paseo Manuel de Lardizabal 4, 20018 San Sebastián, Spain
[2] Centre d'Elaboration de Matériaux et d'Etudes Structurales CEMES-CNRS, 29 Rue Jeanne Marvig, BP 94347, 31055 Toulouse, France
[3] Laboratoire Interdisciplinaire Carnot de Bourgogne, UMR 5209 CNRS-Université de Bourgogne, 9 Avenue A. Savary, BP 47870, 21078 Dijon, France
*Nicolas.Large@cemes.fr

Metal nano-objects and nano-structures have recently attracted much interest due to their possible use in new nanoscale optical devices (nano-antennas, negative refraction lenses, surface wave guides) [1], for biomedical application and for the control of the light emission, absorption and scattering (Raman-Brillouin and Rayleigh scattering) in surface-enhanced spectroscopies (SERS, SEIRA) [2]. We focus here on the interaction between localized surface plasmons (LSP) and acoustic vibrations of metallic nano-objects. The coupling between acoustic vibrations and LSP still presents several theoretical challenges to correctly interpret Raman-Brillouin and pump-probe experiments. Indeed, a lot of theoretical and experimental works have been devoted to the understanding of shape, size, matrix and ordering effects on the LSP whereas only few deal with their dynamical properties (coupling mechanisms to the acoustic vibrations and inelastic light scattering properties).

Methods

We present a theoretical study of the interactions between acoustic vibrations (Fig. 1a) and localized surface plasmons (Fig. 1b) [3,4]. In this work, we introduced the concept of Raman pressure for the first time. It is used as a theoretical tool for the interpretation of resonant Raman scattering mediated by surface plasmons in metallic nano-objects. This physical quantity represents the electromagnetic energy density excited by the Raman probe and modulated by acoustic vibrations of the nano-object (Fig. 1c). The Raman pressure is a local quantity and can be mapped in the near-field region, thus providing a clear picture of the interaction between LSP and acoustic vibrations which give rise to inelastic scattering measurable in the far-field. The surface plasmons/acoustic vibrations coupling is calculated using the Boundary Element Method [5,6].
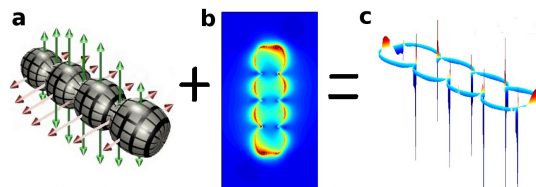
Figure: (a) Deformation of a silver nanocolumn induced by an acoustic vibration mode. (b) Near-field distribution associated with the LSP of the nanocolumn. (c) Modulation of the near-field by the acoustic vibration mode close to the nanocolumn surface.

Results

We show results on spherical nanoparticles, dimers, and nanocolumns. These results clearly show that for every particular acoustic vibration mode, the modulation of the LSP strongly depends on the size, the shape, the defects of the nano-object, and on the interaction between the nano-objects. The calculations/simulations allow us to understand and correctly interpret the activation of acoustic vibration modes and their relative Raman-Brillouin intensities.

References

[1] N. Large et al, *Phys. Rev. B* **82** (2010) 075310
[2] S. Tripathy et al, *Nano Lett.* ASAP
[3] G. Bachelier, and A. Mlayah, *Phys. Rev. B* **69** (2004) 205408
[4] N. Large et al, *Nano Lett*. **9** (2009) 3732
[5] F. J. García de Abajo et al, *Phys. Rev. Lett.* **80** (1998) 5180; *Phys. Rev. B* **65** (2002) 115418
[6] J. Aizpurua et al. *Phys. Rev. Lett.* **90** (2003) 057401.

Tailoring the optical response of self-assembled photonic-plasmonic crystals

Martín López-García[1], Juan F. Galisteo-López[1], Alvaro Blanco[1], Antonio García-Martín[2], Cefe López[1]

[1] Instituto de Ciencia de Materiales de Madrid, Cantoblanco, Madrid, Spain
galisteo@icmm.csic.es, mlopez@icmm.csic.es, ablanco@icmm.csic.es, cefe@icmm.csic.es
[2] Instituto de Microelectrónica de Madrid, Tres Cantos, Madrid, Spain

mlopez@icmm.csic.es

Tuning the optical response of both photonic and plasmonic devices as well as their hybrid structures is a challenging issue. Recently it has been shown that colloidal self-assembled photonic crystals deposited on metallic substrates can yield large field enhancements at well defined wavelengths depending mainly on the diameter of the spheres [1]. It has also been demonstrated that such hybrid modes are strongly dependent on the morphology of the samples, or ,for example, changes on the surrounding media refractive index, as large as those of the best performing plasmon resonances based sensors[2].

In this work we present a complete theoretical and experimental study on how the filling fraction can strongly modify the modes of hybrid photonic-plasmonic crystals working in the visible-NIR range. By continuously reducing the diameter of polystyrene spheres deposited on gold substrates while keeping the lattice constant unchanged, we will show that not just the modal position, but also the field confinement can be strongly modified [3]. Evidence on this modification is carried out by mean of normal incidence reflectance measurements. As a proof of principle for application, dye doped spheres emitting in the visible range have been treated on the same way in order to strongly modify the spontaneous emission. This method allows tuning of the spontaneous emission (both angular and spectroscopic) with a very simple process.

Finally, this system is compared to well known plasmonic and photonic tunable systems showing its potential in future applications as for example solar cell, organic light emitting devices or sensing.

References

[1] M. López-García, J.F. Galisteo-López, A. Blanco, J. Sánchez- arcos, C. López and A. García-Martín, *Small,* **6,** 1757 (2010)

[2] X. Yu, L. Shi, D. Han, J. Zi and P.V. Braun, *Advanced Functional Materials* **20**, 1-7, (2010).

[3] M. López-García, J. F. Galisteo-López, A. Blanco, A. Garcia-Martin and C. Lopez. , *Advanced Functional Materials* **20,** 4338 (2010).

Figures
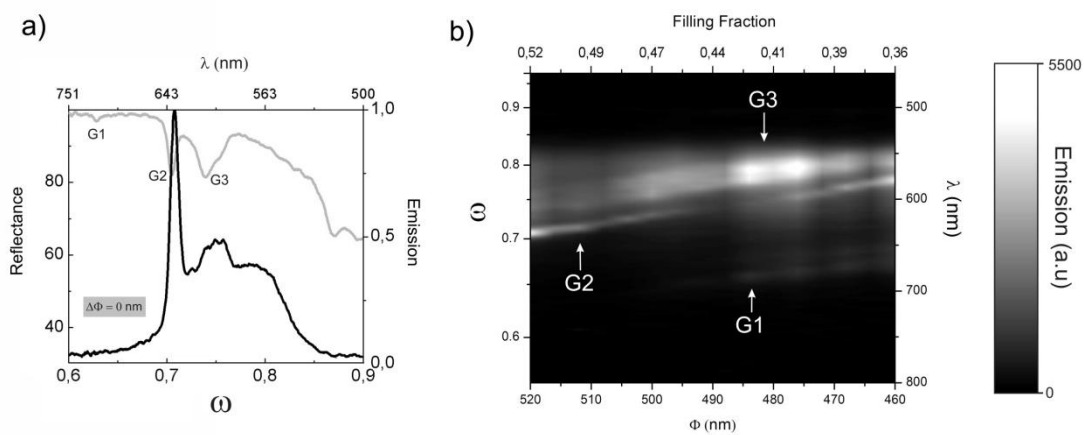
Figure 1. a) Normal incidence reflectance (grey) and emission (black) for close-packed lattice of red dye dopped PS 520 nm polystyrene spheres on gold substrate . b) Evolution of emission with filling fraction variation. G1, G2 and G3 are the best define modes shown as dips in reflectance in a).

Polarization and charge transfer resonances in wired patch-antenna arrays

Dana-Codruta MARINICA, Andrei G. Borisov

Institut des Sciences Moléculaires d'Orsay, Université Paris Sud - CNRS
Bat. 351, 91405 Orsay cedex, France
dana-codruta.marinica@u-psud.fr

We investigated theoretically light interaction with a freestanding structure of subwavelength thin rectangular gold posts arranged periodically in a 2D-lattice. The time-domain approach used is based on an efficient pseudo-spectral solver. The transmission response of the system shows a resonant behavior corresponding mainly to the excitation of localized plasmons of individual posts. When metallic wires interconnect the posts, besides polarization resonances of individual posts (Fig. a) and wires, we emphasized the appearance of resonances which correspond to charge transfer between neighboring metallic objects of the pattern (Fig. b). The dispersion of these resonances crosses the light line, leading to propagating bound states of surface plasmon polariton character.
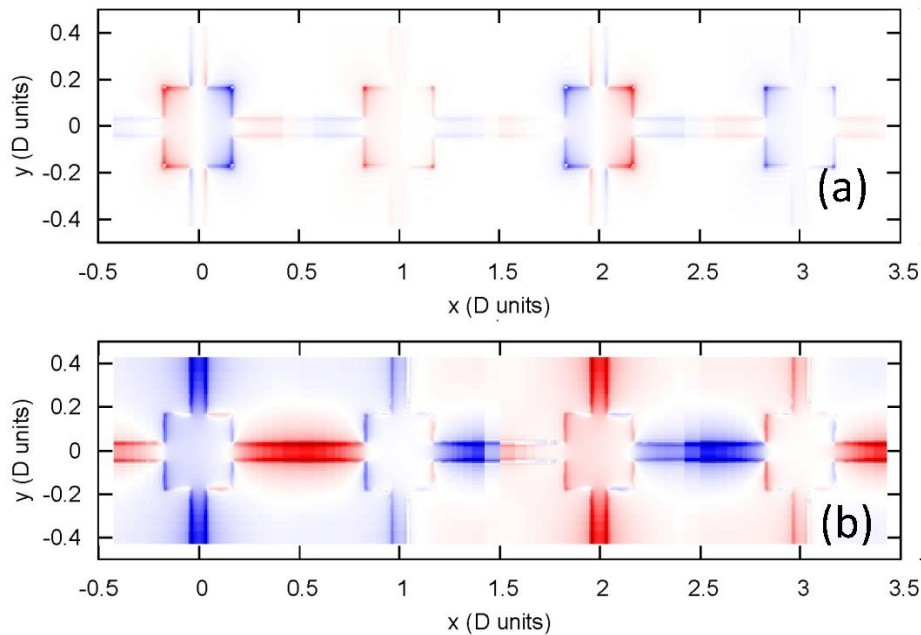
Figure *z-component of the electric field distribution at the resonance frequency in the vicinity of the surface structure for: a) a polarization resonance (λ=450nm) and b) a charge transfer resonance (λ=850nm). The period of the structure is D=300nm, the thickness of the posts and wires is 50nm; here the incident light wavevector component k_x=G/4, with G=2π/D.*

Spectral evolution of the SPP wavevector magnetic modulation in Au/Co/Au films

D. Martín-Becerra[‡,1], J. B. González-Díaz[1], V. V. Temnov[2], G. Armelles[1], T. Thomay[3],
A. Leitenstorfer[3], R. Bratschitsch[3], A. García-Martín[1], M. U. González[1]

[1]IMM-Instituto de Microelectrónica de Madrid (CNM-CSIC), Isaac Newton 8, PTM,
E-28760 Tres Cantos, Madrid, Spain.
[2]Department of Chemistry, Massachusetts Institute of Technology, Cambridge (MA), USA
[3]Department of Physics and Center for Applied Photonics, University of Konstanz, Germany
[‡]diana.martin@imm.cnm.csic.es

Surface plasmon polaritons (SPPs) are quasi-two-dimensional electromagnetic excitations that propagate along a dielectric-metal interface. They have field components decaying exponentially into both neighboring media, which makes them suitable for many possible applications, including miniaturized optical devices. For this reason, it is essential the development of "active" plasmonic configurations, which requires a system where we are able to manipulate plasmon properties with an external agent. Thereby, magnetic field seems a promising choice to play that role, since it is able to modify the dispersion relation of SPP at reasonable values and at a high switching speed [1]. In fact, when we apply the magnetic field, both the real and the imaginary part of the SPP wavevector k_{SP} are modified. This effect is related to the non-diagonal elements of the dielectric tensor, ε_{ij} that appear when applying a magnetic field. Those are too small for noble metals (the ones typically used in plasmonics), while for ferromagnetic metals (whose optical losses are however larger), they are much higher at easily achievable magnetic field magnitudes. Therefore a compromise can be achieved by using multilayers of noble and ferromagnetic metals [2, 3].

In the present work, we analyze the magnetic field induced SPP wavevector modulation (Δk) in Au/Co/Au films as a function of the wavelength and the position of the Co layer inside the trilayer.

The experimental analysis of the SPP wavevector modulation has been performed via surface plasmon interferometry with tilted slit-groove microinterferometers [4]. A sketch of a magneto-plasmonic interferometer is shown in Fig. 1. Illumination with a p-polarized laser beam at normal incidence results in the excitation of SPPs at the groove that propagate towards the slit, where they are reconverted back into free-space radiation (I_{SP}) and interfere with light directly transmitted through the slit (I_r). The total intensity collected from the slit is:

$$I_{DC} = I_r + I_{SP}e^{-2k^i_{SP}d} + 2\sqrt{I_{SP}}e^{-k^i_{SP}d}\sqrt{I_r}\cdot cos(k_{sp}{}^r\cdot d + \varphi_0),$$

where k^r_{SP} and k^i_{SP} are the real and imaginary part of the SPP wavevector respectively, φ_0 is an arbitrary phase, and d is the groove-slit distance.

When the light intensity transmitted through the slit is recorded by scanning a photodiode along the slit axis, a series of maxima and minima appears as a consequence of the different slit-groove distance for each slit position. To detect the magnetic modulation, we apply an external periodic magnetic field high enough to saturate the sample (about 20 mT) in the direction parallel to the slit axis. This generates a variation in the SPP wavevector, therefore shifting the interference pattern. Then, at each point of the slit, with a lock-in amplifier we measure the variation of intensity associated with this pattern shift, I_{MP}, which constitutes the magnetoplasmonic interferogram. Actually, when applying the magnetic field, both the real and the imaginary part of the SPP wavevector k_{SP} are modified and the I_{MP} signal can be expressed, up to a first order approximation, as:

$$I_{MP} = I(M) - I(-M) \approx (-2\cdot\Delta k_{sp}{}^r\cdot d)\sqrt{I_{SP}}e^{-k^i_{sp}d}\sqrt{I_r}\cdot sin(k_{sp}{}^r\cdot d + \varphi_0 + \Phi)\text{, with } \tan\Phi = \frac{\Delta k^i_{sp}}{\Delta k^r_{sp}}$$

Here Δk_{SP} represents the k_{SP} modulation with the sample magnetization and it is defined as Δk_{SP} =$k_{SP}(M)-k_{SP}(-M)$. As we can see in the equation, the modulation of k^r_{SP} (Δk^r_{SP}) is related to the amplitude of the magnetoplasmonic signal, while the modulation of k^i_{SP} (Δk^i_{SP}) induces a phase shift (Φ) between the optical and the magnetoplasmonic signal. We would like to notice here that for $\Delta k^i_{SP}=0$ the optical and magnetoplasmonic interferograms are shifted by exactly 90º due to the cosine and sine dependence of each magnitude, and according to our definition Φ is zero in that case.

Thus, through the comparison of both interferograms we are able to determine the modulation of both the real and imaginary part of k^r_{SP}. We have performed this analysis as a function of the wavelength and Co position. Figure 2 shows the spectral evolution of Δk^r_{SP} and Δk^i_{SP} for three different Co positions. As can be shown, Δk^r_{SP} decays exponentially as the position of the cobalt layer goes deeper in the trilayer, a behaviour that can be correlated with the exponential decay of the SPP field inside the metal [4, 5]. Regarding the wavelength dependence, Δk^r_{SP} decreases as the wavelength increases. This behaviour is related to the dispersion relation of the plasmon, which is associated with the electromagnetic field inside the metal layer. The higher the wavelength, the closer the plasmon is to the light line, and the more its electromagnetic field is spread on the dielectric. On the other hand, for lower wavelengths, the SPP electromagnetic field appears more confined at the interface, probing more inside the metal layer, where the magnetic activity lies.

References:

[1] R. F. Wallis, J. J. Brion, E. Burstein, and A. Hartstein, Phys. Rev. B **9** (1974) 3424.
[2] J. B. González-Díaz, *et al.* Phys. Rev. B **76** (2007) 153402.
[3] E. Ferreiro-Vila, *et al.* Phys. Rev. B **80** (2009) 125132.
[4] V. V. Temnov, *et al.* Nat. Photonics **4** (2010) 107.
[5] D. Martín-Becerra *et al., Appl. Phys. Lett.* **97**, 183114, (2010)

Figures:
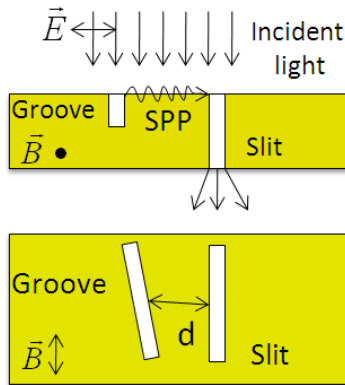
Figure 1: Sketch of the magneto-plasmonic micro-interferometer.
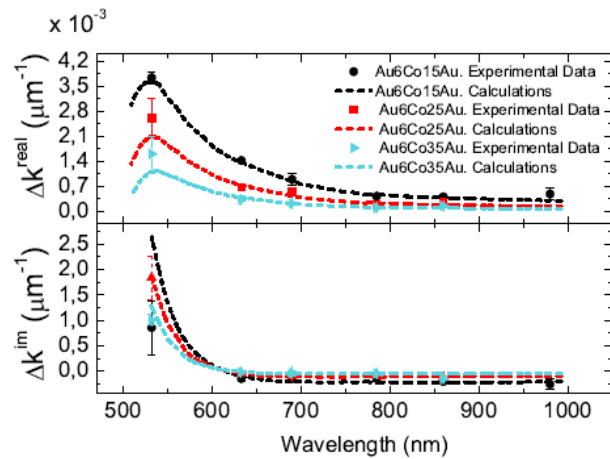

Figure 2: Spectral evolution of the magnetic modulation of real and imaginary part Δk^r_{SP} and Δk^i_{SP} the real part of k_{SP} with the position of the cobalt layer and the incident wavelength.

Modelling and realisation of PDMS microchannel to integrate in a nanostructured magneto-plasmonic gas and biosensor device

G.S. Masi [a,b], M.G. Manera [a], C. Martucci [a], P. Congedo[b], L. Vasanelli [b], R.Rella [a]

[a] *IMM-CNR Lecce, via per Monteroni, Lecce, 73100, Italy*
[b] Department of Innovation Engineering, University of Salento,
via per Monteroni, Lecce, 73100, Italy
gaetano.stefano.masi@gmail.com

Microfluidics provides the ability to analyze small sample volumes and reagents, which leads to lower assay costs as well as sample preparation automation. The integration of these existing techniques provides a number of advantages and challenges when combined with an optical detection platform, such as MOSPR (magneto-optical surface Plasmon resonance). In this work a discussion about recent advances in combining biomolecular microarrays, microfluidics and MOSPR biosensing is presented and its advantages are discussed.

Actually, microfluidic technologies are capable of controlling and transferring tiny quantities of liquids which allow chemical and biochemical assays to be integrated and carried out on a small scale. Such technologies provide to manipulate the fluids and improve the mixing or the separation phase or to increase the temperature of the fluid (some reactions needs high temperature) and reduce the time for analysis. The fabrication of microfluidics device is based on standard photolithography techniques for master realization [1,2].

In this work we have developed a single microfluidic channel for application in a magneto-optical surface plasmon resonance device (Fig.1). The typical dimension of the channel are: 100 μm x 30μm x 1,5 cm (width, height, length). Before the realisation of the device the performances of the system has been evaluated by computational simulations with finite elements analysis.

References

[1] T.M. Squires, S.R. Quake, Rev. Mod. Phys., 77, 2005, 977.
[2] G.M. Whitesides, Nature, 422, 2006, 368.
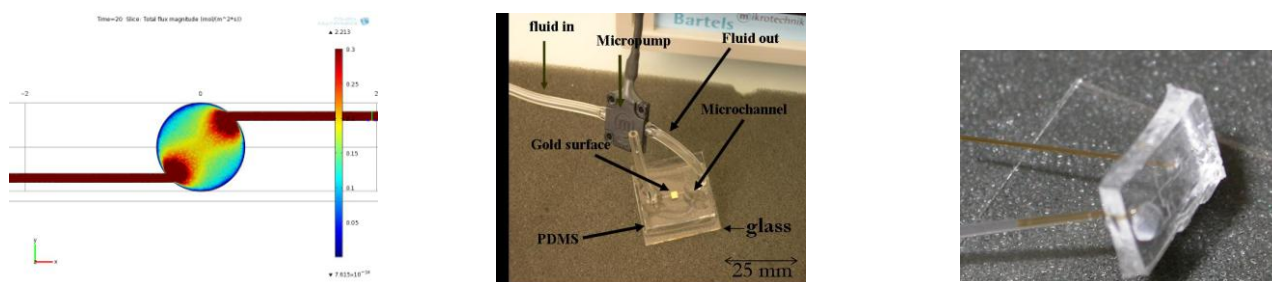
Fig.1: Typical single channel MOSPR microfluidic device

OLIGOPEROXIDE BASED FUNCTIONAL LUMINESCENT NANOCOMPOSITES

N. Mitina[1], S. Meshkova[2], Z. Topilova[2], A. Voloshinovskii[3], R. Stoika[4], A. Zaichenko[1]

[1]Lviv Polytechnic National University, 12 S. Bandera St., Lviv, 79013, Ukraine;
[2]A. Bogatsky Physico-Chemical Institute NASU, 65080 Odessa, Ukraine;
[3]I. Franko Lviv National University, 8 Kyryla i Mefodiya St, Lviv, 79005, Ukraine
[4]Institute of Cell Biology of NASU, 14/16 Drahomanov Str., Lviv, 79005, Ukraine

nem@polynet.lviv.ua

The intensive development of contemporary biotechnology, biochemistry and medicine is based on the purposeful synthesis and application of mineral, polymeric and hybrid nanoparticles with predetermined size and controlled functional properties.

Molecular design and controlled synthesis of novel oligoperoxide based surface-active block, comb-like functional oligoelectrolytes and nanogels of controlled size distribution, porosity, functionality, and biocompatibility were proposed and studied. These substances are capable to form poly dentate coordinating complexes of lanthanide (Ln) (Eu, Pr, Ce, Tb) possessing luminescent ability in wide wavelength range. Other developed route of the obtaining water based nanosized luminescent functional composites consists in encapsulation of low molecular weight organic complexes, for instance, $Eu(TTA)3TFFO$, $Yb(TTA)3$, $Tb(AA)3$, where TTA - thenoyltrifluoroacetone, TFFO - triphenyl phosphineoxide, AA - acetyl acetone, using various techniques, namely:

1) formation of intermolecular complexes of oligoelectrolyte surfactant and low molecular lanthanide - containing substances;
2) solubilization of water insoluble lanthanide - containing complexes in hydrophobic zones of micelle-like structures or porous formed by surface-active oligoelectrolytes or nanogels in water;
3) nanoencapsulation of water insoluble lanthanide - containing complexes in polymeric nanoparticles via multi-stage water dispersion polymerization initiated with oligoperoxide metal complexes.

We have developed also the promising techniques of the synthesis of luminescent (fluorescent), magneto-responsible, X-ray detectable functional nanoscale vehicles for enzymes, proteins, drugs and markers of biological objects including pathological and tumor cells. There are monodisperse polymeric, ferric oxide, gold and silver particles with predetermined size, charge, functionality. Novel functional nanocomposites consist of polymeric including fluorine-containing or siliceous, Fe_3O_4, Fe_2O_3, Pd, silver, gold core and functional oligoelectrolyte based shell. The shell and/or core of luminescent or X-ray detectable markers contain phosphor of organic or mineral nature including complexes of rare earth elements. The size of polymer nanoparticles is in the range of 30÷300nm. The size of hybrid polymer-mineral nanoparticles is 5÷30nm. Functional hybrid nanoparticles contain functional shell, which provides biological compatibility and ability to dispersion in physiological solution as well as to interaction with cell membranes of pathological including tumor cells. These carriers have been successfully tested as magnetic and luminescent markers for detection, separation and killing pathological cells as well as for the study of phagocytosis by granulocytes of human blood.

As a result stable water systems consisting of the functional carrier including luminescent substances in the core, porous or micelle hydrophobic zones of polymer nanoparticles (70-300 nm), nanogels (100-700 nm) or micelle-like structures (50-200 nm), respectively are formed (Fig.). Besides -COOH, -S03H, -SH, -N(CH3)2 groups, the developed nanocomposites contain desired amount of ditertiary peroxide fragments capable to initiate grafting functional reactive spacers of desired length for covalent attachment of cell recognizing vectors of natural origin (lectins, antibodies etc.). The polymeric nanogels were filled with antimicrobial or anticancer drugs including water insoluble ones also.

Functional nanocomposites including nanogels that can bind specific proteins and interact with cell membrane, particularly with rte apoptotic cells, bacteria and fungi were successfully examined as luminescent markers and drug carriers.
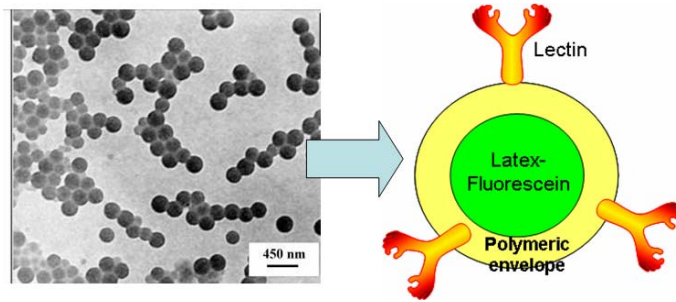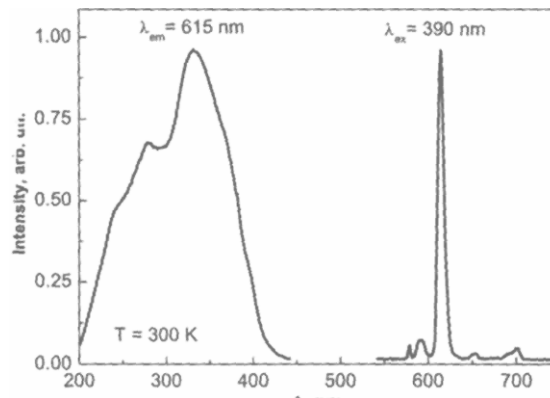
Figure 1

Figure 2

Figure 1

TEM-image of functional polystyrene particles containing fluorescein in the core and the scheme of obtaining lectin-particle conjugate.

Figure 2

Emission (excited at 390 nm) and luminescence excitation (for 615 nm emission) spectra ofEu (TTA)i in the micelle hydrophobic zones of polymer nanoparticles

Plasmonics in the UV: Gallium and Aluminium nanoparticles. A comparison with Gold and Silver

B. García-Cueto, D. Ortiz, F. González and F. Moreno.

Group of Optics. Department of Applied Physics. University of Cantabria. 39005 Santander (Spain)
morenof@unican.es

During the last fifteen years, metallic nanoparticles have attracted the attention of many researchers due to the double possibility of localizing light in nanometric dimensions and getting high intensity local fields (excitation of Localized Plasmon Resonances, LPR's). Their use as plasmonic sensors has found many nanotechnology applications in biosensing [1], nanocircuitry [2], spectroscopy [3], photovoltaic devices [4] and microscopy [5]. Typical plasmonic sensor tools are made of Silver and Gold. Nanoparticles made of these metals show LPR's in the VIS-NIR range [6]. Because of the enormous impact of these tools in biosensing applications and also because many biological molecules and matter respond in the UV part of the spectrum [7], it is necessary to investigate and design plasmonic tools able to work at shorter wavelengths. Aluminium [8] and Gallium [9] have recently shown to be two possible candidates to cover this spectral range. The purpose of this contribution is to show a numerical comparison through the DDA method (Discrete Dipole Approximation) between these metals and the conventional Gold and Silver when nanoparticles made of these materials are located on dielectric substrates. The hemispherical particle shape will be taken as a basic geometrical model to develop this comparison, in part stimulated by the experiments performed in [9].

Figure 1 left shows the real part of dielectric constant of Aluminium, Gallium, Gold and Silver. The spectral response of spherical isolated nanoparticles (R=20nm) are plotted in Figure 1 right, where we show the normalized spectral absorption efficiency for each metal. As can be seen, Gold and Silver have a plasmonic resonance in the visible and near-ultraviolet zone, respectively; while Gallium presents a peak in 3.5 eV and the Plasmon resonance of Aluminium is outside the range represented (UV zone).

In Figure 2 we represent the spectral absorption efficiency of a hemispherical particle (R=20nm) on a sapphire substrate. Our model takes into account two factors: the incident polarization and the angle of incidence. We simulated two polarization states: S and P (perpendicular and parallel components to incidence plane, respectively). A comparison with the isolated particle case shows both the effect of the substrate and particle shape on the positions and structure of the spectra. Particularly notorious is the big shift undergone by the Al resonance due to the presence of the substrate. Concerning the resonant spectral position for each metal, Gold and Silver are in 2.1eV (590nm) and 2.6eV (476nm) respectively, i.e. in visible range. On the other hand, Aluminium has a LPR in 3.9eV(318nm) and Gallium presents two clear resonances, one in 2.5eV (496nm) associated to S polarization and other in 4.7eV (264nm) associated to P polarization. The choice of incidence angle is also important. At normal incidence S and P polarizations cannot be distinguished (both components are parallel to the substrate). However, for angles different to normal, P component (parallel to the incidence plane and perpendicular to the substrate) increases, leading to changes in her spectral response.

References

[1] Romain Quidant, Mark Kreuzer, Nature Nanotechnology, **5** (2010) 762.
[2] N. Engheta, Science, **317** (2007) 1698.
[3] R.G. Freeman, K.C. Grabar, K.J. Allison, R.M. Bright, J.A. Davis, A.P. Guthrie, M.B.Hommer, M.A. Jackson, P.C. Smith, D.G. Walter, and M.J. Natan, Science **267** (1995) 1629.
[4] H.A. Atwater, A. Polman, Nat. Materials **9** (2010), 205.
[5] T. Kalkbrenner, U. Hakanson, A. Schädle, S. Burger, C. Henkel, V. Sandoghdar, Phys. Rev. Lett. **95** (2005) 200801.

[6] K. Lance Kelly, Eduardo Coronado, Lin Lin Zhao, and George C. Schatz, Journal Of Physical Chemistry B **107** (2003) 668.

[7] Itai Lieberman, Gabriel Shemer, Tcipi Fried, Edward M. Kosower, and Gil Markovich, Angewandte Chemie **120** (2008) 4933.

[8] Mustafa H Chowdhury, Krishanu Ray, Stephen K Gray, James Pond, and Joseph R Lakowicz, Analytical Chemistry **81** (2009) 1397-403.

[9] P.C. Wu, T. Kim, A.S. Brown, M. Losurdo, G. Bruno and H.O. Everitt, Appl. Phys. Lett. **90** (2007) 103119.

Figures
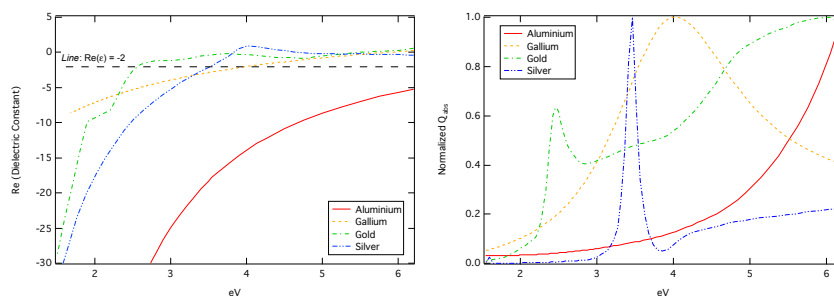
Figure 1. *Left*: Comparison of the real part of dielectric constant for Aluminium, Gallium, Gold and Silver. In addition, it includes a line-mark of Re(ε) = -2. *Right*: DDA calculations of the normalized absorption efficiency (Q_{abs}) of isolated spheres (R=20 nm) made of Aluminium, Gallium, Gold and Silver respectively.
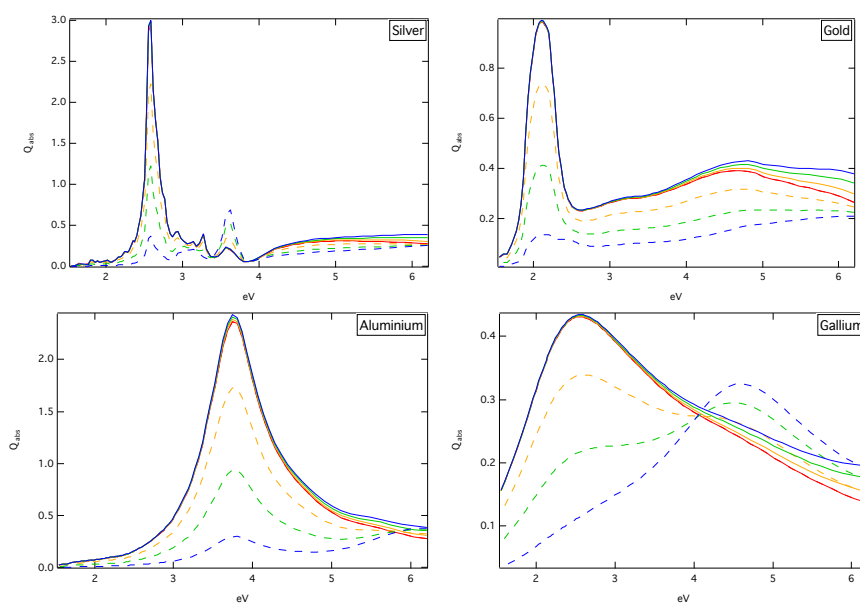
Figure 2. DDA calculations of the absorption efficiency (Q_{abs}) of Aluminium, Gallium, Gold and Silver hemispherical nanoparticles (radius 20nm) on Sapphire substrate. P (dashed lines) and S (solid lines) incident polarization are shown for different angles of incidence: 0º (red lines), 30º (orange lines), 50º (green lines) and 70º (blue lines). Silver and Gold have LPR's in the visible zone (1.50-3.10 eV), Aluminium and Gallium in UV zone (>3.10 eV).

Acknowledgements

Investigation of non-reciprocal magneto-plasmonic waveguides for compact integrated optical isolators on silicon

Patrick Nedel and **Ségolène Olivier**

CEA-Leti, Minatec Campus, 17 rue des Martyrs, 38054 Grenoble Cedex 9, France
patrick.nedel@cea.fr; segolene.olivier@cea.fr

Introduction

Creating compact on-chip non-reciprocal components is of fundamental interest in integrated optics at telecom wavelength of 1.55 µm. Today a lot of integrated functions are available commercially such as lasers, couplers, filters, modulators, but there is a lack of non-reciprocal integrated functions like optical isolators and circulators. Commercial optical isolators are expensive bulk components operating in the Faraday configuration (with a longitudinal external magnetic field) not suited for integration. They are based on garnet magneto-optical material which has very low absorption at telecom wavelength.

Integrated optical isolators based on Mach-Zehnder designs in the Kerr configuration (i.e. with a transverse external magnetic field with respect to the propagation direction) have been proposed using also garnet as magneto-optical material [1]. There have been a large number of demonstrations of stand-alone optical isolators and circulators based on iron garnet waveguides, but they have not become commercial devices due to their lack of compatibility with InP or Si-based photonic platforms. Up to now, the expensive technique of wafer bonding is necessary to combine garnets with InP- or Si-based semiconductor materials [2].

Another approach is the use a ferromagnetic material like FeCo which exhibits a much larger magneto-optical activity, thus leading to more compact devices. Moreover FeCo is fully compatible with InP or Silicon chips. Recently, FeCo has been used in an integrated laser system with direct isolation operating at 1.3 µm wavelength, demonstrating isolation ratio close to 100 dB/cm [3].

As a metal, FeCo can sustain surface plasmon polaritons. In this paper, we study so-called magneto-plasmonic waveguides combining both magneto-optical and plasmonic properties. We investigate numerically the non-reciprocal properties of such waveguides to assess their potential for optical isolators.

Results

We study compact SOI ridge waveguides with a FeCo capping layer of varying thickness on top. The waveguides have a typical width of 500 nm and a height of 220 nm and are embedded in a SiO_2 matrix. Finite element simulations were performed to analyze the modes supported by the waveguides as a function of the FeCo thickness. The refractive indices of Si and SiO2 were taken as $n_{Si} = 3.47$, $n_{SiO_2} = 1.44$ and the complex permittivity tensor of FeCo, with external magnetization applied along the

x axis was taken as $\varepsilon_{FeCo} = \begin{pmatrix} -10+29i & 0 & 0 \\ 0 & -10+29i & -1.7+1.8i \\ 0 & 1.7-1.8i & -10+29i \end{pmatrix}$.

Without FeCo, the reference SOI waveguide supports two fundamental TE and TM photonic modes with an effective index of 2.43 and 1.84 respectively. For thin FeCo thickness on top of the waveguide, i.e. in the range 0-20 nm, both TE and TM modes show a smooth evolution of their effective index, as shown in Figure 1a. Above 20 nm of FeCo, plasmonic modes, with a maximum field intensity at the interface between FeCo and Si start to appear. These modes are typical of dielectric-loaded surface Plasmon polariton waveguides (DL-SPP) [4].

The non-reciprocity NR induced by the magneto-optical material FeCo is defined as the relative difference between the effective index of the forward and backward propagating modes under saturated magnetization with respect to the effective index under zero magnetization. The non-reciprocity therefore reads $NR = \dfrac{n_{eff}(+M) - n_{eff}(-M)}{n_{eff}(M = 0)}$. For each mode, magnetization is applied in the Kerr configuration in order to avoid polarization conversion. For the TE mode, magnetization is applied along the y axis, whereas for the TM photonic and DL-SPP modes, magnetization is applied along the x axis. Results are presented in Figure 1b. For the TE and TM photonic modes, there is an optimal FeCo thickness for which the non-reciprocity is maximum. The optimal FeCo thickness is 25 nm for the TE photonic mode with a relative effective index variation of $0.4\ 10^{-3}$ and 15 nm for the TM photonic mode with a relative effective index variation of $3.6\ 10^{-3}$. For the DL-SPP fundamental mode, the behaviour is different. The non-reciprocity increases exponentially and progressively reaches saturation. The relative effective index variation reaches $9\ 10^{-3}$ for a FeCo thickness of 50 nm. The corresponding Mach-Zehnder isolator devices defined by $L = \lambda_0 / 8\Delta n_{eff}$ are 215 µm for the TE photonic mode, 32 µm for the TM photonic mode and only 7 µm with the DL-SPP mode.

Conclusion and persepctives

We have studied numerically a magneto-plasmonic waveguide consisting of a classical silicon ridge waveguide with a magneto-plasmonic layer of FeCo on top. For a FeCo thickness above 20 nm, the waveguide supports a plasmonic guided mode, for which the relative non-reciprocal effective index variation between forward and backward propagation reaches $9\ 10^{-3}$, allowing to reduce the size of optical isolator devices down to 7 µm. These waveguides can be fabricated on 300 mm wafers using standard microelectronic tools. Other more compact waveguide configurations like metallic slot waveguides can be envisioned in the future [5].

References

[1]   H. Dötsch et al., J. Opt. Soc. Am. B, **22** (2005) 240

[2]   R. Espinola et al., Opt. Lett. **29** (2004) 941

[3]   W. Van Parys et al., Appl. Phys. Lett., **88** (2006) 071115

[4]   A.V. Krasavin et al., Appl. Phys. Lett., **90** (2007) 211101

[5]   C. Delacour et al., Nanolett., **10** (2010) 2922

Figures

(a)   **(b)**
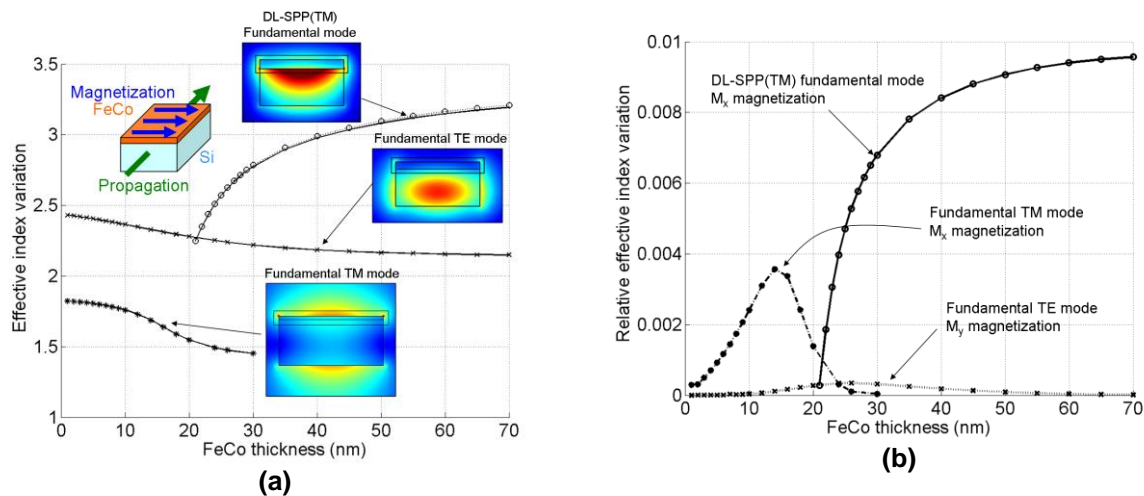
Figure 1: (a) Effective index of the modes supported by a silicon ridge waveguide with a FeCo layer of varying thickness on top. The associated electromagnetic field maps are represented as insets; (b) Relative effective index variation between forward and backward propagating modes illustrating the amount of non-reciprocity effect in the Si/FeCo magneto-plasmonic waveguide.

Magnetic properties of high permittivity dielectric nanoparticles applied to optical metamaterials.

Ramón Paniagua-Domínguez*, F. López-Tejeira*, José A. Sánchez-Gil*, L. Jelinek[+], R. Marqués[++].

*Instituto de Estructura de la Materia, Consejo Superior de Investigaciones Científicas, Serrano 121, 28006, Madrid, Spain
[+]Department of Electromagnetic Field, Czech Technical University in Prague, 166 27, Prague, Czech Republic
[++]Departamento de Electrónica y Electromagnetismo, Universidad de Sevilla, 41012, Sevilla, Spain

ramon.paniagua@iem.cfmac.csic.es

In the last decade, great deal of attention has been brought to artificially tailored materials exhibiting electromagnetic properties non-attainable in naturally occurring media. The so called metamaterials can present extraordinary properties such as a negative refractive index [1]. One of the current open issues in this field is pushing these properties from the microwave range of the electromagnetic spectrum to the visible range [2]. One major difficulty in this task is achieving a strong magnetic response capable of generating a magnetic moment strong enough as to obtain a negative effective permeability. Most of the many attempts are based on designs with a profound analogy with the canonical split-ring design, but taking advantage of the plasmonic behaviour of metals at visible frequencies [3,4]. One important drawback of these designs is the inherent absorption of metals, which prevents from making an effective bulk material.

Our theoretical proposal is, instead of using metals, to take advantage of the strong confinement of the field that happens in high-permittivity dielectrics. Following the proposal of L. Jelinek and R. Marqués [5] we present several designs that could lead to the realization of left-handed bulk media in the IR-visible frequencies. These include the SiC torus configuration, the SiC spherical-shell (see Fig.1) for the magnetic response in the IR regime, and the α-hexagonal Si spherical-shell for the visible regime.

Finally, a 2D medium is also shown to exhibit left-handedness in the near-infrared based exclusively in dielectric cylinders. The effect is a consequence of the excitation of dipolar magnetic resonances together with an appropriate election of the lattice spacing (see Fig.2).

References

[1] V. Veselago, Sov. Phys. Uspekhi, **10** (1968) 509-514.
[2] V. M. Shalaev, Nature Photonics, **1,** (1968) 509-514.
[3] Soukoulis et al., Science, **315,** (2007) 41-48.
[4] A. Alú, A. Salandrino, N. Engheta, Optics Express, Vol. 14, **4**, (2006) 1557-1567.
[5] L. Jelinek, R. Marqués, J. Phys.:Condens. Matter, 22, (2010) 025902(6pp)

Figures.

(a)

(b)
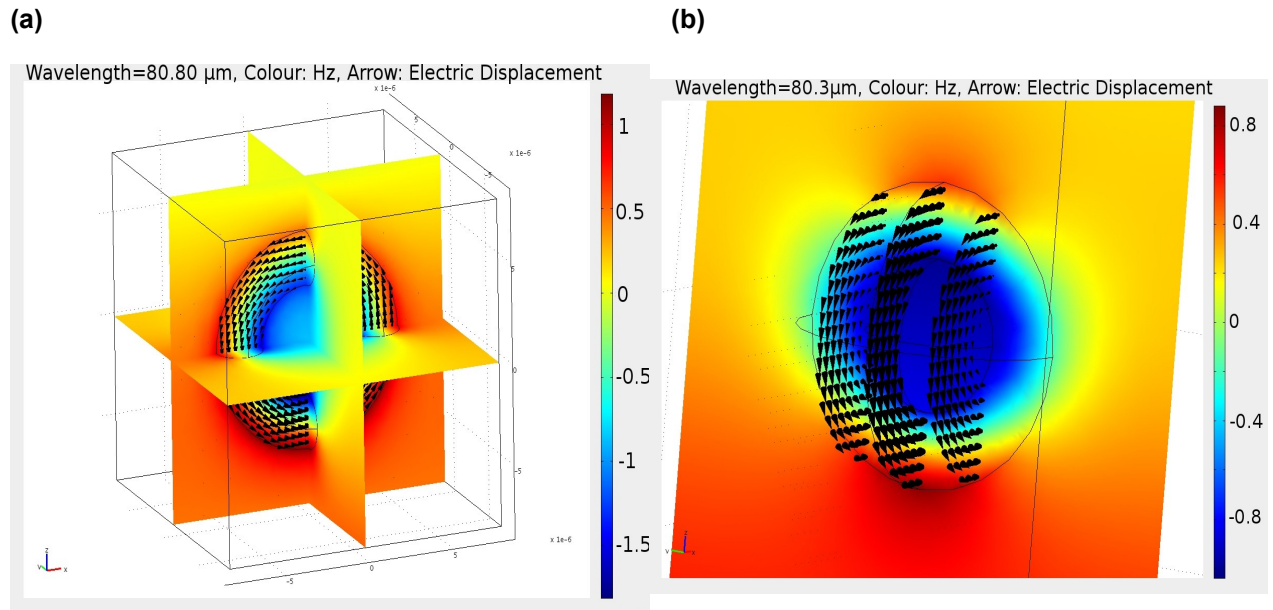
Fig.1: Dielectric Ring (a) and Shell (b) made of SiC. The incident magnetic field is directed along the y-axis. The induced displacement currents generate a strong magnetic response reversing the field inside the structures.
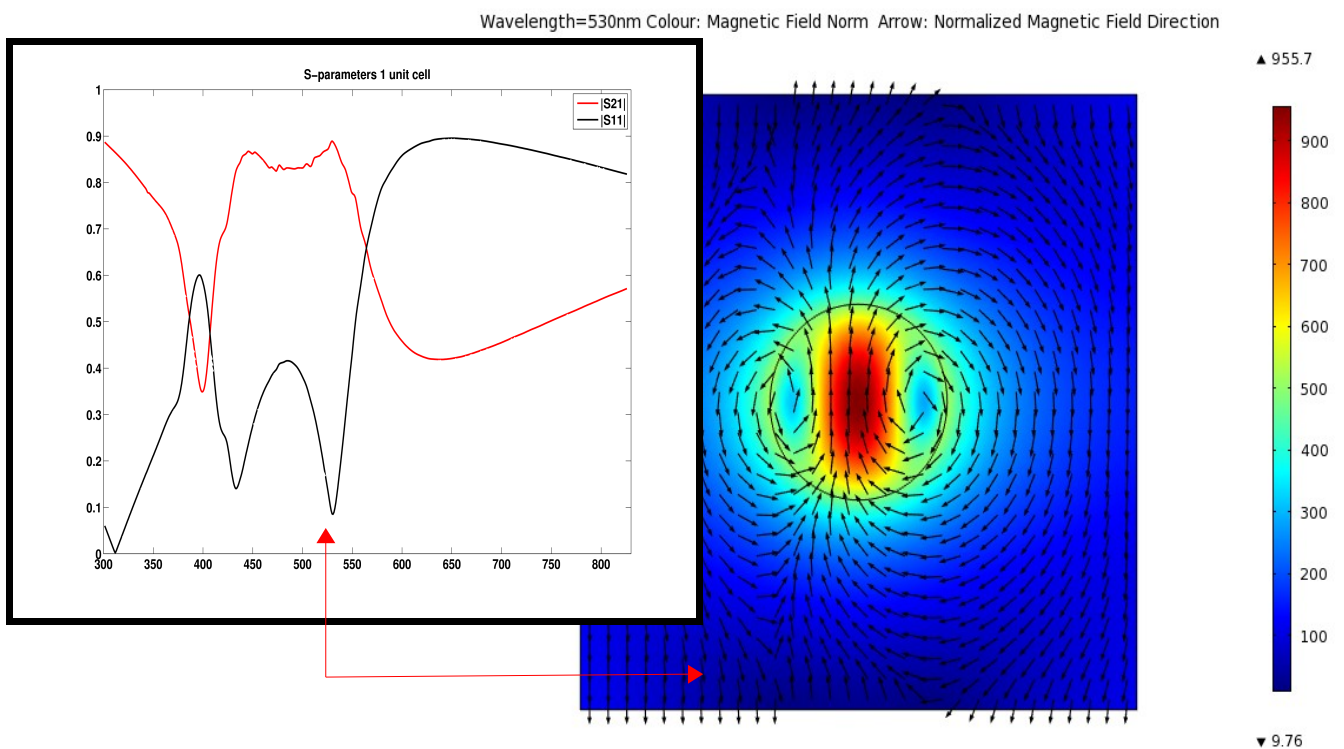
Fig.2: Dielectric cylinder made of Si with R=50nm serves as the unit cell for the 2D left-handed medium. The incident magnetic field is directed along the y-axis. As is readily observed a strong magnetic dipolar mode is excited in the structure.

60

Self-Organization of Cholesteric Liquid-Crystal Polymers on Metal Substrates

Mercedes Pérez-Méndez[1], Paloma Tejedor[2]

[1]*Instituto de Ciencia y Tecnología de Polímeros (ICTP). CSIC. C/ Juan de la Cierva, 3. 28006-Madrid. Spain*
[2]*Instituto de Ciencia de Materiales de Madrid (ICMM), C.S.I.C. C/ Sor Juana Inés de la Cruz, 3. Cantoblanco. 28049-Madrid. Spain*

perezmendez@ictp.csic.es

Optoelectronic Cholesteric liquid-crystal-polymers (ChLCP), synthetized in our lab [1], when dispersed in solution, self-organize on metal surfaces, such as: Si(111); Pt / TiO2 / SiO2 /Si(001), Ag, Au, either colloidal spheres or thin layers [2].

Under spin coating controlled conditions growth has been obtained in multilayer ordered structures, Figure 1.

Their HELICAL MACROMOLECULES, Figure 2, uncoil and get adsorbed on the metal via π-interaction, with the aromatic rings extended parallel to the interface and the aliphatic chains directed towards the bulk solution, according to the scheme depicted in Figure 3.

The interaction of these ChLCP with metals could be applied to the design of functionalized surfaces provided with physico-chemical properties of interest.

Besides, our synthetic cholesteric liquid-crystals, exhibit OpticalRotatory Dispersion(ORD), complex Circular Dichroism (CD) patterns, transmitance and reflectance, with potential application in various areas of nanotechnology, such as: CHLC DISPLAYS WITH PHOTOCHROMIC RESPONSE [3], FIBER COUPLED CHOLESTERIC LIQUID CRYSTAL LASERS [4], BIOSENSORS IN RECOGNITION PHENOMENA and MEMs [5].

References

[1] a) M. Pérez-Méndez and C. Marco Rocha, Acta Polymerica, **1997**, 48, 502-506; b) M. Pérez-Méndez and C. Marco Rocha, " Preparing cholesteric liquid crystals - by adding acid dichloride and butanediol to chloro-naphthalene, heating in nitrogen, decanting into toluene, etc", Patent with nº EP1004650-A; WO9831771-A; WO9831771-A1; AU9854863-A; ES2125818-A1; ES2125818-B1; EP1004650-A1; US6165382-A; MX9906732.

[2] S. Sánchez-Cortés, R. Marsal-Berenguel, M. Pérez-Méndez, "Adsorption of a Cholesteric Liquid-crystal Polyester on Silver and Gold Nanoparticles and Films Studied by Surface-Enhanced Raman Scattering", Applied Spectroscopy **2004** Vol. 58 Nº 5, pp 562 -- 569

[3] T. Yoshioka, T. Ogata, T. Nonaka, M. Moritsugu, S.N. Kim and S. Kurihara, "Reversible-Photon-Mode Full-Color Display by Means of Photochemical Modulation of a Helically Cholesteric Structure ", Adv. Mater. **2005**, 17, 1226-1229.

[4] B. Taheri, P. Palffy-Muhoray, and H. Kabir, ALCOM Symposium. Chiral Materials and Applications, Cuyahoga Falls, Feb. 18-19 (1999)

[5] Emerging Liquid Crystal Technologies (Proceedings Volume), Proceedings of SPIE Volume: 5741 Editor(s): Liang-Chy Chien, April 2005, ISBN: 9780819457158

[6] C. Munuera, E. Barrena and C. Ocal, "Scanning Force Microscopy three-dimensional modes applied to conductivity measurements trough linear chain organic SAMs" Nanotechnology 18, 125505 (2007)

[7] T.R. Matzelle, G. Geuskens and N. Kruse, "Elastic properties of poly(N-isopropylacrylamide) and poly(acrylamide) hydrogels studied by scanning force microscopy" Macromolecules (8): 2926-2931 APR 22 2003
Figures
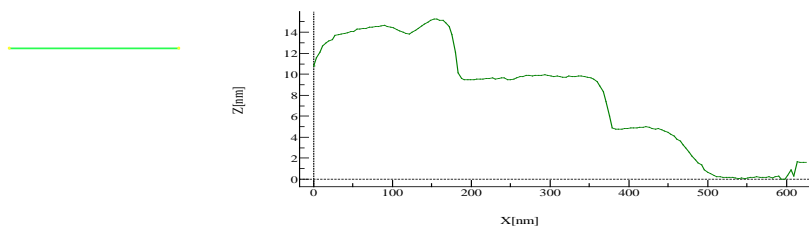
*Figure 1. Multilayered structure of ChLC polymer grown by spin coating.*


Figure 2: ChLC polymer helical molecule   *Figure 3: Adsorption of extended ChLC polymer on Ag thin layer.*
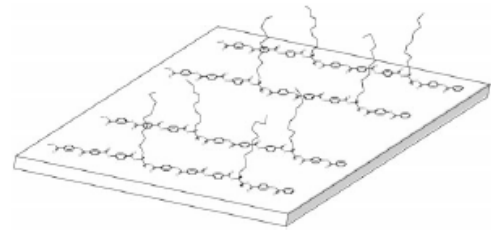
62

Spectral signature of molecular linkers in plasmonic cavities

Olalla Pérez-González[1-2], Nerea Zabala[1-2], Peter Nordlander[3] and Javier Aizpurua[2]

[1]Electricity and Electronics Department, University of the Basque Country, Bilbao, Spain.
[2]Donostia International Physics Center (DIPC) and Centre for Materials Physics (CSIC-UPV/EHU), Donostia-San Sebastián, Spain.
[3]Laboratory for Nanophotonics, Rice University, Houston, USA.

olalla_perez@ehu.es

In the last decade fundamental advances have been achieved in the fields of molecular electronics [1] and plasmonics [2]. In particular, the optical properties of plasmonic dimers with different shapes have been deeply studied and explained using exact numerical calculations and hybridization models [3]. Recent experiments, such as the simultaneous measurements of electronic conduction and Raman spectroscopy in molecular junctions [4], have suggested the possibility of sensing individual molecules, connecting both fields.

Following this emerging connection, we related optical properties to transport processes in a recent letter using a model consisting of a conductive bridge linking two gold nanoshells [5]. For the sake of simplicity, we modelled the linker as a pure conductor with real conductivity so that the variation of conductivity affected only the imaginary part of the dielectric function characterizing the junction. Now, boosted by the recent interest in molecular switches [6], we have improved this simple model to make it more realistic. In this work, we study the effect on the optical response of a molecular junction bridging a gold nanoparticle dimer, where the dielectric response of the junction is characterised by a Lorentz model, which takes into account the resonant frequency ω_0 of the linking molecule. In this work, both the real and imaginary parts of the dielectric function characterizing the junction are affected by the nature of the linker.

As a first step, we have considered junctions with transition frequency ω_0 = 1.51eV - (λ_0 = 820nm), corresponding to rotaxane molecules [6]. Fixing the radius of the gold particles (R = 50nm) and the separation distance between them (d = 1nm), the plasmonic resonance of the disconnected dimer is found at λ_p = 665nm, below the transition wavelength of the molecular linker. Then, we connect the gold particles with a cylindrical molecular region of radius a mimicking the molecules, and we observe the evolution of the far-field and near-field properties of the whole system as the bridge becomes wider. Electromagnetic fields and optical extinction spectra are obtained by solving Maxwell's equations exactly with the Boundary Element Method (BEM) [7].

Figure 1(a) shows the evolution of the optical extinction spectra of our system as the radius of the molecular junction is increased up to 35 nm. As for the pure conductor, we observe that the Bonding Dimer Plasmon (BDP) mode, arising from the coupling between the dipole modes of the individual nanoparticles (initially found around λ_{BDP} = 665nm), is slightly blue-shifted as the radius of the linker is increased. In contrast to our previous study, for longer wavelength values, in addition to the appearance of a Charge Transfer Plasmon (CTP) mode around λ_{CTP} = 970nm, where a real charge transfer between the particles occurs, we also observe the emergence of a new resonance between the BDP and the CTP modes.

For small molecular junctions, in contrast to the pure conductor case, where the CTP mode vanishes with a dramatic red-shift towards longer wavelength values as size is decreased, the CTP mode disappears slightly blue-shifting as the linker size is reduced. These BDP and CTP resonances are prominent for small sizes of the molecular linker, whereas the new resonance gains spectral weight dramatically as the linker size is increased, suggesting a strong influence of the molecular transition in the optical behaviour of the system. The nature of the three different resonances described above is analyzed with the help of near-field contour plots.

The results are generalized to consider molecular linkers presenting different resonances in the range of λ_0 = 400-1200 nm (Figure 1(b)). In this case, where we have fixed the radius of the molecular linker to 5 nm, we observe that the position of the BDP remains unaltered, whereas its intensity is stronger for longer λ_0 values. In contrast, the CTP mode presents a parabolic red-shift and loss of spectral weight as the resonance of the connecting molecules λ_0 is found at longer wavelength values.

We believe that the study of this kind of spectral changes in plasmonic cavities connected by molecular linkers might lead to control the switch on and off of the different emerging plasmon modes.

References

[1] T. Dadosh, Y. Gordin, R. Krahne, I. Khivrich, D. Mahalu, V. Frydman, J. Sperling, A. Yacoby and I. Bar-Joseph, *Nature* **436**, (2005) 677.
[2] J. Aizpurua, G.W. Bryant, L.J. Ritcher and F.J. García de Abajo, *Phys. Rev. B* **71**, (2005) 235420.
[3] J.B. Lassiter, J. Aizpurua, L.I. Hernández, D.W. Brandl, I. Romero, S. Lal, J.H. Hafner, P. Nordlander and N.J. Halas, *Nano Lett.* **8**, (2008) 1212.
[4] D.R. Ward, N.J. Halas, J.W. Ciszek, J.M. Tour, Y. Wu, P. Nordlander and D. Natelson, *Nano Lett.* **8**, (2008) 919.
[5] O. Pérez-González, N. Zabala, A.G. Borisov, N.J. Halas, P. Nordlander and J. Aizpurua, *Nano Lett.* **10**, (2010) 3090.
[6] Y.B. Zheng, Y.W. Yang, L. Jensen, L. Fang, B.K. Juluri, A.H. Flood, P.S. Weiss, J.F. Stoddart and T.J. Huang, *Nano Lett.* **9**, (2009) 819.
[7] F.J. García de Abajo and A. Howie, *Phys. Rev. Lett.* **80**, (1998) 5180.

Figures
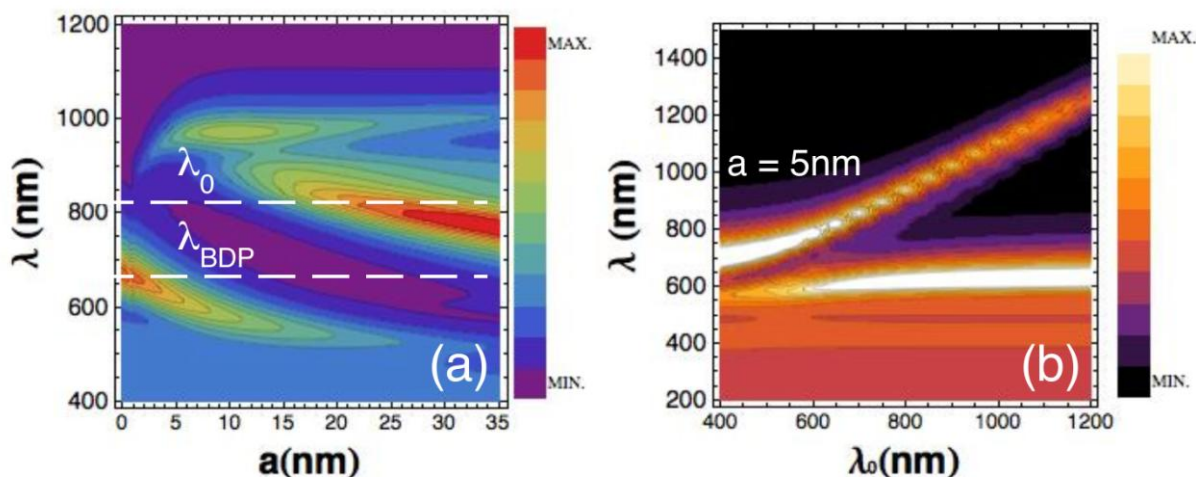
Figure 1: (a) Evolution of the optical extinction spectra of a molecular junction bridging a gold nanoparticle dimer as the radius of the molecular linker a is increased. The dashed lines indicate the spectral position of the considered molecular transition at 1.51eV (λ_0) and the initial spectral position of the BDP mode (λ_{BDP}), which also appears when the dimer is disconnected. (b) Plasmonic resonances of a gold nanoparticle dimer connected by a molecular bridge of radius a = 5 nm formed by different molecules, as a function of their resonance wavelengths.

Wavelength-dependent magneto-optical coercivity in cobalt ferrite nanoparticles

Francesco Pineider[1,2], Cesar De Julian Fernandez[1], Giulio Campo[1], Elvira Fantechi[1], Claudia Innocenti[1], Dante Gatteschi[1] and Claudio Sangregorio[1]

1. Università di Firenze & INSTM, Italy 2. Università di Padova & ISTM-CNR, Italy
francesco.pineider@unifi.it

Polarized photons are powerful probes to enucleate magnetic properties of nanoparticles: their interaction with materials returns information in which spin population and spectroscopic attributes are intertwined. In particular, the possibility of using photons of different energy allows to separate contributions arising form different phases of the material and to link magnetic properties to single electronic transitions or delve into more elaborate physical mechanisms otherwise very hard - if not impossible - to observe.

We recently carried out an extensive magneto-optical (MO) study using magnetic circular dichroism (MCD) at cryogenic and room temperatures on magnetite and cobalt ferrite nanoparticles to correlate structural and stoichiometric parameters to their MO response, and found clear correlations between particle composition and MCD spectrum.

In addition to this by recording hysteresis loops using as a probe light of different wavelengths (i.e. sampling different spectral regions), we found that coercivity in cobalt ferrite depends strongly (>30%) and linearly on the wavelength used as a probe (see figure). Comparison SQUID-based experiments carried out under irradiation confirm that the effect is not due to light-induced heating or charge transfer due to photon absorption. The mechanism underlying this effect is still under debate and is likely to be related to the polarisation of valence band transitions of the material with respect to the axes of anysotropy of single cobalt ferrite nanocrystals.

Figures
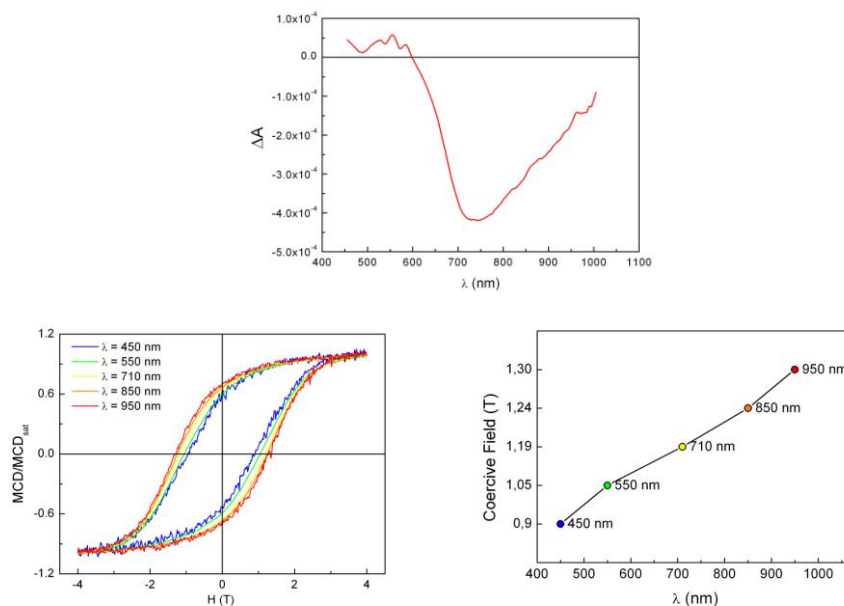
(Top) MCD spectrum of a Cobalt ferrite nanoparticle sample at 2 K under 5 T applied field. (Bottom left) wavelength-dependent coercivity (2 K) of the same sample and (Bottom right) plot showing the linear dependence of coercivity vs wavelenght

Plasmon Resonances of Flexible Shape Nanoparticles

Rogelio Rodríguez-Oliveros, Jose Antonio Sánchez-Gil

Institute of the Structure of the Matter (CSIC), Serrano 121, Madrid, Spain.
rogelio@iem.cfmac.csic.es

We present an advanced numerical formulation to calculate the optical properties of 3D nanoparticles (single or coupled) of arbitrary shape and lack of symmetry [1]. The method is based on the (formally exact) surface integral equation formulation, implemented for parametric surfaces describing particles with arbitrary shape through a unified treatment that we call flexible surfaces based on the so called Gieli's formula [2].

Flexible surfaces can be consider an extremely appealing tool in a numerical implementation of a scattering method, since selecting a few number of parameters can lead to very different surfaces, that mimic the most common shapes of nanoparticles experimentally synthesized on plasmonics, as sphere, cubes, cylinders and stars. Moreover this remarkable feature of the flexible surfaces not only saves computational time, since we only have to implement a program to achieve different shapes instead one program each, but also avoids problems in the implementation of the scattering method related to the matching and sharpness of the surfaces.

In figure [1] we show a sort of surfaces achievable by a flexible surface called *SuperShape* [3] described by the following parametric equations:

$$r(\phi) = \left(\left| \frac{1}{a} sin\left(\frac{m}{4}\phi \right) \right|^{n_2} + \left| \frac{1}{b} cos\left(\frac{m}{4}\phi \right) \right|^{n_3} \right)^{-\frac{1}{n_1}}$$

$$x(t,s) = r_1(s)r_2(t)sin(t)cos(s)$$
$$y(t,s) = r_1(s)r_2(t)sin(t)sin(s)$$
$$z(t,s) = r_2(t)cos(t)$$

In order to show the flexibility and reliability of the formulation, we plot in figure [2] the surface field at the resonance wavelength for a 5-fold star made of silver. In figure [3] we study the dependence of the scattering cross section of a insulate cube made of silver on the sharpness of the edges. The scattering cross section shows a blue shift when the sharpness of the vertex increase. Finally, figure[4] shows the electric field on the surface of a spherical dimer made of gold, it illustrates the fact this approach deals with all sorts of complex surfaces as the star in figure[1] along the less complex ones as spheres.

The implementation of flexible surfaces in the 3d scattering methods based on the green theorem makes it specially suitable for complex scattering problems in Nano-Optics and -Photonics.

References

[1] Rodriguez-Oliveros, R. Sánchez-Gil J.A., submitted to optics express.
[2] Gielis, J. American Journal of Botany, **90** (2003) 333
[3] Bourke, P. http://local.wasp.uwa.edu.au/~pbourke/geometry/supershape3d/.
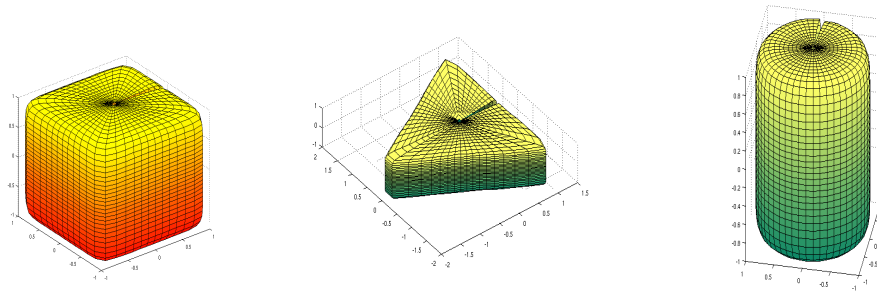
Figures

**Figure1 .-** *Geometrical shapes achievable to the SuperShape changing the parameters.*
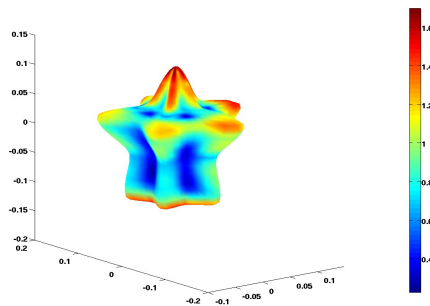
**Figure2 .-** *Electric field on the surface of a silver nanostar with r=50nm at λ=531nm*
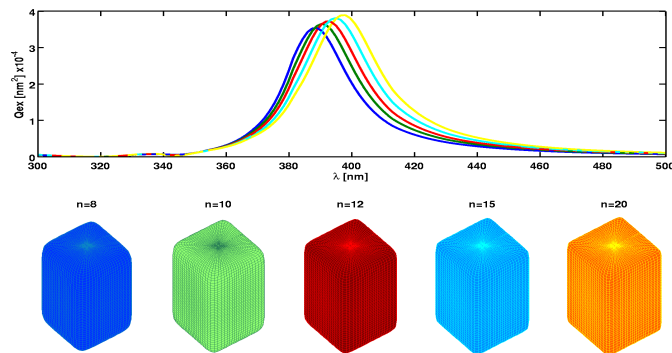

Figure3.- *Scattering cross section for silver nanocubes L=50nm with increasing sharpness*
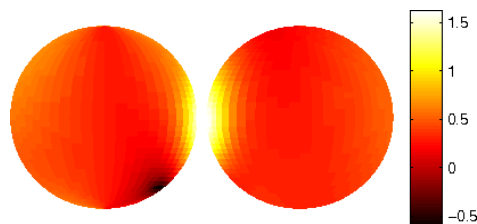
Figure4.- *Electric field on the surface for a gold dimer with r=15nm and gap=2nm at resonance wavelength λ=535nm*

Light emission statistics in correlated random photonic nanostructures

N. de Sousa[1], J. J. Saenz[1], A. García-Martín[2] and L. S. Froufe-Pérez[3]

[1] Departamento de Física de la Materia Condensada,
Universidad Autónoma de Madrid, 28049 Madrid, Spain

[2] Instituto de Microelectrónica de Madrid, CSIC,
Isaac Newton 8, Tres Cantos, 28760 Madrid, Spain

[3] Instituto de Ciencia de Materiales de Madrid, CSIC,
Campus de Cantoblanco, 28049 Madrid, Spain

nuno.teixieira@uam.es

The statistical properties of light transport and emission in disordered media has been a matter of intense research during the last century. Being the basis of coherent multiple scattering of waves well known, the phenomenon itself is not yet fully explored and understood. These multiple wave scattering effects are at the heart of emerging behaviors like Anderson localization of light and electrons, band structure in crystalline solids or photonic crystals (PhC), among many others.

Although the limits of perfectly ordered systems on the one hand, and uncorrelated and relatively weakly scattering systems on the other hand, are quite well understood. There is a gap between both limits which is largely unexplored. In particular, it has been shown in many different situations that disordered systems exhibiting certain structural correlations can share properties of both crystalline and fully disordered systems. For instance, the conductivity of liquid metals [1] or the cornea transparency [2] can be understood in the same footing: a disordered but correlated system can present spectral regions of high transparency for electron or light transport.

The effects of disorder in an initially ordered structure, such as a PhC, might lead to strong Anderson localization, as the scattering mean free path can be severely reduced in the band edges [3]. Also, strongly correlated charged colloids can scatter light in such a way that the transport mean free path presents a strong chromatic dispersion [4]. Even in the absence of practically any long range correlations, the structure of the scatterers itself can be used to modify the light emission and transport properties of a disordered system in such a way that transport parameters [5], or even the threshold of a random laser [6], can present resonances which can be tuned in advance.

The effect of correlations in a disordered structure regarding light emission properties of single fluorescent emitter has been a matter of much less intense research efforts. It is clear that the structure surrounding a single emitter can largely alter its emission dynamics [7]. In the last years, several groups considered such effects in a statistical way suitable for the description of disordered systems [7,8,9]. In particular, in ref.[9] it was shown that several structural properties near a phase transition can be accessed via fluorescence intensity fluctuations.

Is has been theoretically proven that near field scattering in random systems alters fluorescence dynamics in such a way that microscopic information about the surroundings of a single emitter can be obtained from lifetime fluctuations or from the shape of the statistical distribution tails [10,11].

In this presentation, we theoretically show how, in the previous context, fluorescence emission rate statistics are largely altered due to the appearance of structural correlations in a disordered system.

We have developed a model of point resonant interacting scatterers which are placed at random. Emission dynamics of a single emitter is calculated for each sample of an ensemble of structural realizations of the system.

While keeping constant the scattering properties of single scatterers, the global geometry, and scatterers density, the structural correlations are controlled changing the temperature of the interacting set of scatterers.

It is shown that fluorescence decay rate statistics of a the single emitter correlates with the structural phase transitions of the system. In the low temperature limit, the structure freezes in an face center cubic lattice. This structure presents a gap (frequency range of low photonic density of states) corresponding to a vanishing fluorescence decay rate. As usual, it also presents narrow frequency windows of high density of states, corresponding to band edges of the perfect infinite crystalline structure, leading to high decay rates.

At frequencies corresponding to both a band gap and a band edge, we perform decay rate statistics varying the temperature of the system. It is shown that, at low temperature, decay rates hardly fluctuates and its average value corresponds to the crystalline one. On temperature raising, fluctuations of decay rate grow, and the averaged values undergoes a relatively sharp transition to a different value. This transition can be identified with a structural phase transition in the system.

References

[1] N. W. Aschcroft and J. Lekner, Phys. Rev. **145** (1966) 84.
[2] R. W. Hart and R. A. Farrell, J. Opt. Soc. Am. **59** (1969) 766.
[3] Sajeev John, Phys. Rev. Lett. **58** (1987) 2486.
[4] L. F. Rojas-Ochoa, J. M. Mendez-Alcaraz, J. J. Sáenz, P. Schurtenberger, and F. Scheffold, Phys. Rev. Lett. **93** (2004) 073903.
[5] P. D. García, R. Sapienza, A. Blanco, and C. López, Adv. Mater. **19,** 2597 (2007); R. Sapienza, P.D. García, J. Bertolotti, M.D. Martín, A. Blanco, L. Viña and C. López, D.S. Wiersma, Phys. Rev. Lett. **99**, (2007) 233902.
[6] S. Gottardo, R. Sapienza, P.D. Garcia, A. Blanco, D. S. Wiersma and C. Lopez, Nat. Phot. **2** (2008) 429.
[7] Jordi Hernando, Erik M. H. P. van Dijk, Jacob P. Hoogenboom, Juan-José García-López, David N. Reinhoudt, Mercedes Crego-Calama, María F. García-Parajó, and Niek F. van Hulst, Phys. Rev. Lett. **97** (2006) 216403.
[8] H. Gersen, M. F. García-Parajó, L. Novotny, J. A. Veerman, L. Kuipers, and N. F. van Hulst, Phys. Rev. Lett. **85** (2000) 5312.
[9] R. A. L. Vallee, M. Van der Auweraer W. Paul and K. Binder, Phys. Rev. Lett. **97** (2006) 217801.
[10] L. S. Froufe-Pérez, R. Carminati and J. J. Sáenz, Phys. Rev. A **76** (2007) 013835.
[11] L. S. Froufe-Pérez and R. Carminati, Phys. Stat. Sol. (a) **205** (2008) 1258.

Infrared Nanophotonics based on Metal Antennas and Transmission Lines

M. Schnell[1], P. Alonso-González[1], F. Casanova[1,2], L. Arzubiaga[1], L. E. Hueso[1,2], A. Chuvilin[1,2], R. Hillenbrand[1,2]

[1] CIC nanoGUNE Consolider, Tolosa Hiribidea 76, 20018 Donostia – San Sebastian, Spain
[2] IKERBASQUE, Alameda Urquijo 36-5, Basque Foundation for Science, 48011 Bilbao, Spain
m.schnell@nanogune.eu

Metal antennas and transmission lines are common devices for receiving and transporting signals in the radiofrequency regime. Here, we demonstrate that by reducing the size down to the micrometer range, these devices can be operated at infrared frequencies (~30 THz) [1,2]. We apply our recently introduced vector near-field microscopy technique [3] for directly visualizing the reception and transport of infrared energy [4]. The combination of antenna plus transmission line is a promising platform technology for designing future mid-infrared devices which require subwavelength-scale integration.

The transmission line that is used here consists of two parallel wires that are isolated by a small gap (Fig. 1b). This structure is the miniature version of a very common TV cable known as the ladder line for connecting the roof antenna with the television set. A dipole antenna is connected to one end of the transmission line for converting free-space radiation into a confined mode. By illuminating the antenna with infrared radiation ($\lambda \approx 10\mu m$), a surface wave is launched which is travelling along the transmission line to the right side. Fig. 1c shows the momentary near-field distribution of the surface wave that is tightly bound to the metal wires. The image reveals that the surface mode has an asymmetric charge distribution. Moreover the image allows for determining the wavelength of the surface mode. Numerical calculations confirm the experiment with excellent agreement (Fig. 1a).

Based on these transmission lines, we compress infrared energy to a nanoscale focus spot of 60 nm [4]. This is achieved by tapering the end of the transmission line, i.e. gradually reducing the lateral dimensions. By propagating along the taper, the surface mode is compressed to deep subwavelength scale dimensions ($\lambda/150$). Interestingly, we observe that the wavelength of the surface wave is still of the order of the free-space wavelength. This is in strong contrast to plasmon compression where the field confinement is connected with a large increase of the wave vector.

The compression of infrared surface waves with tapered transmission lines opens the door for the development of ultra-small integrated infrared sensor and spectroscopy devices for chemical and (bio)medical diagnostics.

References

[1] T. Mandviwala et al., *Microw Opt Techn Let* **47**, 17 (2005).

[2] P. M. Krenz et al., *Opt. Express* **18**, 21678 (2010).

[3] M. Schnell et al., *Nano Lett.* **10**, 3524 (2010).

[4] M. Schnell et al., *submitted*

Figures
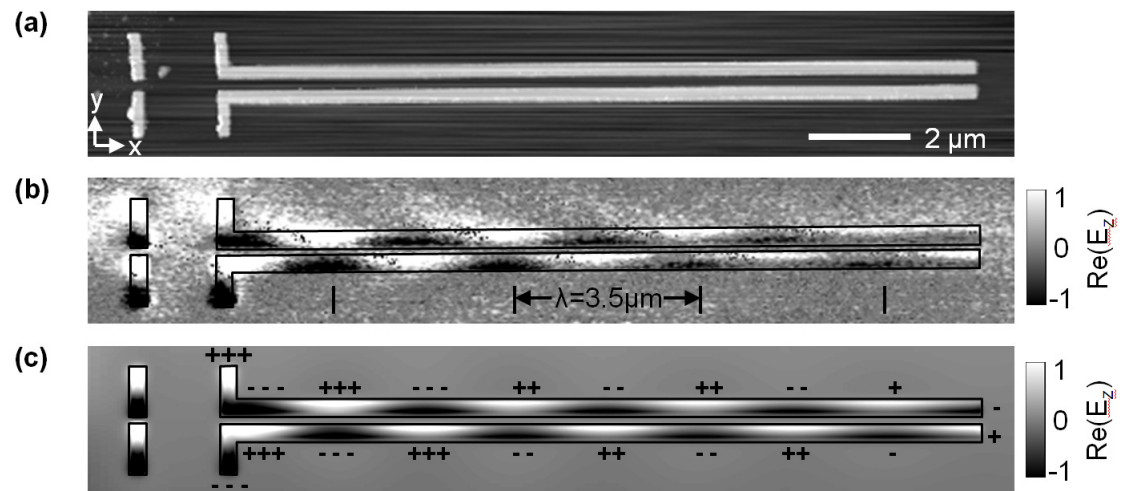
Fig. 1: Energy transport and propagation properties in two-wire transmission lines. (a) Topography image of an antenna-coupled two-wire transmission line, consisting of two 40nm height Au wires, 200nm wide, separated by a 300nm wide gap, on a Si substrate. (b) Experimental near-field image taken at λ = 9.3 µm, showing $Re(E_z)=|E_z|cos(\varphi_z)$. (c) Numerically calculated near-field image showing $Re(E_z)=|E_z|cos(\varphi_z)$.

FLUORESCENCE LIFETIME NEAR RESONANT NANOPARTICLES

I. Suárez-Lacalle, N. de Sousa, L. Froufe-Pérez, J.J. Sáenz

Departamento de Física de la Materia Condensada, Universidad Autónoma de Madrid, Madrid, Spain
irene.suarez@uam.es

The **spontaneous emission rate of a single emitter** (e.g., atom, molecule, quantum dot) depends on the environment. The control of the decay rate through the Photon Local Density of States (PLDOS) was first pointed out (at radio frequencies) by Purcell [1]. Modifications of the spontaneous decay rate of molecules close to metallic surfaces [2,3] or atoms in simple cavities [4] are well known examples nowadays. Nanometer scale objects behave as **nanoantennas for single-emitter fluorescence** modifying the   radiative emission rate as well as the far-field angular radiation pattern [5].

Theoretical discussions are usually based on electric dipolar interactions. Analytical formulas based on a dipole–dipole model have been derived [6] for radiative, Γ^R, and non-radiative, Γ^{NR}, decay rate versus the distance between a single emitter close to a **metallic nanoparticle**. Γ^R is dominated by a z_0^{-3} dependence, a z_0^{-6} dependence being visible at plasmon resonance.

A drawback when using metallic objects is the presence of absorption, which creates additional non-radiative channels. **Resonant dielectric structures** provide an alternative way to control both field enhancements and emission rates [7]. Very recently it has been shown [8,9] that submicron silicon spheres present non-absorbing dipolar magnetic and electric resonances in the near infrared.

As it is known, small dielectric particles present an electric dipolar response. However, as the size increases (or the wavelength deacreases) the first Mie-resonance always corresponds to a magnetic dipolar resonance. In absence of absorption, at resonant conditions, the extinction cross section   does not depend on the particle size or material properties.

In this work we study the spontaneous decay rate of a single (electric) dipole emitter close to a dielectric resonant subwavelength particle using an analytical approach. As we will show, both lifetime and angular emission near a dielectric particle at the magnetic resonance present unexpected properties that differ from those predicted for metallic nanoparticles. Lifetime near magneto-optical particles will also be discussed [11].

References
[1] E.M. Purcell., Physical Review, **69** (1946), 681
[2] R.R. Chance, A. Prock, and R. Silbey, Adv. Chem. Phys., **37** (1978), 1.
[3] W.L. Barnes , J. Mod. Optics, **45** (1998), 661.
[4] *Cavity Quantum Electrodynamics.* P. Berman (Ed.) ,Academic Press, New York, 1994.
[5] H. Gersen, M. F. García-Parajó, L. Novotny, J. A. Veerman, L. Kuipers, and N. F. van Hulst., Phys. Rev. Lett., **85** (2000), 5312.
[6] R. Carminati, J.-J. Greffet, C. Henkel, J.M. Vigoureux, Opt. Commun., **261** (2006), 368.
[7] M. Laroche,S. Albaladejo, R. Carminati, and J.J. Sáenz , Opt. Lett., **32** (2007), 2762.
[8] García-Etxarri , R. Gómez-Medina, L. S. Froufe-Pérez, C. López, L. Chantada, F. Scheffold, J. Aizpurua, M. Nieto-Vesperinas and J. J. Sáenz, Optics Express, **19** (2011), 4815.
[9] M. Nieto-Vesperinas, R. Gómez-Medina and J.J. Sáenz . J. Opt. Soc. Am. A, **28** (2011) 54-60.
[10] J.M. Wylie and J.E. Sipe. Phys. Rev. A, **30** (1984), 1185.
[11] S. Albaladejo, R. Gómez-Medina, L. S. Froufe-Pérez, H. Marinchio, R. Carminati, J. F. Torrado, G. Armelles, A. García-Martín and J. J. Sáenz, Optics Express, 18 (2010), 3556

Propagation of morphology dependent resonances in sets of nanocylinders in front of supertransmitting slits

Francisco Javier Valdivia-Valero, Manuel Nieto-Vesperinas

Instituto de Ciencia de Materiales (ICMM), Consejo Superior de Investigaciones Científicas (CSIC), C/ Sor Juana Inés de la Cruz 3 (Campus de Cantoblanco), Madrid, Spain
mnieto@icmm.csic.es fvaldivia@icmm.csic.es

Microcylinders and microspheres, as well as their arrangements such as in photonic molecules and waveguiding chains, have been a subject of active research. These microcavities present new effects on enhancement, confinement, spectroscopic splitting and transport of optical energy [1]. On the other hand, near field optics has shown the relevance of some of these effects at the subwavelength scale. This takes place via eigenmodes such as whispering gallery modes (WGM) in sets of dielectric nanoparticles, and localized surface plasmons (LSP) in metallic ones.

In addition, extraordinary, or enhanced, optical transmission through subwavelength apertures is a resonant effect that has received much attention in connection with its importance for light concentration, detection and wavefront steering [2]. Here we inquire on the interplay between the transmission characteristics of nanoapertures and its coupling to morphology dependent resonances (MDR) in nanocylinders in front of them; these being WGMs, and LSPs.

When the apertures make a metallic grating, the set of particles is a photonic crystal (PC). The role of Mie resonance propagation in both dielectric and metallic PCs has been a subject of interest as regards its influence on the crystal bandgap size and position. An interplay between both the band structure and the excitation of particle resonances rules the enhancement and propagation of the light through the PC-slit grating system. This process is favored by the high field concentration inside, or around, the particles, for either WGMs or LSPs, respectively.

We address different sets of either dielectric or metallic nanocylinders in front of a subwavelength metallic slit [3]. Next, we extend this study to photonic crystals close to gratings of such slits. The effects on light transmission and localization in the system when morphology-dependent resonances are excited in the particles, are analysed.

Calculations are done both by the finite element method and using FDTD simulations. We discuss the effect of these excitations on extraordinary transmission by either the slit or the array.

We show the dominant role of the MDR over the aperture resonances, as regards the resulting transmitted intensity and its concentration in the cylinders. When sets of these particles are placed in front of the slit, like linear or bifurcated chains, with or without bends, one can control the localization and enhancement of MDRs by appropriate design of the parameters. So that these surface waves are coupled by both waveguiding of the nanocylinder eigenmodes and by scattered propagating waves.

For the case of PCs, by changing the crystal parameters we can select the frequency range in which a partial PC bandgap and a MDR appear. This allowing us to manipulate the light transmitted through the grating [4].

The excitation of Mie resonances of nanocylinder sets and PCs placed in front of subwavelength slits, dramatically enhances the extraordinary resonant transmission that these apertures would produce alone. The transmitted intensity concentrated either inside or on the nanoparticles (according to whether they are WGMs or LSPs, respectively), is scarcely influenced by the transmission characteristics of the slits, and can be further enhanced by introducing corrugation on the slab surface by focalization onto the particle set.

We conclude that the arrangements of metallic nanoparticles is not superior to that of dielectric ones as regards localized enhancements of transmitted light. In addition, transmission by WGMs is substantially less dissipative than by LSPs. These last are useful, notwithstanding, when they play the role of e.g. *nanoantenna* or *spaser* emitters.

References

[1] K. J. Vahala, Nature, **424** (2003) 839.
[2] F.J. García-Vidal, L. Martín-Moreno, T.W. Ebbesen, L. Kuipers, Rev. Mod. Phys. **82** (2010) 729.
[3] F. J. Valdivia-Valero and Manuel Nieto-Vesperinas, Opt. Express, **18** (2010) 6740.
[4] F. J. Valdivia-Valero and Manuel Nieto-Vesperinas, Opt. Commun., (2010) « article in press ».

Figures
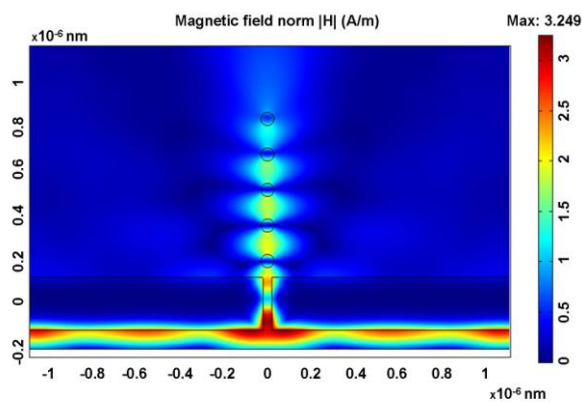
Map of |H| when a linear chain of Ag cylinders (radius= 30nm; distance between cylinders= 100nm) is at 346nm from a slit practized in a Tungsten slab (slab width= 2610nm; slab thickness= 237.55nm; slit width= 39.59nm). A p-polarized plane wave at λ= 400 nm incides from below. Localized surface plasmons are excited around the cylinders.
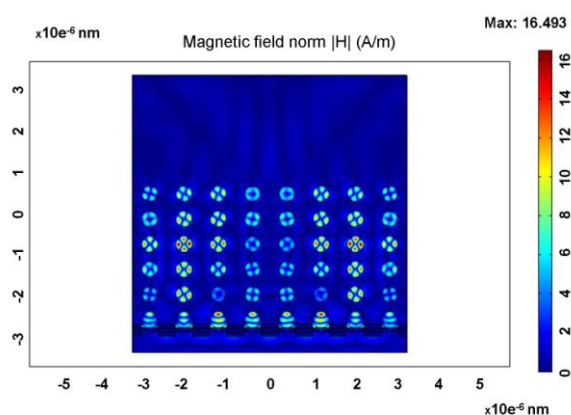
A Si cylinder photonic crystal (radius= 200nm; horizontal period= 826.87nm; vertical period= 600nm) in front of a perfectly conducting corrugated grating (refractive index= i32; period= 826.87nm; slab width= 8·period; slab thickness= 283.5nm; slit width= 118.12nm; corrugation period= period; corrugation amplitude= 99.2244nm). A p-polarized plane wave at λ= 945 nm incides from below. Whispering gallery modes are excited inside the cylinders.